

PAH RADICAL SCAVENGING IN FUEL-RICH PREMIXED BENZENE FLAMES

by

Timothy George Benish

B.ChE. Chemical Engineering
Georgia Institute of Technology, 1992

M.S. Chemical Engineering Practice
Massachusetts Institute of Technology, 1996

Submitted to the Department of Chemical Engineering
in Partial Fulfillment of the Requirements for the Degree of

Doctor of Philosophy

at the

Massachusetts Institute of Technology

June 1999

© 1999 Massachusetts Institute of Technology
All Rights Reserved

Signature of Author: _____
Department of Chemical Engineering
March 1999

Certified by: _____
Jack B. Howard
Hoyt C. Hottel Professor of Chemical Engineering
Thesis Supervisor

Accepted by: _____
Robert E. Cohen
St. Laurent Professor of Chemical Engineering
Chairman, Committee for Graduate Students

PAH Radical Scavenging in Fuel-Rich Premixed Benzene Flames

by

Timothy George Benish

Submitted to the Department of Chemical Engineering on March 11, 1999 in partial fulfillment of the requirement for the degree of Doctor of Philosophy in Chemical Engineering.

Abstract

Combustion systems operating under optimum conditions produce only carbon dioxide and water. But in real systems, inadequate mixing of fuel and oxygen produces fuel-rich “pockets”, where incomplete oxidation results in carbon growth, first through small radicals, then through larger species, including polycyclic aromatic hydrocarbons (PAH), and finally into visible carbon particulates (soot). The negative health impacts of PAH and soot have motivated research into their formation mechanisms in flames. The mechanisms are believed to involve acetylene addition to PAH radicals and PAH radical reactive coagulation. Extensive efforts to model carbon growth in flames have elucidated the mechanism for the formation of the first benzene ring, but mechanisms for further growth are as yet speculative.

PAH have been measured in flames by molecular beam / mass spectrometry (MB/MS) and microprobe sampling. These methods produce questionable measurements of PAH, and are unable to detect PAH radical intermediates. Hausman and Homann (1995) developed a technique which includes high quality molecular beam-type sampling of flames with stabilization of radical intermediates by a scavenger. The scavenger, dimethyldisulfide (DMDS) and the sampled flame gases are frozen together, and upon warming, the radicals react with the DMDS to form methylthio compounds: $R\cdot + CH_3SSCH_3 \rightarrow R-SCH_3 + CH_3S\cdot$. High quality measurements of the highly reactive flame compounds can be obtained with this technique.

In this study, fuel-rich, low pressure, premixed benzene/oxygen/argon flames were studied by a similar radical scavenging technique using DMDS, but developed specifically for the accurate quantitation of PAH and PAH radicals. Fifty-five compounds were measured by GC/MS in previously studied $\phi=1.8$ and $\phi=2.0$ benzene flames, including 12 aromatic radicals. Compounds measured in this study that had not been previously measured unequivocally in these flames included 1- and 2-ethynyl-naphthalene, biphenylene, 1- and 5-ethynyl-acenaphthylene, and the acenaphthyl, fluoranthenyl, and pyrenyl radicals. PAH analysis by this radical scavenging technique showed that PAH are in significantly higher concentrations in the benzene $\phi=1.8$ flame than were measured by MB/MS studies by Bittner and Howard (1981). The inventory of PAH less than 300 amu does not change significantly by increasing the equivalence ratio past the sooting limit of the flame.

Ab initio density function calculations of the thermodynamic properties of PAH and PAH radicals show that the aryl C-H bond dissociation energies around the periphery of PAH are roughly the same as those for benzene, regardless of the size of the PAH. The σ radicals created by hydrogen abstractions from PAH are unaffected by the resonance π structures of the PAH. The vinyl-type C-H bonds in the five-membered rings of PAH are 4-kcal/mol stronger than their aryl counterparts. The high bond dissociation energy of these vinyl groups may be a result of the

inability of the already strained C-C bonds of the 5-membered ring to relax upon loss of the hydrogen. The C-H bonds of the methylene-type 5-membered ring of cyclopenta[def]phenanthrene are 32 kcal/mol weaker than the aryl C-H bonds due largely to stabilization by the adjacent π system.

Calculations of the equilibrium between PAH, PAH radicals, H, and H_2 suggest that kinetic mechanisms dominate over thermodynamics in the PAH growth and consumption region of the flame, but that thermodynamic considerations can be significant. Thermodynamics predict that the percentage of PAH that contain a radical site depends almost exclusively on the number and general types of C-H bonds on the periphery of each molecule. At least in the early stages of the flame, thermodynamics alone significantly overestimates the radical concentrations.

The kinetic flame model developed by Richter et al. (1999) was critically tested with the data from this study. It showed that acenaphthylene appears to be formed by the addition of C_2H_2 to the 1-naphthyl radical, but suggests that another acenaphthylene formation pathway is necessary in the benzene flame to account for the high concentrations of acenaphthylene. A reaction between two phenyl radicals (or a reaction between phenyl and benzene) followed by a rearrangement has been postulated as the dominant pathway for the formation of acenaphthylene in the benzene flames.

PAH and soot were measured by microprobe sampling in the atmospheric ethylene-air flames studied by Harris and Weiner (1983a) when they concluded that acetylene is the only significant reactant in soot growth. In the present study, PAH were found in sufficiently high concentrations that their contribution to soot growth appears to be important. The observed mass growth rates of the total PAH and soot are consistent with a simple mechanism in which both C_2H_2 and PAH react with soot, and C_2H_2 also reacts with PAH. The PAH-soot reaction occurs with a collision efficiency of order 5000-times larger than the C_2H_2 -soot value, and contributes 95% or more of the soot mass growth.

Thesis Supervisor: Jack B. Howard
Hoyt C. Hottel Professor of Chemical Engineering

Acknowledgements

I would first like to thank my advisor, Professor Jack Howard, a shining example of everything a professor should be. His guidance has been invaluable, and his friendly and easy-going personality has made my life as a graduate student a pleasant experience. I could not ask for a better role model. I would also like to thank my thesis committee members, Dr. Art Lafleur, Prof. Preetinder Virk, and Prof. Adel Sarofim for their time and effort in guiding me through this process. The members of the CORE lab deserve special thanks, especially Koli Taghizadeh, who has taught me everything I know about chromatography, and John LaRusso, whom I depended on to get things running and to keep them that way. I would also like to express thanks to Prof. Bill Green for his support and advice on molecular modeling. I am grateful to K. Das Chowdhury and Lenore Rainey for their electron microscopy efforts.

It has been a pleasure to work with the members of my group over the years, whether slaving away in the basement or solving the world's problems over a pizza. First and foremost I would like to thank Bill Grieco, for teaching me how to build almost everything I needed, for constantly letting me bounce ideas off of him, for his extensive personal advice, and for telling me, "You're not stupid. You're just unlucky!" as my equipment failed almost daily. I would also like to thank Rich Shandross for getting me started with the crazy system I inherited from him and Henning Richter, who's help in modeling and constant support in the last few months of this work were absolutely critical.

It is impossible to imagine how this project would have evolved without the help of Prof. Larry Scott and Dr. Atena Necula at Boston College. Atena's amazing ability to synthesize virtually any compound I imagined led to almost every interesting finding in this work. I have also enjoyed spending time with the members of the Scott lab. And speaking of, I would like to thank Shelly for all of her encouragement and for being the light at the end of my tunnel.

Finally, I would like to thank my family. Mom, Don, and Grandma, your love and support is unmatched anywhere in the world. I would like to dedicate this to my father, who's incredible foresight and guidance has allowed me to get to this point. For everything I have accomplished and for everything I am, I will be forever indebted to you.

I would like express my gratitude for financial support from the Division of Chemical Sciences, Office of Basic Energy Sciences, Office of Energy Research, U.S. Department of Energy under Grant DE-GF02-84ER13282 and for analytical support from the MIT Center for Environmental Health Sciences under Center Grant NIH-5P30-ES02109 and Program Grant NIH-5P01-ES01640 of the National Institute of Environmental Health Sciences.

Table of Contents

Chapter 1	Introduction and Background	11
1.1	Health Effects of PAH and Soot	11
1.2	PAH and Soot Formation in Flames	12
1.2.1	PAH Growth by Acetylene	13
1.2.2	PAH Growth by PAH Coagulation	14
1.3	Measuring PAH and Radicals in Flames	14
1.3.1	Molecular Beam Mass Spectrometry	15
1.3.2	Sample Collection and Chromatography	17
1.3.3	Radical Scavenging	19
1.4	Objectives	21
Chapter 2	Experimental Apparatus and Procedures	22
2.1	Combustion Apparatus	22
2.1.1	Burner	22
2.1.2	Molecular Beam-Type Sampling	23
2.1.3	Gas and Liquid Fuel Delivery	27
2.2	Sampling Procedure	29
2.3	Flame Conditions	31
2.4	Scavenger Selection	31
2.5	Sample Analysis	32
2.5.1	Calculation of Mole Fraction	35
2.5.2	Problems Associated with Concentrating Sample Solutions	37
2.5.3	Effect of Washing the Trap	39
2.5.4	Analysis of Scavenged Radicals with Sulfur Chemiluminescence	40
Chapter 3	Results	43
3.1	Mole Fractions of Stable Aromatics in Flames	43
3.1.1	Small Condensed PAH	43
3.1.2	Substituted Aromatics	46
3.1.3	Biaryls	50
3.1.4	Larger PAH	52
3.1.5	Oxy-PAH	54
3.2	Mole Fractions of Aromatic Radicals in Flames	57
3.2.1	Phenyl and Benzyl Radicals	57

3.2.2	Naphthyl Radicals	60
3.2.3	Acenaphthyl Radicals	62
3.2.4	Pyrenyl and Fluoranthenyl Radicals	65
3.2.5	Other Radicals Detected and Undetected	69
Chapter 4	Modelling and Discussion	71
4.1	Thermodynamic Calculations	71
4.1.1	Heats of Formation and H-Dissociation	72
4.1.2	Equilibrium Calculations	76
4.2	Flame Model	79
4.2.1	Base Case Model	79
4.2.2	Modified Model	83
Chapter 5	Soot Surface Growth	88
5.1	Microprobe Sampling of an Atmospheric Ethylene Flame	89
5.2	Results	90
5.3	Discussion	96
Chapter 6	Conclusions and Recommendations	99
Appendices		102
Appendix A	Radical Scavenging with Dibromomethane	103
Appendix B	Tabulated Mole Fractions	110
Appendix C	Detailed Sampling Procedure	113
Appendix D	Tabulated Thermodynamic Data from DFT Calculations	118
References		122

List of Figures

Figure 1.1	Mutagenesis by benzo[a]pyrene	12
Figure 1.2	Naphthalene formation by acetylene addition	13
Figure 1.3	Naphthalene formation by cyclopentadienyl combination	14
Figure 1.4	Cross-section of an MB/MS system (Bittner, 1981)	15
Figure 1.5	Collection of condensable material from flames (McKinnon, 1992)	18
Figure 1.6	Cross section of radical scavenging system (Griesheimer and Homann, 1998)	20
Figure 2.1	Cross-section of cold trap and burner.	23
Figure 2.2	Diffusion pump oil contaminants.	24
Figure 2.3	Molecular beam/radical scavenging system and cold trap.	25
Figure 2.4	Molecular beam/radical scavenging system schematic.	26
Figure 2.5	Gas feeds and benzene vaporizer.	28
Figure 2.6	Sample retrieval.	30
Figure 2.7	Mole fractions of phenylacetylene and phenol calculated from injections 1 and 2.	38
Figure 2.8	Mole fractions of benzo[ghi]fluoranthene and cyclopenta[cd]pyrene calculated from injections 2 and 3.	39
Figure 2.9	GC/SCD chromatogram of a flame sample.	42
Figure 3.1	Structures of small condensed PAH.	44
Figure 3.2	Benzene and toluene mole fractions in the $\phi=1.8$ flame. (Bittner and Howard, 1981)	44
Figure 3.3	Prevalent PAH mole fractions in the $\phi=1.8$ and $\phi=2.0$ flames.	45
Figure 3.4	Small PAH mole fractions in the $\phi=1.8$ and $\phi=2.0$ flames.	46
Figure 3.5	Structures of substituted PAH.	47
Figure 3.6	Phenylacetylene and styrene mole fractions in the $\phi=1.8$ and $\phi=2.0$ flames.	47
Figure 3.7	1-Methylnaphthalene and 2-vinylnaphthalene mole fractions in the $\phi=1.8$ and $\phi=2.0$ flames.	48
Figure 3.8	GC/MS chromatogram of a flame sample extracting molecular ions 152 and 176. ($\phi=1.8$, 7.75 mm, HP-50+ column)	49
Figure 3.9	Ethynylnaphthalene mole fractions in the $\phi=1.8$ and $\phi=2.0$ flames.	49
Figure 3.10	Ethynylacenaphthylene mole fractions in the $\phi=1.8$ and $\phi=2.0$ flames.	50
Figure 3.11	Structures of some biaryls.	50
Figure 3.12	Biaryl mole fractions in the $\phi=1.8$ and $\phi=2.0$ flames.	51
Figure 3.13	Structures of larger condensed PAH.	52
Figure 3.14	Mole fractions of the mass 226 and 228 compounds in the $\phi=1.8$ and $\phi=2.0$ flames.	53
Figure 3.15	Mole fractions of the mass 252 and 276 compounds in the $\phi=1.8$ and $\phi=2.0$ flames.	54
Figure 3.16	Structures of oxy-PAH.	55

Figure 3.17 Phenol mole fractions in the $\phi=1.8$ and $\phi=2.0$ flames.	55
Figure 3.18 Naphthol and dibenzofuran mole fractions in the $\phi=1.8$ and $\phi=2.0$ flames.	56
Figure 3.19 Oxy-PAH mole fractions in the $\phi=1.8$ and $\phi=2.0$ flames.	57
Figure 3.20 Structures of 1-ring methylthio compounds.	58
Figure 3.21 Mass spectra for 1-ring methylthio compounds: methylthiobenzene, benzylmethylsulfide, p-tolyl sulfide.	59
Figure 3.22 Phenyl and benzyl radical mole fractions in the $\phi=1.8$ and $\phi=2.0$ flames.	60
Figure 3.23 Structures of methylthionaphthalene.	60
Figure 3.24 Mass spectra for the methylthionaphthalenes: 1-methylthionaphthalene, 2-methylthionaphthalene.	61
Figure 3.25 Naphthyl radical mole fractions in the $\phi=1.8$ and $\phi=2.0$ flames .	62
Figure 3.26 Structures of methylthioacenaphthylene.	62
Figure 3.27 GC/MS chromatogram of the extracted fragment ions for methylthioacenaphthylene. (HP-50+ column)	63
Figure 3.28 Mass spectrum for 4-methylthioacenaphthylene	63
Figure 3.29 Mass spectra for 1-methylthioacenaphthylene, 3-methylthioacenaphthylene, and 5-methylthioacenaphthylene.	64
Figure 3.30 Acenaphthyl radical mole fractions in the $\phi=1.8$ flame.	65
Figure 3.31 Structures of methylthiopyrene and methylthiofluoranthene.	66
Figure 3.32 GC/MS chromatogram of the extracted fragment ions for methylthiopyrene and methylthiofluoranthene. (HP-50+ column)	66
Figure 3.33 Mass spectra for the three isomers of methylthiopyrene: peak A, 1-methylthiopyrene, peak C.	67
Figure 3.34 Mass spectra for 5-methylthiofluoranthene.	68
Figure 3.35 Pyrenyl and fluoranthenyl radical mole fractions in the $\phi=1.8$ flame.	68
Figure 4.1 Optimized geometry of 4-acenaphthyl radical from BLYP/DZVP calculations.	75
Figure 4.2 Base case model results for naphthalene, acenaphthylene, and related species.	81
Figure 4.3 Acenaphthylene formation via biphenyl.	82
Figure 4.4 Base case model results for the mass 178 and mass 202 species.	83
Figure 4.5 Modified model results for naphthalene, acenaphthylene, and related species.	86
Figure 4.6 Modified model results for the mass 202 species.	87
Figure 5.1 Atmospheric flame burner and sampling apparatus.	90
Figure 5.2 Soot and Σ PAH concentrations at different positions in flame.	91
Figure 5.3 HPLC chromatogram of soot extract at 368 nm waavelength (C/O=0.70, 10 mm).	91
Figure 5.4 Effect of the relative reactivity of soot and Σ PAH on the calculated soot growth contribution by Σ PAH.	95
Figure 5.5 Collision efficiencies at different distances from burner.	96
Figure 5.6 Carbon densities of acetylene and Σ PAH for premixed C ₂ H ₄ -air flat flames at different pressures.	97

Figure A.1	GC/MS chromatogram of bromonaphthalene and mass spectrum of 1-bromonaphthalene.	104
Figure A.2	PAH radical mole fractions determined from scavenging with dibromomethane (DBM) and dimethyl disulfide (DMDS).	109
Figure C.1	Operating procedure reference schematic	117
Figure D.1	Numbering schemes for select PAH.	118

List of Tables

Table 2.1	Flame Conditions.	31
Table 2.2	GC/MS Specifications.	32
Table 2.3	Identification and Quantitation Methods for each Compound Studied.	34
Table 2.4	PAH in Cold Trap Drippings and Washings.	40
Table 3.1	Other Methylthio Compounds Detected.	70
Table 4.1	Standard Heats of Formation and H-Disassociation Energies.	74
Table 4.2	Naphthalene/Hydrogen Equilibrium.	78
Table 4.3	Pyrene/Hydrogen Equilibrium.	78
Table 4.4	Acenaphthylene/Hydrogen Equilibrium.	79
Table 4.5	Added Reactions for Base Case Kinetic Model.	79
Table 4.6	Modifications to the Base Case Model.	84
Table 4.7	Effect of Thermodynamics on Model Predictions	84
Table 5.1	Identified flame compounds and their estimated mass fractions of total PAH.	92
Table 5.2	Additional measurements and calculated values.	93
Table A.1	Selected Bond Dissociation Energies .	104
Table A.2	Scavenged Products of Standard and Deuterated Dibromomethane.	106
Table A.3	Relative Amounts of Brominated PAH Using Different Scavengers.	107
Table A.4	Calculation of Side Reactions of CH ₂ Br ₂ .	108
Table B.1	Measured Species Mole Fractions, $\phi=1.8$ Flame, 0.3 to 0.74 cm HAB.	110
Table B.2	Measured Species Mole Fractions, $\phi=1.8$ Flame, 0.76 to 1.09 cm HAB.	111
Table B.2	Measured Species Mole Fractions, $\phi=2.0$ Flame.	112
Table D.1	Formation and Zero-Point Energies from DFT Calculations.	118
Table D.2	Enthalpy Corrections and Entropies from DFT Calculations.	119

Chapter 1

Introduction and Background

The vast majority of energy production in the U.S. and the world comes from the combustion of fossil fuels, including oil, natural gas, and coal. Burning of these hydrocarbon fuels releases heat, which is used to produce work, as well as chemical by-products. If the fuel is perfectly mixed with adequate oxygen upon burning, the products are simply carbon dioxide and water. However practical combustors, including power plant burners and automobile engines, can not achieve perfect mixing, so in fuel-rich pockets of a combustor, the reactive fragments of the fuel molecules begin to combine with each other. As the hydrocarbon molecules grow, they organize into planar hexagonal carbon rings, because the electronic structure of the rings makes them very stable (Haynes, 1991). The resulting planar multi-benzenoid ring structures, termed polycyclic aromatic hydrocarbons (PAH), the most prevalent containing 2 to 5 rings, continue to grow and coagulate until they become visible carbon particulates, or soot (McKinnon and Howard, 1992).

1.1 Health Effects of PAH and Soot

Extreme levels of air pollution have been correlated to mortality in a number of case studies, beginning with the infamous London Fog in 1952, which resulted in about 4,000 excess deaths due primarily to respiratory diseases (Schenker, 1993). Associating lower levels of air pollution with health effects has been difficult, because of hundreds of confounding factors people are exposed to, including cigarette smoking. However, recent studies have suggested that fine particulate matter, most of which is produced in combustion sources, contributes to excess mortality in the U.S., predominantly from lung cancer and cardiopulmonary disease (Dockery et al., 1993).

The tendency for soot to cause cancer was first identified in chimney sweeps by Sir Percival Pott in London in 1775. Although work to date has failed to conclusively find the mechanism for disease, there is considerable speculation that it may be linked to the PAH which are adsorbed to the surface of the airborne soot particles (Allen et al., 1996). Many PAH have been found to be both carcinogenic (causing cancer) and mutagenic (mutating DNA) in bioassays of bacteria, rodent, and even human cells (Durant et al., 1996). Only a few of the PAH seen in flames

account for the majority of the mutagenicity of typical combustion products. Some of the most active species include PAH containing 5-membered rings, such as cyclopenta[cd]pyrene (Howard et al., 1995), and oxygen-containing PAH (Durant et al., 1996).

Benzo[a]pyrene (B[a]P) is the most studied of the mutagenic PAH, and much of how it is processed in the body has been revealed. Although B[a]P itself is a very non-reactive compound in cellular conditions, cells expressing the P₄₅₀ gene (including lung epithelium) attempt to make it more polar by adding hydroxyl groups so that the body can eliminate it in waste water. One of the intermediates in this process, (+)anti-benzo[a]pyrenediol-epoxide (BPDE, Figure 1.1), has been found to intercalate within DNA while the reactive epoxide reacts with the N⁷ position of guanine bases within the DNA. The resulting DNA adduct has been detected by x-ray crystallography and NMR (Cosman et al., 1992). Upon replication, the DNA undergoes G → T mutations at the adduct sites (Mackay et al., 1992). It is not known if this particular mutation (or any mutation) is responsible for the carcinogenic potential of B[a]P, or if other mutagenic PAH follow a similar mechanism.

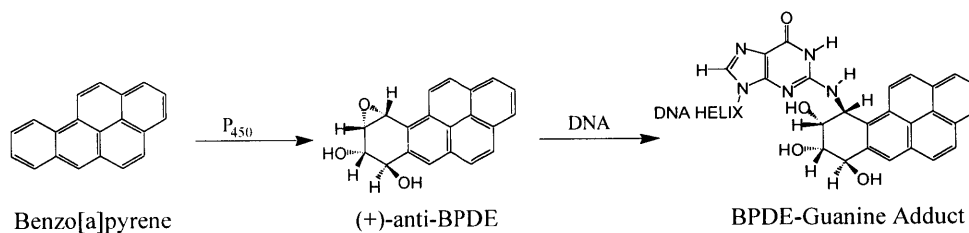


Figure 1.1 Mutagenesis by benzo[a]pyrene

1.2 PAH and Soot Formation in Flames

Concerns about the health impacts of PAH and soot have created interest in how the compounds are produced, as this knowledge may lead to control strategies, especially for the most mutagenic species. A number of detailed kinetic models have been developed in an effort to identify the most important pathways to the formation and growth of PAH and soot. An overview of the recent progress in the development of elementary kinetic models has been presented by Lindstead (1998). The effort thus far has been dedicated primarily to understanding the formation of the first benzene ring. Although some of the mechanisms for benzene formation are still debated, most of the rate constants for the various reactions have been studied in detail. Less understood are the growth processes that lead to further ring growth. A number of kinetic models have been developed to explain PAH growth in specific flames (Marinov et al., 1996, Wang and Frenklach, 1997, Cataldi, et al., 1996), but the mere number of

possible pathways for carbon growth and lack of thermodynamic and kinetic data for the molecules involved makes the development of a flame-independent model difficult.

1.2.1 PAH GROWTH BY ACETYLENE

A frequently used hypothesis within the combustion community is that PAH growth occurs primarily through sequential addition of acetylene. The first testing of this hypothesis using detailed elementary reaction modelling of PAH formation was performed by Frenklach et al. (1984). Comparisons of model prediction against experimental data from shock-tube pyrolysis studies of acetylene supported the hypothesis, which has continued to be supported by numerous additional experimental and computational investigations. The first step in this proposed growth mechanism is the abstraction of a hydrogen atom from the aromatic ring, forming a σ radical site, to which acetylene adds. The formation of naphthalene by this mechanism is detailed in Figure 1.2. In this case, three different pathways have been envisioned for the addition of a second acetylene group, which is followed by ring closure. Although the mechanisms for acetylene addition to different PAH structures may vary slightly, the basic concept can be easily applied to all PAH. A number of investigators have applied this mechanism to the surface growth of soot as well, which is discussed in Chapter 5.

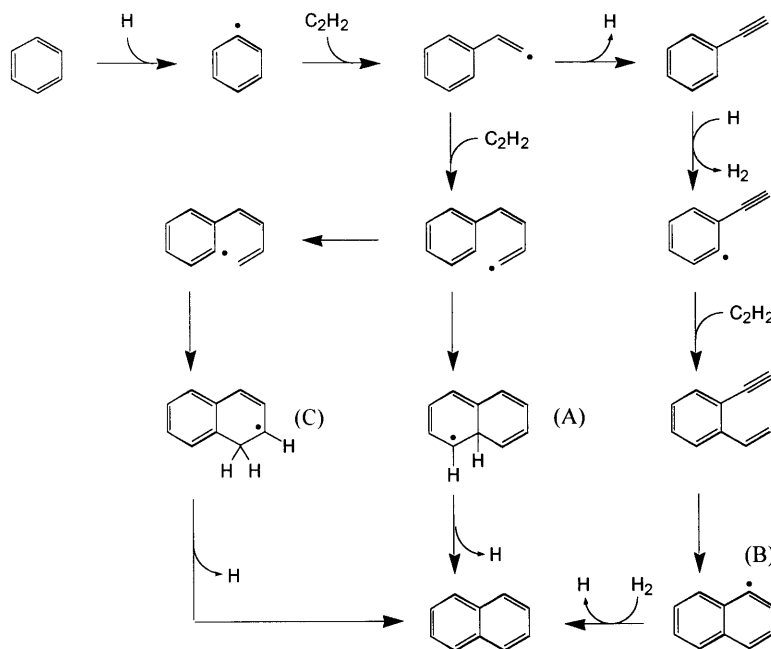


Figure 1.2 Naphthalene formation by acetylene addition

Two different radical types are expected as intermediates in the mechanism of Figure 1.2. Hydrogen abstraction reactions and ring closure by the right pathway produce a σ radical (B). The ring closure by the center pathway produces a π radical intermediate (A). Although the π radical is stabilized by resonance, the loss of the benzene ring structure produces a relatively unstable compound. Numerical studies have indicated that between these two pathways, the right one is the dominant pathway in PAH growth mechanisms (Frenklach, 1988). The leftmost pathway (C), suggested by Scott (1999), includes a hydrogen transfer step which may dramatically lower the activation energy for the formation of a π radical, since the first aromatic ring is unaffected by the closure of the second.

1.2.2 PAH GROWTH BY PAH COAGULATION

Another potential pathway for PAH growth involves the reaction between two aromatic species. The prevalence of biphenyl in benzene flames (McKinnon, 1992) and binaphthyl in naphthalene flames (Griesheimer and Homann, 1998) suggests that these reactions can be significant. Marr (1993) calculated that an alternate pathway to naphthalene formation by combination of cyclopentadienyl radicals followed by rearrangement (Figure 1.3) may be dominant over acetylene addition. The cyclopentadienyl radical is also a π radical, but it may be created by simply abstracting a hydrogen, and is thus more stable than the previously discussed case.

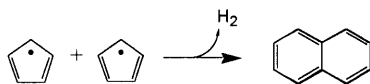


Figure 1.3 Naphthalene formation by cyclopentadienyl combination

1.3 Measuring PAH and Radicals in Flames

Validation of the various proposed PAH formation mechanisms requires measurements of the species involved. Several techniques have been used to measure the compounds within flames. Non-intrusive techniques, including optical methods, allow study of soot and a few classes of molecules, but can not distinguish between the hundreds of different compounds within the flames. The data are obtained by withdrawing samples of the flame gases and feeding them directly to analytical equipment for on-line processing, or by collecting the gas or condensable materials and analyzing them by separate techniques. Physical sampling of compounds with spatial

resolution requires insertion of a probe, which perturbs the flame, often to an unknown extent. In addition, special care must be taken to ensure that the compounds entering the sampling system do not react before analysis.

1.3.1 MOLECULAR BEAM / MASS SPECTROMETRY

One of the most exploited techniques for obtaining flame species data is molecular beam / mass spectrometry (MB/MS). MB/MS, unlike the analysis techniques before it, could be used to measure a wide variety of species, including radicals, with only one method. Homann et al. (1963), Homann and Wagner (1965), and Bonne et al. (1965) first used MB/MS quantitatively to measure dozens of species in sooting flames. Others, including Bittner and Howard (1981), have extended this method to obtain detailed profiles of more compounds, including PAH, in a wide variety of flames.

In MB/MS, gases are sampled by a probe into a low-pressure environment where molecular collisions become negligible. The core of the sampled gases are subsequently sampled by a second probe, or *skimmer*, followed by a collimating orifice, creating a narrow beam of molecules which travel unimpeded into a mass spectrometer (Figure 1.4). The sampling process of MB/MS is considered to be of high quality. Since only the core of the sample reaches the mass spectrometer, the molecules can not react with surfaces, and the low pressures ensure that the molecules do not react with each other after being sampled from the flame.

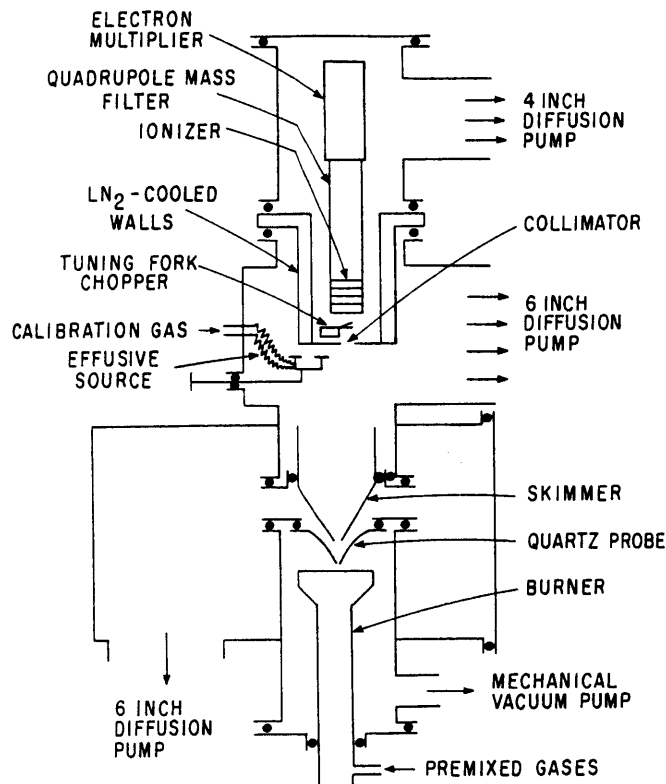


Figure 1.4 Cross-section of an MB/MS system (Bittner, 1981)

In an electron-impact mass spectrometer, the typical type used in this application, the molecules are subjected to a stream of electrons in the ion source, which knocks electrons from the molecules, leaving a small fraction with a positive charge. The energy of the impact can also cause the molecule to fracture, resulting in fragment ions. The molecular and fragment ions then pass through an electric field, which is tuned to let only ions of a specific mass to charge ratio (m/z) reach the detector (generally an electron multiplier). The electric field is varied so that the ions are counted for each m/z over the range of the scan, resulting in a mass spectrum. Fragmentation of the molecular ion in a mass spectrum can be useful for identifying a single compound (or several compounds which are first separated by chromatography), but would be catastrophic for MB/MS studies of flames, as hundreds of different molecules enter the mass spectrometer at the same time. Therefore, a great deal of effort is made to accurately control the ion source to ensure that only molecular ions are made.

Much of the difficulty in obtaining accurate concentrations for the species in the flame using this technique lies in the calibration methods. First, the sampling procedure tends to enrich the molecular beam with high-molecular weight compounds. This phenomenon, termed mass discrimination, is caused by the diffusion of lighter species out of the centerline of the expansion, scattering of the beam by surrounding gases, and other factors (Knuth, 1973). However, mass discrimination is not expected to significantly impact the measurement of large molecules, like PAH.

Even though the mass spectrometer can be calibrated for some compounds, the temperature of the flame can not be duplicated, so a number of assumptions and estimations are necessary. But most importantly, the mass spectrometer can not be directly calibrated for a number of compounds, including nearly all radicals and compounds that are difficult to introduce into the system, like PAH, which generally have low vapor pressures. The energy needed to ionize each compound efficiently without fragmenting it must be known, because this is the only way of separating the hundreds of compounds which impact the detector. Therefore estimations of ionization cross-sections are used to calibrate the response of the mass spectrometer to each compound. The detection efficiency of the ionized molecules must also be estimated. The errors incurred from these estimations are expected to increase as the concentrations of the species of interest decrease (Bittner, 1981). Many PAH approach the detection limit for this

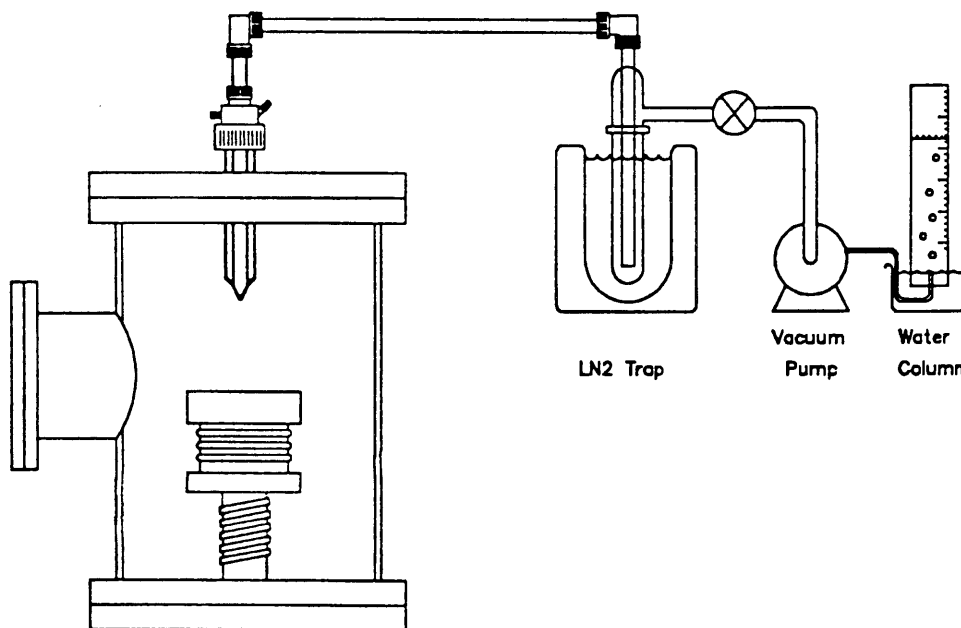
technique, so their quantitation may be quite poor. Also, almost all PAH have several isomers, which can not be separated with MB/MS.

In the case of radicals, additional care must be taken to differentiate them from a parent molecule that may have fragmented in the mass spectrometer. Avoidance of fragmentation is very difficult, because the tendency for a molecule to fragment is related in part to the internal energy of the molecule that is ionized in the mass spectrometer. The internal energy of the molecules is difficult to quantify because of many unknowns in the dynamics of the sampling process as well as the physical properties of the molecules themselves. Because of the limitations of MB/MS, the largest aromatic radicals measured in flames by this method are the phenyl and benzyl radicals.

1.3.2 SAMPLE COLLECTION AND CHROMATOGRAPHY

Many of the limitations of the on-line methods can be overcome by collecting a sample of the flame gases over a period of time and employing various separation and detection techniques to identify each compound. Gas and liquid chromatography are generally used to separate the hundreds of flame compounds, which are then detected with mass spectrometry, flame ionization, or a host of optical techniques.

Generally, the flame is sampled with the smallest probe that can be used in order to minimize flame perturbation. The gases can be collected in a tank and later fed to a GC to determine the concentrations of the major flame species. But PAH comprise only 1% of the total concentration of flame compounds and they condense upon sampling, so they must be collected by passing the sampled flame gases through filters or cooled traps where the PAH condense (Figure 1.5). The temperature of the collecting surface is important, because small PAH are volatile enough to stay in the gas phase at room temperature. The surfaces are then washed with a solvent, which extracts the PAH. Methylene chloride is a common and sufficient solvent for small PAH (less than 6-7 rings), while larger PAH and small fullerenes require different solvents. The solution of PAH is then injected directly into a chromatograph. Gas chromatography with mass spectrometry (GC/MS) is frequently used for identification and quantitation of small PAH (less than 300 amu), while high performance liquid chromatography with ultra-violet detection (HPLC/UV) is often used to study larger species.



Burner and Chamber

Figure 1.5 Collection of condensable material from flames (McKinnon, 1992)

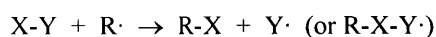
While on-line methods are subject to the detection limits of the analysis techniques, the sample collection methods are not, because the flame can be sampled over a sufficiently long period of time so that the most minute compounds can be extracted and concentrated by repeated separation processes. In addition, mass isomers can easily be separated with chromatography. Finally, quantitation of the flame species is relatively simple and does not rely on theoretical estimations. Quantitation of PAH requires only authentic standards of the compounds of interest, which can be analyzed in the same way as the flame samples. As a result of these features, over 50 PAH have been measured in flames using this technique.

However, an overriding concern regarding this method is that the effects of collecting a sample of reactive material are not known. Reactions can occur in the gas phase within the sampling device (as pressures in these systems are generally too high for a collision-free environment) or on the collecting surface. PAH radicals, which may be somewhat stable in the flame, can be very reactive at room temperature, so they do not exist long enough to be identified. Also, given the high radical character of PAH in flames, it is possible that sampled species reactively coagulate, forming larger PAH. For example, two sampled phenyl radicals may react on a surface to form biphenyl, a compound that may or may not actually be present in the flame. In addition, PAH having low volatilities may

condense onto the internal surfaces of the probe and transfer line before reaching the target collecting surface. For these reasons, data obtained by simple sample collection must be interpreted with caution (Haynes, 1991).

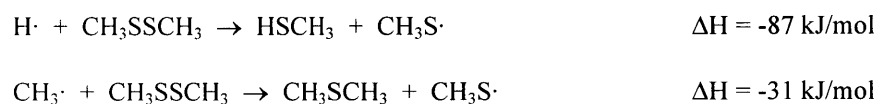
1.3.3 RADICAL SCAVENGING

Because neither of the methods discussed have been useful for studying PAH radicals, a new radical scavenging technique has been developed. Radical scavenging, often termed spin trapping, refers to a process in which a particular radical reacts with a scavenger molecule, producing a stable compound and a scavenger radical or a stable radical complex:



Nitroso and nitrene compounds are the most commonly used scavengers for the analysis of reactive radicals, though mostly used to study solution chemistry (Church, 1994). Small flame radicals (H, O, OH, and CH₃) have been detected by scavenging with N₂O, D₂, and NO (Fristrom and Westenberg, 1965) as well as NO₂ and CCl₄ (Fristrom, 1983) and I₂ (Smyth and Miller, 1987). Large polyacetylene radicals have been stabilized by capping with CF₃ and CN radicals (Lagow et al., 1995).

Quantitative radical scavenging in flames has been best demonstrated by Homann and coworkers. Schottler and Homann (1987) combined the sample quality of the MB/MS method and the benefits of the sample collection methods with their new radical scavenging technique. A molecular beam-type probe sampled microwave discharges of H, O, and CH₃ radicals, which then impacted a liquid nitrogen-cooled plate in a high-vacuum chamber. Dimethyl disulfide (DMDS) was added as a scavenger simultaneously to the plate, producing a frozen matrix of radicals and scavenger. Upon warming, the radicals reacted with the weak S-S bond of DMDS to form methylthio adducts:



The scavenging products were collected in liquid form and analyzed by GC/MS. The discharge was then replaced with an acetylene flame in order to measure flame radicals.

The cold plate was later replaced by a more sophisticated cold trap (Figure 1.6) to improve the collection efficiency of the flame species (Hausmann and Homann, 1990). The trap consisted of two liquid-nitrogen-cooled hemispherical surfaces that collected about 90% of the material that entered the opening. DMDS was added through

a small sphere, drilled with holes, located in the center of the trap. Sampling of the flame lasted for 30 minutes. Then the trap was allowed to warm, and the melted scavenger and flame species dripped into a vial through a hole in the trap. The material in the vial was analyzed immediately by GC/MS without further processing. Using this design, PAH and radicals were measured in fuel-rich, laminar, premixed acetylene and benzene flames (Hausmann and Homann, 1990, Hausmann, et al., 1992). The aromatic radicals measured included phenyl, benzyl, indenyl, phenoxy, and naphthyl, but the uncertainties in their measurements are not clear. A more recent study of a naphthalene flame by the same apparatus resulted in discovery of $C_{16}H_9$ radicals, though structures could not be assigned (Griesheimer and Homann, 1998).

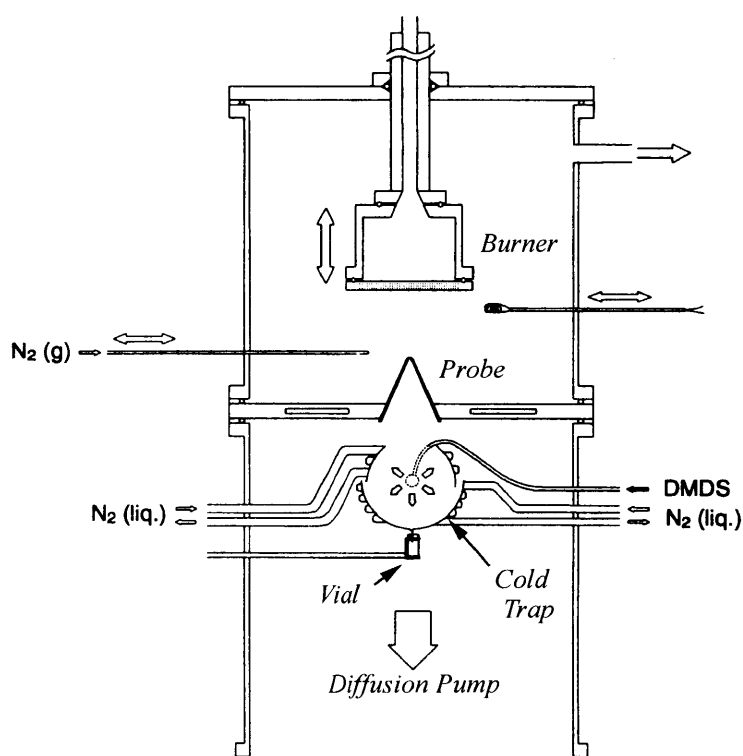
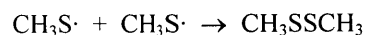
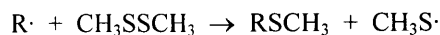


Figure 1.6 Cross section of radical scavenging system (Griesheimer and Homann, 1998)

The chemistry of the scavenging reactions is discussed in detail by Hausmann and Homann (1995). DMDS reacts with monovalent hydrocarbon radicals to form methylthio adducts, and if the scavenger is added in excess, the resulting methylthio radicals react only with themselves:



The reaction of the scavenger with the radicals goes nearly to completion. Side reactions, including hydrogen abstractions and hydrocarbon radical capping, were found to be negligible when DMDS was added in excess with the exception of DMDS adding across double and triple bonds. However, these artifacts could be easily distinguished from scavenged monovalent radicals, because they contained two methylthio groups.

Not only does radical scavenging allow for the detection of PAH radicals in flames, but it also eliminates the concerns of collecting a reactive sample, because the reactive species are quenched by the scavenger. As a result, the data obtained for stable PAH may be of higher quality than those obtained by any method thus far.

1.4 Objectives

The first objective of this study is to obtain an additional set of data for the low-pressure benzene flame studied by Bittner and Howard (1981), since it has become one of the most used sets of data in which kinetic model builders can test their models. But unlike the study by Bittner and Howard, the emphasis of this work is on PAH, some of which have been measured by a significantly different method and others that have not been detected in flames thus far. Second, this work extends the radical scavenging methods developed by Homann and coworkers to the study of larger PAH radicals than have been previously detected and provides the first radical data for the sooting flame studied by McKinnon (1992). Finally, the new data are compared with predictions from a state-of-the-art kinetic model in order to locate inadequacies in the proposed mechanisms and reaction rates.

Chapter 2

Experimental Apparatus and Procedures

Premixed, laminar flat flames were studied at a pressure of 20 torr. Though these types of flames do not completely represent industrial conditions, they exhibit one-dimensional behavior, which greatly simplifies the task of modeling the reactions within the flame. The low-pressure conditions allowed for detailed probing of the flame, as the thickness of the flame zone scales inversely with pressure. Low pressure was also necessary to avoid overloading the sampling system, and allowed for comparisons with numerous previously published studies for which temperature measurements were already available.

2.1 Combustion Apparatus

The combustion apparatus include the burner, sampling system, and reactant feed systems.

2.1.1 BURNER

The burner, which has been used previously (Bittner, 1981; Cole, 1982; Westmoreland, 1986; Shandross, 1996), is shown in Figure 2.1. After being well-mixed, the fuel, oxidant, and diluent gases first passed through a compartment filled with steel wool, which was used to help distribute the gases uniformly across the burner surface and to avoid flashback. The flow then entered a flow straightener, consisting of a copper plate drilled with hundreds of holes, and finally exited upward through a horizontal copper disk, 71 mm in diameter, which was drilled with about 730 1 mm dia. holes arranged in a hexagonal array and spaced 2.5 mm between hole centers. The burner was water-cooled, and the use of copper allowed for an even temperature distribution across the burner surface, although the surface temperature was not measured.

Premixed acetylene/oxygen flames were ignited on the burner surface with an arc from a wire held within a quartz tube and connected to a tesla coil. The flame was directed upward, and the burnt gases turned radially outward and then downward around the flame and exited from the bottom of the burner chamber. The burner

pressure was measured in the 2 in. dia. exhaust pipe, approximately 10 ft. from the burner by a capacitance transducer (MKS Baritron 170, 100 torr). The pressure drop from the burner to this point was negligible. The gases were then pumped through a high capacity vacuum pump (Stokes Microvap model 149-11) which maintained the vacuum in the burner chamber, but could be isolated by a gate valve. The pressure in the burner chamber was controlled by a second adjustable vacuum valve and by a controllable air leak to the pump. The pressure was consistently held to within 0.04 torr of the set point.

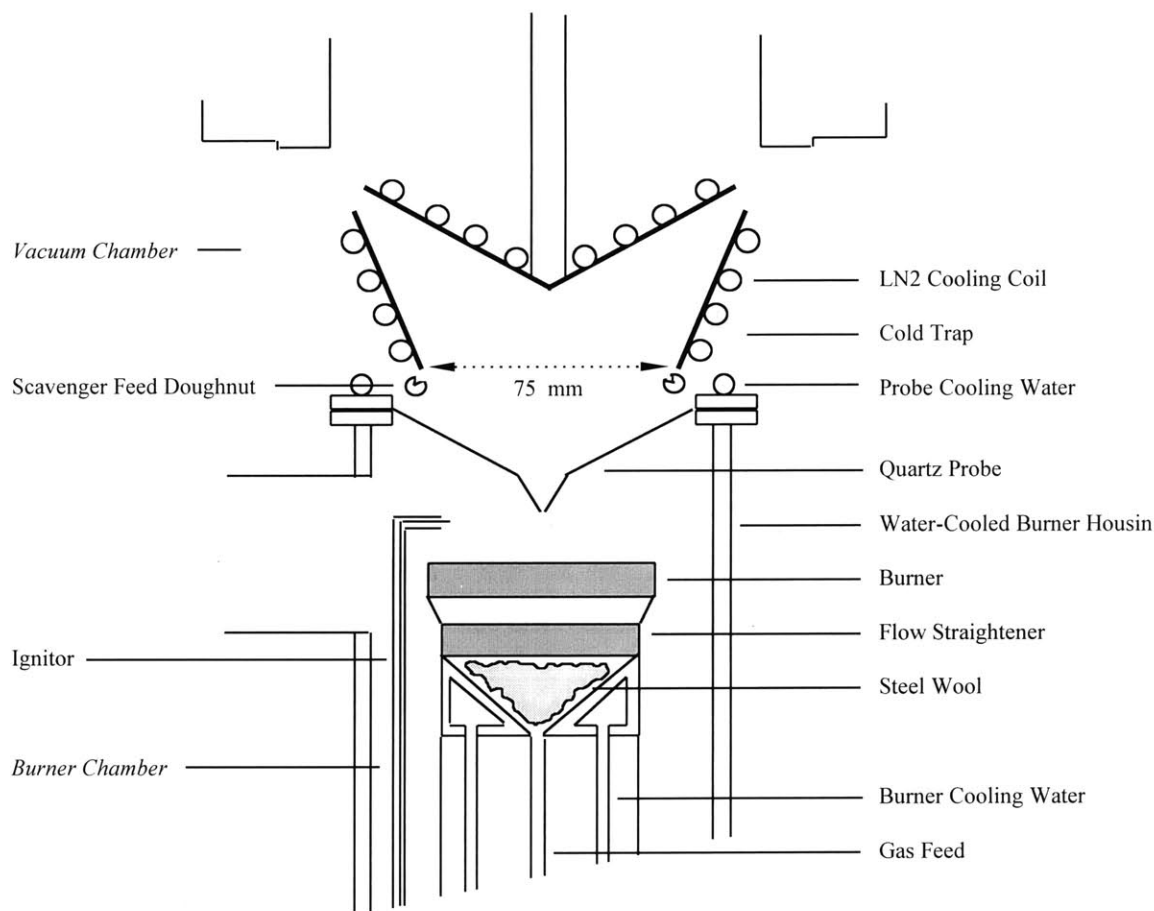


Figure 2.1 Cross-section of cold trap and burner.

2.1.2 MOLECULAR BEAM-TYPE SAMPLING

The flame was sampled along the centerline by a quartz probe. The burner design and low gas flow rates produced laminar, two-dimensional flames, which could be probed vertically, without considerations to radial effects. The flame was considered to be one-dimensional up to a distance equal to the burner diameter, where radial

influences are believed to reach the centerline. In order to sample at various positions, the burner was moved vertically with the aid of a translation stage and was leveled by a rotatable shim at the bottom of the burner. The distance between the probe and burner was measured through a quartz window with a cathetometer. Two separate measurements, precise to ± 0.1 mm were taken at the midpoint of the sampling period.

The probe, made by G. Finkenbeiner, Inc., was a 40° - 90° hybrid design, the type used in previous molecular beam/mass spectrometry (MBMS) sampling of flames (Bittner and Howard, 1981; Cole, 1982; Westmoreland, 1986; Shandross, 1996). The small angle at the probe tip minimized perturbation of the flame, while the large angle facilitated a fast quenching of reactions as the sampled molecules entered the high vacuum atmosphere. The probe was ground so that the bottom 1mm of the probe had a wall thickness of only 0.1 mm, again to minimize flame perturbation. The probe was water-cooled and had an orifice diameter of 0.70 mm.

The high temperature, reactive flame gases passing through the probe expanded into a high vacuum environment (of order 10^{-4} torr), where the mean free path for collisions between molecules was more than a meter. Therefore, bimolecular reactions were quickly quenched. The high vacuum environment was maintained by two six-inch diffusion pumps, which used a polyphenyl ether oil (Santovac 5), to entrap and remove the gases under molecular flow conditions. The oil had a tendency to flow out of the pump inlet, or “backstream”, in small quantities, so water-cooled baffles were added to dramatically decrease backstreaming and contamination of the sample with pump oil. A consideration given during sample analysis was that the oil when broken down could resemble PAH from the flame (Figure 2.2). The pressure in the vacuum chamber was monitored with two bayard-alpert type ionization gauges. The entire system, shown in Figures 2.3 and 2.4, was the modification of a previous MBMS system (Bittner and Howard, 1981; Cole, 1982; Westmoreland, 1986; Shandross, 1996), with the skimmer and third vacuum stage having been removed.

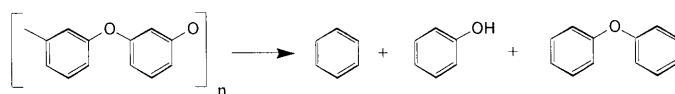


Figure 2.2 Diffusion pump oil contaminants.

The flame gases were finally frozen upon impacting the “cold trap.” The trap, shown in Figures 2.1 and 2.3, was fabricated from 1/16” stainless steel sheets into two concentric cones, with the outside one opened to let

the gases in. This configuration satisfied numerous conditions. The opening where the gases entered had the same area as the opening where any non-condensed gases exited, preventing a pressure build-up within the trap. The opening was also large enough to let most of the sampled gases in. Two surfaces allowed for condensing of any molecules that were reflected off the first impact point. Finally, the trap could be removed from the system and the surfaces easily washed into a sample jar.

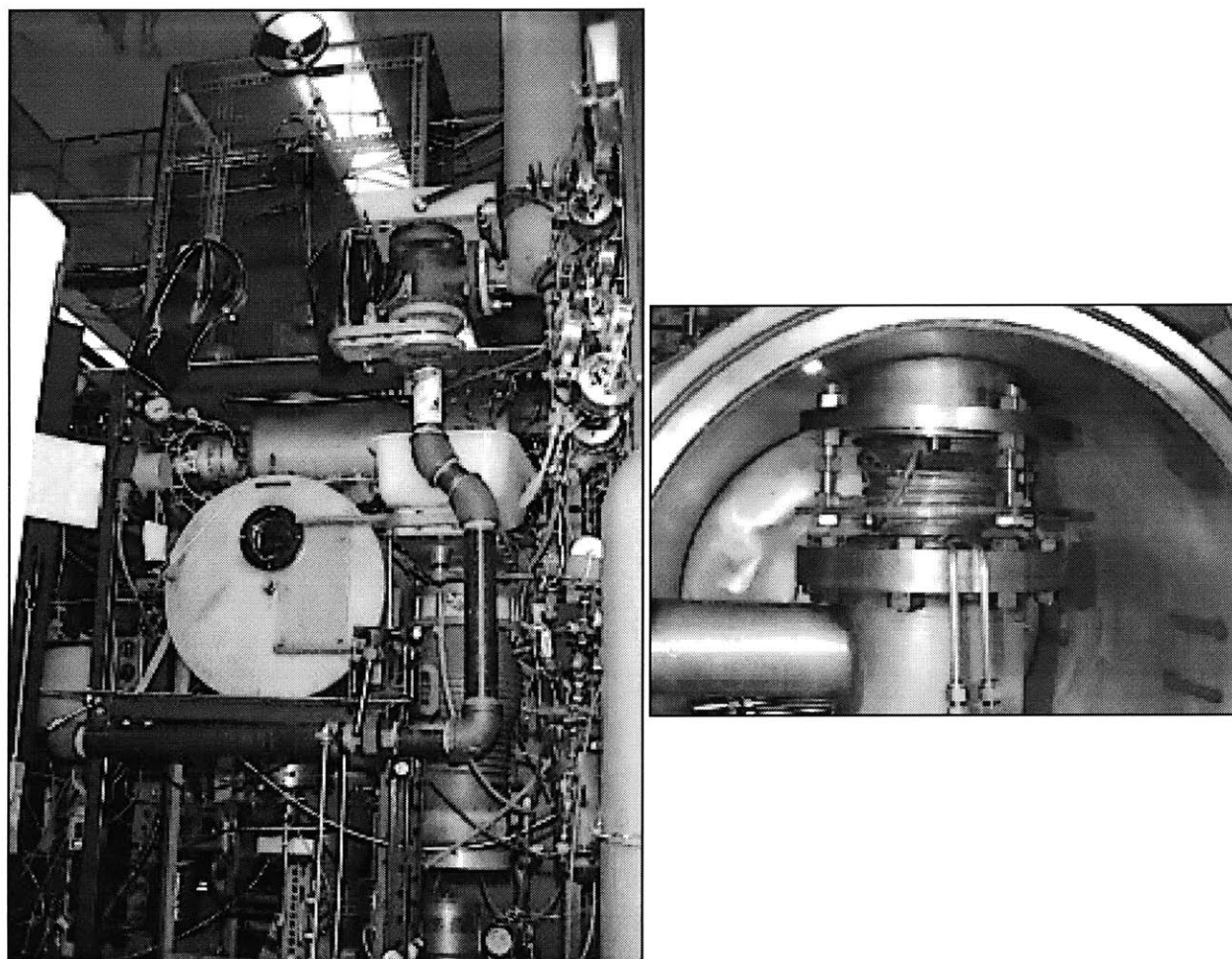


Figure 2.3 Molecular beam/radical scavenging system and cold trap.

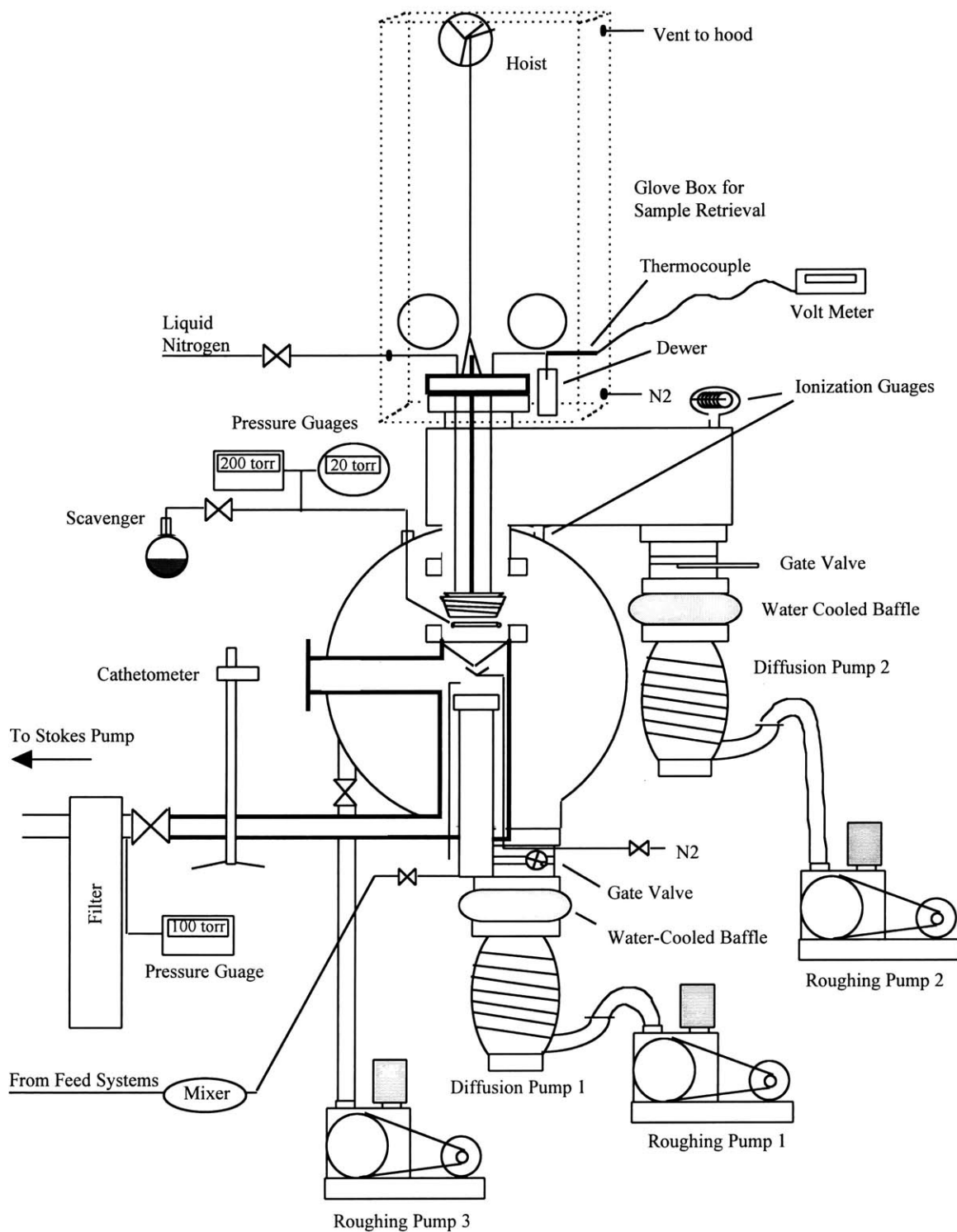


Figure 2.4 Molecular beam/radical scavenging system schematic.

The trap was cooled by liquid nitrogen passing through copper coils welded to the sides and top of the trap. The liquid nitrogen flow rate was controlled so that a small amount exited the system still in liquid form, ensuring that the trap was held at liquid nitrogen temperature, -196 °C. At this temperature, all but the lightest flame gases (such as H₂, CO, O₂, and small radicals) condensed.

Scavenger was added through a 1/4-in. tube formed in a circle and perforated with 14 equally spaced 0.5 mm holes at a 45° angle upward from the center (see Figure 2.1). This *scavenger feed doughnut* evenly distributed the scavenger across the surfaces of the cold trap, while allowing the core of the sampled gases to reach the cold trap unhindered. The scavenger, originally in liquid form, was vaporized at room temperature by exposing it to the vacuum system through the feed doughnut. The pressure in the doughnut was measured by a gauge using piezoresistive pressure sensors. Critical flow was maintained across the holes of the feed doughnut, so the flow could be calibrated and controlled by the upstream pressure. The flow of scavenger was set at 3×10^{18} molecules per second, compared to the total flow of flame gases through the probe of approximately 2×10^{19} molecules per second. Hausmann et al. (1992) showed that increasing the flow beyond this rate did not affect the scavenging reaction, so it is believed that nearly all of the flame radicals reacted only with the scavenger molecules.

2.1.3 GAS AND LIQUID FUEL DELIVERY

Fuel, oxidant, and diluent gases were fed into a mixing chamber (a steel container filled with steel wool), then to the burner. The gas and benzene feed systems are shown in Figure 2.5. Flows of cylinder gases were controlled by adjusting the upstream pressures at critical flow orifices, since critical flow was dependent only on the upstream pressure and temperature:

$$m = CAP \left[\frac{\gamma M}{RT} \left(\frac{2}{\gamma + 1} \right)^{(\gamma+1)/(\gamma-1)} \right]^{0.5} \quad (\text{Eqn. 2.1})$$

where m =mass flow rate, C =flow coefficient, A =orifice area, P =upstream pressure, R =gas constant, M =molecular weight, T =temperature (K), $\gamma=C_p/C_v$, and C_p and C_v are heat capacities at constant pressure and constant volume respectively.

Critical orifices were made from watch jewels drilled with holes of diameter 0.040 cm for acetylene, 0.038 cm for oxygen, and 0.032 cm for argon. Oxygen and argon pressures were monitored by mercury-filled manometers backed by a reference vacuum of 0.5 torr. Acetylene pressure was monitored by a digital pressure gauge (Meriam Instrument Series 2000, 1500 torr absolute). Upstream pressures for all gases were maintained around 1100 torr, while the downstream pressure was near 100 torr.

Since critical flow was not dependent on the downstream pressure, flows were calibrated by measuring the pressure change (via an MKS Baritron 170 capacitance transducer, 100 torr) in an evacuated 17.65 liter tank placed downstream of the critical orifices. The flow rates for a range of upstream pressure settings were calculated from the pressure rises via the ideal gas equation. Flows were corrected for temperature differences using a thermometer located near the cylinder regulators. The accuracies of the measured gas flows were estimated at $\pm 0.5\%$ for oxygen and $\pm 0.4\%$ for argon.

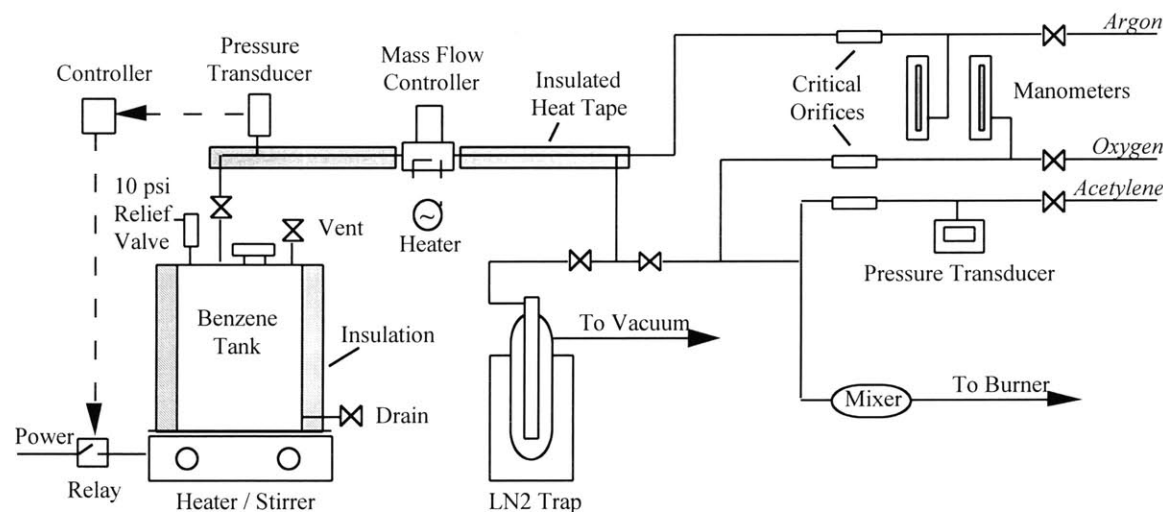


Figure 2.5 Gas feeds and benzene vaporizer.

Benzene, housed in a 12-liter stainless steel tank, was vaporized using a hot plate with a magnetic stirrer. Pressure in the tank was held within 250-310 millibar with a pressure transducer/controller (Omega PX205/CN76000) that controlled power to the hot plate via a relay, which kept the liquid benzene temperature relatively constant in order to help maintain a steady benzene flow. The flow rate of the benzene vapor was controlled by a mass flow controller (Tylan General VC-4900VRH, 0.5 SLPM), which was heated internally to

80°C to keep benzene from condensing within. The line between the tank and the point where argon was added as diluent was wound with heat tape and maintained at 80°C. When not being routed through the burner, the benzene vapor was condensed in a vacuum trap filled with liquid nitrogen (LN₂).

The mass flow controller was calibrated by collecting the metered benzene in the evacuated LN₂ trap over a period of time. The LN₂ trap was isolated from the downstream vacuum system to assure that all of the benzene condensed in the trap. The condensation rate was high enough to accommodate the flow, as no pressure rise was seen upstream of the mass flow controller. The trap was weighed before insertion into liquid nitrogen, then after 30 min. to 2 hr., the trap was removed and heated by a heat gun to melt most of the benzene collected within and water that had frozen to the outside of the trap. Care was taken to assure that benzene loss by evaporation was minimal. Finally the trap, containing 40-60 g benzene, was weighed with a scale accurate to 0.01 g. The accuracy of the benzene flow rate was estimated at ±0.5%.

2.2 Sampling Procedure

The cold trap was removed between experiments, scrubbed with a DCM-soaked clean-room wiper (Texwipe Alphasorb 10), rinsed with clean DCM, then inserted into the vacuum chamber. The trap fit into a PVC ring, which held it at a consistent position. The inside of the probe and the scavenger feed doughnut were also wiped with a DCM-soaked cloth to remove any PAH that had deposited.

The vacuum chamber was sealed and the system was evacuated (see Appendix C for a more detailed description of the sampling procedure). The burner pressure was set to 20 torr by an air leak valve, the burner chamber was purged by a stream of gaseous dry nitrogen, and the distance between the burner and probe was set, as the liquid nitrogen feed valve was opened. After approximately 6 min., the cold trap temperature reached less than 200 K, and the scavenger feed was begun. After 7 min. and a cold trap temperature of less than 150 K, a lean acetylene/oxygen flame ($\phi < 1.0$) was ignited. Benzene was slowly added to the flame as the acetylene flow was decreased, the process lasting about 10 seconds. As the gas and fuel flows and burner pressure were quickly adjusted to the appropriate values, the diffusion pump gate valves were opened, lowering the vacuum chamber pressure from 1×10^{-2} torr to approximately 3×10^{-4} torr.

The cold trap was maintained at liquid nitrogen temperature (77 K), as sampling of the flame continued for 45 min. Then the flame was extinguished, the system was brought to atmospheric pressure by adding desiccated nitrogen gas, and the cold trap was raised into a sealed glove box (Figure 2.6) and placed over a glass jar, shielded from light by aluminum foil. The liquid nitrogen flow was halted and the trap was allowed to warm. Much of the warmed scavenger and flame compounds dripped from the trap into the jar, which contained a small amount of DCM so that the compounds would go immediately into solution, keeping evaporation and precipitation of flame compounds to a minimum. After 30 min., the trap was rinsed with DCM in order to collect the remaining substances adhered to the trap.

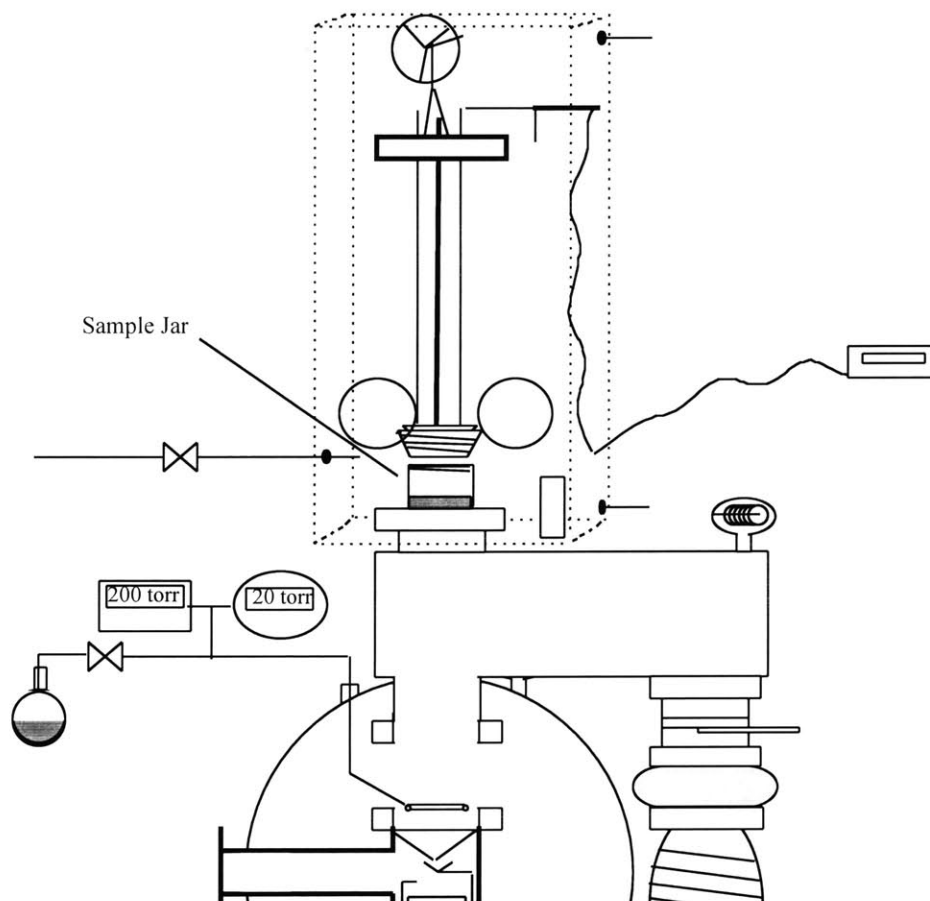


Figure 2.6 Sample retrieval.

2.3 Flame Conditions

Flame conditions, shown in Table 2.1 were chosen so that the data could be compared with literature values. The fuel equivalence ratio, ϕ , is defined by Eqn. 2.2.

$$\phi = \frac{\left(\frac{[\text{fuel}]}{[\text{oxidant}]}\right)_{\text{actual}}}{\left(\frac{[\text{fuel}]}{[\text{oxidant}]}\right)_{\text{stoich}}} \quad (\text{Eqn. 2.2})$$

At $\phi=1.0$, the flame is stoichiometric, and all of the fuel and oxygen are converted to CO_2 and H_2O . The $\phi=1.8$ flame is just below the sooting limit of $\phi=1.9$ (Bittner, 1981) and is one of the most referenced flames for comparing model calculations to flame data. The $\phi=2.0$ flame is slightly sooting and has been studied by more than one researcher.

Table 2.1 Flame Conditions.
(percentages are mole fractions)

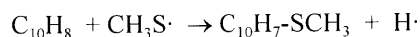
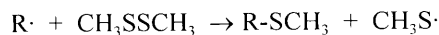
	$\phi=1.8$	$\phi=2.0$
Benzene	13.5%	14.7%
Oxygen	56.5%	55.3%
Argon	30.0%	30.0%
Pressure	20 torr	20 torr
Cold gas velocity	50 cm/s	50 cm/s
Studied by	Bittner (1981) Hausmann, et al. (1992) ^a	Bittner (1981) McKinnon (1989)

^awith the same pressure, velocity, and ϕ , but with no argon

2.4 Scavenger Selection

Initial attempts at studying flame radicals were made using dibromomethane (CH_2Br_2) as a scavenging compound. After this proved unsuccessful (see Appendix A), the scavenger was replaced with dimethyl disulfide (DMDS), which had already been demonstrated as an adequate scavenger by Schottler and Homann (1987), and is discussed in Chapter 1. The following sample analysis methods and results pertain only to the experiments in which DMDS was used.

One may question whether side reactions take place with the methylthio radicals that may lead to analytical artifacts. For instance, a scavenging reaction could produce methylthio radicals, which could theoretically form methylthionaphthalene by the displacement of a hydrogen from naphthalene:



or a similar reaction that would lead to an inaccurate measurement of the naphthyl radical. To determine if these types of hydrogen abstraction reactions occur, perdeuterated naphthalene (C_{10}D_8) was mixed with the scavenger and fed to the cold trap while sampling a flame as described earlier. Though large amounts of C_{10}D_8 were found in the resulting sample solution (3 times more than naphthalene), no $\text{C}_{10}\text{D}_7\text{SCH}_3$ was found, even though the concentration of methylthionaphthalene was around 2% of the concentration of naphthalene. Therefore, PAH hydrogen displacement reactions are believed not to be caused by methylthio radicals, which agrees with the conclusions reached in thermodynamic calculations by Hausmann and Homann (1995).

2.5 Sample Analysis

The volume of the collected sample, including the solvent, totaled approximately 40 ml. To this was added an internal calibration standard: 50-100 μl of a prepared solution of perdeuterated PAH, including styrene (C_8D_8), naphthalene (C_{10}D_8), acenaphthene ($\text{C}_{12}\text{D}_{10}$), anthracene ($\text{C}_{14}\text{D}_{10}$), and pyrene ($\text{C}_{16}\text{D}_{10}$). The addition of the internal standard allowed the total amount of each compound in solution to be determined without knowing the sample volume or injection volume. One microliter of this solution was injected into a gas chromatograph (HP 5890 Series II Plus) with a mass selective detector (HP 5972). The column specifications and temperature program for the GC/MS are shown in Table 2.2. Then high purity nitrogen was blown over the sample, evaporating some of the DCM, until the sample volume reached approximately 3 ml. Another 1 μl injection was made, and the sample was further concentrated under nitrogen to a volume of 0.1 to 0.2 ml. At this point, all of the DCM and much of the DMDS from the solution had evaporated, and a final 1 μl injection was made.

Table 2.2 GC/MS Specifications.

Column Type:	HP50+ (50% cross-linked phenyl-methyl-silicone) capillary column
Column Dimensions:	30m length, 0.25 mm I.D.
Carrier Gas Flow Rate:	1 ml/min (Helium)
Injector Temperature:	250° C
Detector Temperature:	280° C
Oven Temperature Program:	50° C for 1.5 min., then increase 8° C per min to 310° C and hold for 5 min.

Separately, a standard solution containing 34 PAH as well as the internal standard was prepared in 5 different dilutions and injected into the GC/MS in triplicate. The molecular ion for each compound was extracted from the chromatogram, and the resulting peak was integrated. A calibration curve was constructed for each compound, relating peak area to concentration. The calibration curves were nearly linear in many cases, but appeared quadratic in others. The same integration process was applied to each of the sample injections, and the calibration curves were utilized to provide sample concentrations of each of the compounds that were also present in the standard. Concentrations for some compounds that were not in the standard were estimated by calculating the following *relative response factor* between each compound and a PAH for which a calibration curve was fit, where:

$$\text{Relative Response Factor} = \frac{\text{Concentration of Species A} / \text{Peak Area of Species A}}{\text{Concentration of Species B} / \text{Peak Area of Species B}} \quad (\text{Eqn. 2.3})$$

Relative response factors could be determined by a single injection of two compounds, although it was considered a less accurate method, because many of the calibration curves were not linear. The concentrations of the compounds for which quantitative standards were not available were estimated by assuming that the calibration curves (again, by measuring the molecular ion only) were the same as those for a compound of similar structure. The last method was considered the poorest because it is often difficult to estimate response factors without measuring them. The methods in which each of the PAH studied was identified and quantitated are outlined in Table 2.3 as well as estimates of the uncertainties in the calculated mole fractions for each species.

Identifications of PAH were made by comparing both the retention times and the mass fragmentation patterns of the sample peaks and those of the known compounds. However, in a few cases, structures were deduced from similarities to other compounds. These cases are detailed individually in Chapter 3. The ability to extract individual fragment ions from the chromatogram was critical in identifying several compounds, as the total ion count was often several orders of magnitude higher than the ion counts of the molecules of interest.

Table 2.3 Identification and Quantitation Methods for each Compound Studied.

Name	MW	Retention Time (min)	Identification and Quantitation ^a	Uncertainty Factor ^b
Phenol	94	8.0	A,F,1,J	1.2
Phenylacetylene	102	5.6	A,F,1,J	1.2
Styrene	104	5.7	A,F,1,J	1.3
Indene	116	9.1	A,F,1,J	1.2
Methylthiobenzene	124	10.3	A,F,1,K	1.2
Naphthalene	128	12.2	A,F,1,K	1.2
Benzylmethylsulfide	138	11.8	A,F,2,K	1.4
1-Methylnaphthalene	142	14.5	A,F,2,K	1.3
1-Naphthol	144	18.5	C,H (2-Naphthol),2,L	1.5
2-Naphthol	144	18.6	A,G (Phenol),2,L	1.4
2-Ethynylnaphthalene	152	16.2	A,F,2,L	1.3
1-Ethynylnaphthalene	152	16.3	A,F,2,L	1.3
Biphenylene	152	17.0	A,F,2,L	1.4
Acenaphthylene	152	17.3	A,F,1,L	1.2
Biphenyl	154	15.7	A,F,1,L	1.2
2-Vinylnaphthalene	154	16.4	A,F,2,L	1.3
Acenaphthene	154	17.7	A,F,2,L	2.0
Fluorine	166	19.1	A,F,2,L	1.3
Dibenzofuran	168	18.0	A,F,2,L	1.3
1-Acenaphthenone	168	21.3	A,G (Pyrene),2,M	1.4
1-Methylthionaphthalene	174	20.0	C,H (2-Methylthionaphthalene),2,M	1.3
2-Methylthionaphthalene	174	20.2	A,F,2,M	1.3
1-Ethynylacenaphthylene	176	20.5	A,F,2,M	1.3
5-Ethynylacenaphthylene	176	20.7	A,F,2,M	1.3
Phenanthrene	178	22.4	A,F,2,M	1.3
Anthracene	178	22.5	A,H (Phenanthrene),2,M	1.5
9-Fluorenone	180	21.8	A,G (Pyrene),2,M	1.4
Phenalenone	180	24.0	A,G (Pyrene),2,M	1.4
Cyclopenta(def)phenanthrene	190	24.3	A,F,2,M	1.3
A-Methylthioacenaphthylene	198	24.3	A,H (2-Methylthionaphthalene),3,M	1.5
5-Methylthioacenaphthylene	198	24.4	A,H (2-Methylthionaphthalene),3,M	1.7
3-Methylthioacenaphthylene	198	24.6	A,H (2-Methylthionaphthalene),3,M	1.7
1-Methylthioacenaphthylene	198	24.7	A,H (2-Methylthionaphthalene),3,M	1.7
Fluoranthene	202	26.1	A,F,2,N	1.3
Acephenanthrylene	202	26.5	A,H (Pyrene),2,N	1.3
Aceanthrylene	202	26.8	A,H (Pyrene),2,N	1.3
Pyrene	202	27.0	A,F,2,N	1.3
1-Phenylnaphthalene	204	23.3	A,F,3,N	1.3
2-Phenylnaphthalene	204	24.7	A,F,3,N	1.3
Cyclopenta(cd)pyrene	226	30.8	A,F,2,N	1.3
Benzo(ghi)fluoranthene	226	30.0	B,H (Cyclopenta(cd)pyrene),2,N	1.3
Benz(a)anthracene	228	30.4	A,G (Pyrene),3,N	1.5
Chrysene	228	30.7	A,G (Pyrene),3,N	1.5
Benzanthrone	230	31.5	A,G (Pyrene),3,N	1.5

Table 2.3 Cont.

Name	MW	Retention Time (min)	Identification and Quantitation ^a	Uncertainty Factor ^b
Methylthiofluoranthene (total)	248	31.6-31.9	A,C,H (2-Methylthionaphthalene),3,N	2.0
A-Methylthiopyrene	248	32.4	C,H (2-Methylthionaphthalene),3,N	1.7
1-Methylthiopyrene	248	32.5	A,H (2-Methylthionaphthalene),3,N	1.7
C-Methylthiopyrene	248	32.6	C,H (2-Methylthionaphthalene),3,N	1.7
Benzo(b)fluoranthene	252	33.6	A,G (Pyrene),3,N	1.5
Benzo(k)fluoranthene	252	33.7	A,G (Pyrene),3,N	1.5
Benzo(a)pyrene	252	34.7	A,G (Pyrene),3,N	1.5
Benzo(a)pyrene	252	34.8	A,G (Pyrene),3,N	1.5
Benzo(a)pyrenone	254	35.3	A,G (Pyrene),3,N	1.5
Indeno(1,2,3-cd)pyrene	276	38.7	A,G (Pyrene),3,N	1.5
Benzo(g,h,i)perylene	276	40.3	A,G (Pyrene),3,N	1.5

^aIdentification: (A) Match of retention time and fragmentation pattern with authentic standard, (B) High-probability library match from fragmentation pattern, (C) Estimated from fragmentation pattern. Quantitation: (F) Standard curve for compound injected into GC/MS (G) Relative response with another compound (named), (H) Assumed same response as another compound (named). Injection: (1) Injection 1, (2) Injection 2, (3) Injection 3. Internal Standard: (J) Styrene-d8 (C₈D₈), (K) Naphthalene-d8 (C₁₀D₈), (L) Acenaphthene-d10 (C₁₂D₁₀), (M) Anthracene-d12 (C₁₄D₁₀), (N) Pyrene-d10 (C₂₀D₁₀).

^bUncertainty range: $([X]/\delta) < [X] < ([X] \times \delta)$, where $[X]$ = species mole fraction and δ = uncertainty factor

2.5.1 CALCULATION OF MOLE FRACTIONS

The mole fraction of each flame compound of interest (x_i) was calculated by:

$$x_i = \frac{(C_i)(Cd_{i,a})(Vd)}{(Cd_{i,b})(\epsilon)(MW_i)(F_h)(t)} \times 10^{-9} \quad (\text{Eqn. 2.4})$$

where C_i = Concentration of species i in the sample solution calculated from an injection into the GC/MS ($\mu\text{g/ml}$), $Cd_{i,a}$ = Concentration of a perdeuterated PAH in the prepared internal standard ($\mu\text{g/ml}$), Vd = Volume of the internal standard added to the sample (μl), $Cd_{i,b}$ = Concentration of the same perdeuterated PAH calculated from the GC/MS injection of the sample solution ($\mu\text{g/ml}$), MW_i = Molecular weight of species i (g/mol), ϵ = Collection efficiency of the cold trap (fraction), F_h = Flow through the probe at the height above burner studied (mol/min), and t = Sampling time (min). The perdeuterated PAH used in this formula was the one which had a retention time on the GC closest to that of the compound of interest. It is important to note that no additional variables, such as injection volume, were needed due to the use of the internal standard.

The flow through the probe was determined experimentally by measuring the rate of pressure increase in the isolated vacuum chamber, downstream of the probe. This method did not rely on any critical flow calculations

that require estimation of the temperature at which critical flow is established, as temperature is difficult to estimate at the probe orifice given the high temperatures of the flame and the cold temperature of the probe. Gases could be fed to the vacuum chamber (the volume which held the cold trap) through two different orifices: the probe, through which gases passed from the burner chamber, and a calibrated critical orifice, through which argon was fed at a known flow rate. The critical orifice could be isolated from the vacuum chamber, but the probe orifice could not. The vacuum chamber was first pumped to a few millitorr, and the pressure in the burner chamber was set to 2.0 torr. The chamber was isolated from the pump, and the pressure rise in the chamber $(dP/dt)_1$ due only to the flow of gases through the probe $(dn/dt)_{\text{probe}}$ into the chamber was measured by a Baritron capacitance manometer (0-1 torr) over a period of 2 min, so that:

$$(dP/dt)_1 = (RT/V) (dn/dt)_{\text{probe}} \quad (\text{Eqn. 2.5})$$

where R=the gas constant, T=temperature, and V=chamber volume. The temperature of the gas within the chamber was measured with a thermocouple. The chamber was then evacuated again and isolated from the pump, the calibrated orifice flow $(dn/dt)_{\text{c.o.}}$ was established, and the pressure rise in the chamber $(dP/dt)_2$ was measured so that:

$$(dP/dt)_2 = (RT/V) [(dn/dt)_{\text{probe}} + (dn/dt)_{\text{c.o.}}] \quad (\text{Eqn. 2.6})$$

Then the pressure rise due only to the calibrated flow was calculated by subtracting Eqn. 2.5 from Eqn. 2.6:

$$(dP/dt)_2 - (dP/dt)_1 = (RT/V) (dn/dt)_{\text{c.o.}} \quad (\text{Eqn. 2.7})$$

Since $(dn/dt)_{\text{c.o.}}$ had been measured by the techniques described in Section 2.1.3, the chamber volume (V) was calculated from Eqn. 2.7. The calibrated flow orifice was isolated from the chamber, and the pressure rise in the chamber $(dP/dt)_3$ was measured while sampling the benzene/oxygen/argon $\phi=1.8$ flame by the probe at various heights above burner. The molar flow rate through the probe (F_h) was then calculated by Eqn. 2.8:

$$F_h = (V/RT) (dP/dt)_3 \quad (\text{Eqn. 2.8})$$

The F_h values measured in flame conditions by this technique match closely the flows that are estimated by critical flow theory applied to the temperatures and pressure of the flame.

To calculate the cold trap collection efficiency, ϵ , a flow of argon and 3% benzene was sent through the burner, and the sampling system was operated as if sampling a flame. After 20 minutes, the cold trap was removed and DCM was immediately sprayed on the surfaces to minimize benzene evaporation upon warming of the trap. After warming, the trap was rinsed with DCM, toluene was added as an internal standard, and the resulting solution

was injected on the GC/MS. Standards of benzene and toluene in DCM were used to calculate the amount of benzene that had been collected. From this and a measure of the flow through the probe performed as above, the collection efficiency of the cold trap was calculated to be $64\% \pm 5\%$. However, it was thought that larger compounds might have higher collection efficiencies than benzene. To explore this possibility, a sooting flame was sampled with the cold trap replaced by a large sheet of perforated paper. After 20 min., the paper held a circular pattern of the soot particles, 60% to 80% of which would have impacted the cold trap had it been there. Since the observed collection efficiency for benzene is within this range, it is considered to be within the existing experimental error to assume that all of the compounds of interest (each larger than benzene) had the same collection efficiency as benzene.

2.5.2 PROBLEMS ASSOCIATED WITH CONCENTRATING SAMPLE SOLUTIONS

The first injection of each sample solution into the GC/MS (injection 1) was unconcentrated so only a few aromatics were in high enough concentration for reliable quantitation, producing a total peak area of at least 500,000 counts. Injection 2 was concentrated under nitrogen so that the remaining aromatics and a few of the scavenged radicals could be quantitated. However, concentrating the sample had a significant effect on some of the concentration profiles, the greatest being on those that had a significantly different volatility than the internal standards to which they were compared. Figure 2.7 shows comparisons of flame mole fractions of compounds calculated from each of the first two injections. Styrene-d8, the internal standard for these two compounds, had a retention time close to that of phenylacetylene but significantly less than that of phenol. As a result, the data for phenylacetylene are not as affected as those for phenol when the samples are concentrated. Where possible, injection 1 was used for the quantitation of the compounds.

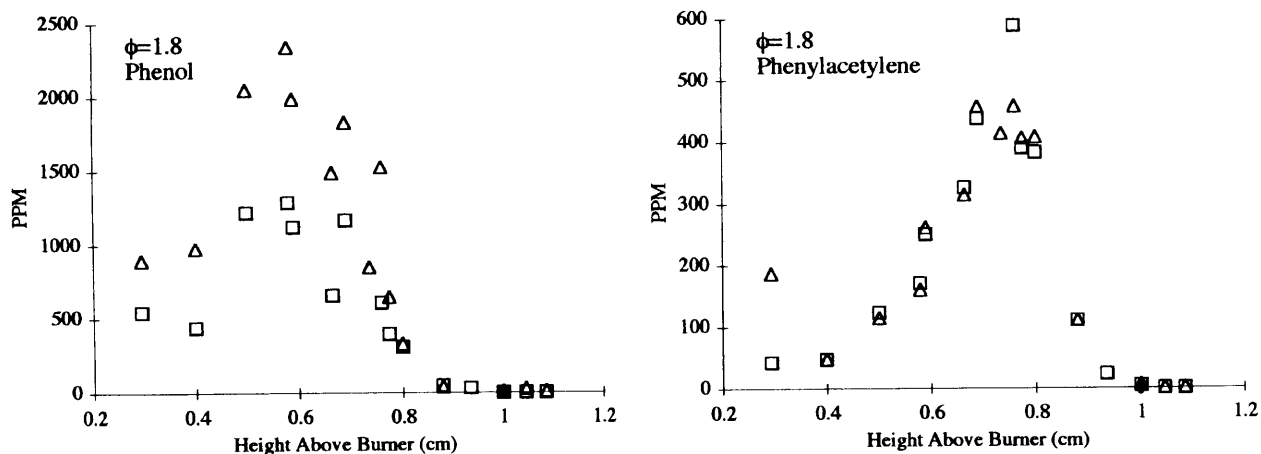


Figure 2.7 Mole fractions of phenylacetylene and phenol calculated from injections 1 (□) and 2 (Δ).

Similar problems were seen as the samples were further concentrated for injection 3. Only a few of the compounds were quantitated at both injections 2 and 3, since one of the requirements for quantitation was well defined GC peaks. Most, including fluorine and benzo[ghi]fluoranthene, showed calculated flame concentration decreases up to 50%, which is similar to those of other compounds analyzed with injections 1 and 2 (Figure 2.8). But in this case, the problem probably stems from a reduction in solubility as the solution concentration increases and the solvent changes from mostly DCM to DMDS. Consequentially, compounds that could not be quantitated with injection 1 were quantitated with injection 2 if possible.

Cyclopenta[def]phenanthrene and cyclopenta[cd]pyrene exhibited a drop in the calculated concentrations of up to 90% upon concentrating (Figure 2.8). This is a particularly important observation because many other compounds could not even be identified, much less quantified using either of injections 1 or 2. Therefore it is possible that the flame concentrations calculated for some of the studied compounds, including the acenaphthylene and pyrene radicals and all PAH larger than cyclopenta[cd]pyrene could be low by up to one order of magnitude. However, the large PAH appeared not to show this behavior, as is discussed in Chapter 3. Also, it is unlikely that the methylthio compounds would precipitate as easily as PAH of the same molecular weight, because the polar methylthio groups should allow them to be more soluble in the mostly-DMDS solvent.

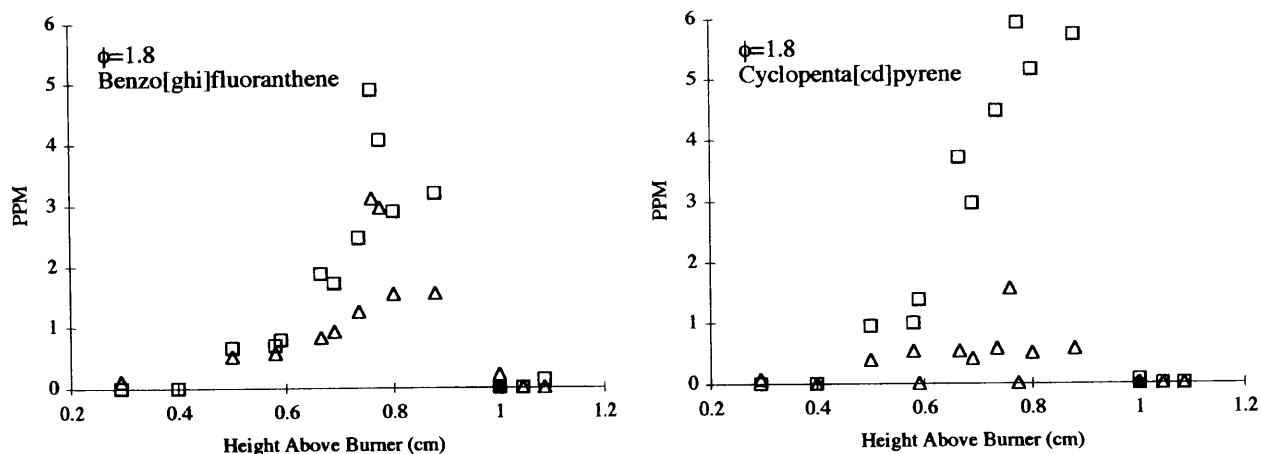


Figure 2.8 Mole fractions of benzo[ghi]fluoranthene and cyclopenta[cd]pyrene calculated from injections 2 (□) and 3 (Δ).

In summary, The data used for calculation of the mole fraction profiles for all of the compounds were taken from the injections that gave an adequate response for quantitation with the least amount of sample concentration. In general, the mole fractions obtained from less concentrated samples are considered more reliable. Unfortunately the errors in a few of the calculated compound concentrations may be more significant than reported, but they can not be quantified.

2.5.3 EFFECT OF WASHING THE TRAP

A sample collected in the cold trap could be divided into two parts: the *drippings*, which fell into the sample jar as the trap warmed, and the *washings*, the remaining sample removed from the trap by rinsing with DCM. Washing of the trap, which was not done by Hausmann and Homann (1995), was performed because it was believed that heavier PAH may adhere to the trap preferentially. The washings and drippings of a single sample were analyzed by GC/MS. However, the samples were too dilute to analyze without concentrating, so they were diluted to the same volume, then concentrated to approximately 6 ml each. The percentages of some select compounds in the washings and the amount that the calculated mole fractions are increased by adding the washings to the sample solution are shown in Table 2.4. The compounds are sorted by increasing volatilities.

Table 2.4 PAH in Cold Trap Drippings and Washings.

Compound	MW	% in Washings	Increases Mole Fraction by
Phenylacetylene	102	27%	38%
Phenol	94	32%	48%
Indene	116	29%	41%
Naphthalene	128	35%	53%
Acenaphthylene	152	39%	65%
Pyrene	202	38%	60%

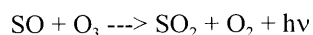
Obviously, washing the trap has a significant impact on the amount of the collected sample that eventually goes into solution. However, the important issue is whether the compounds of interest adhere to the trap more than benzene, for which the trap was calibrated. From Table 2.4 it appears that the larger compounds preferentially stick to the trap, showing the necessity of washing the trap in order to get an accurate measure of flame mole fractions, but it is possible that much of the effect seen is from error stemming from concentrating the sample solutions.

2.5.4 ANALYSIS OF SCAVENGED RADICALS WITH SULFUR CHEMILUMINESCENCE

PAH radical concentrations in the flames were calculated directly by measuring the concentrations of the scavenging products. Four standards of methylthio-aromatics were available in *quantitative amounts*: methylthiobenzene, benzylmethylsulfide, p-tolyl sulfide, and 2-methylthionaphthalene, so that direct quantitation by GC/MS was possible for only 4 radicals. To study the remaining scavenged radicals, a sulfur chemiluminescence detector (Sievers model 355 SCD) was employed.

The SCD, a detector for gas chromatography, has been used to detect sulfur compounds with high sensitivity and selectivity. It has been found to produce an approximately equimolar response to sulfur-containing compounds (Tang et al., 1997). The SCD can be used in conjunction with a flame ionization detector (FID), which responds well to hydrocarbons and can be used to match the retention times from the GC/SCD to those of the GC/MS so that the identification ability of the second can be combined with the quantitative ability of the first. In the operation of the SCD, separated compounds first elute from a GC column into the FID, which burns the sample in a hydrogen/air flame. A portion of the FID exhaust is sampled by a small probe, and the gases pass through a furnace to which air and excess hydrogen are added. Presumably, the flame and furnace convert a significant

portion (about 15%) of the sulfur found in the compounds to SO (Burrow and Birks, 1997). The SO is then contacted with ozone, resulting in the following reaction:



where $h\nu$ is light, which is detected by a photomultiplier. As a result, the signal of the detector is linear with respect to the number of sulfur atoms which pass through it, regardless of the nature of the pre-combusted compound.

Therefore once a compound detected by the SCD is identified (with the aid of the GC/MS), it can be quantified by simply comparing the response to the concentration of a known standard. Calibration of the SCD requires only a few sulfur-containing compounds, eliminating the need for quantitative standards for all of the compounds of interest.

It was initially believed that the scavenged radicals from the flame could be individually quantitated by the SCD by injecting the flame samples. But due to the large number of compounds in the flame and the complex possibilities of scavenging reactions, this was impossible. Figure 2.9 shows the SCD output from injection of a flame sample using the DMDS scavenging technique. Only the most prevalent of the scavenged radicals of interest can be extracted from the chromatogram, and even their identities are questionable. Most of the large peaks in Figure 2.9 correspond to compounds like $\text{CH}_3\text{SSSCH}_3$ and $\text{CH}_3\text{SCH}_2\text{SSCH}_3$, which are probably formed by reactions of methylthio radicals (formed as a side product of the scavenging reaction) with DMDS.

Several methylthio compounds were synthesized in order to identify the scavenged flame radicals, but the compounds, which were in solution, had unknown concentrations, so calibration curves could not be constructed for quantitation by GC/MS. But the solutions could be injected into the GC/SCD along with a standard of known concentration, and because of the equimolar response of the SCD, the concentration of the methylthio compound of interest could be determined. Then calibration by GC/MS would be possible. However, when this method was applied, the reproducibility of the SCD was very poor ($\pm 50\%$), so no useful results were obtained. Therefore, the GC/MS response factor for 2-methylthionaphthalene was applied to all methylthio compounds of equal or greater size that were studied. The uncertainty in this assumption was believed to be $\pm 30\%$.

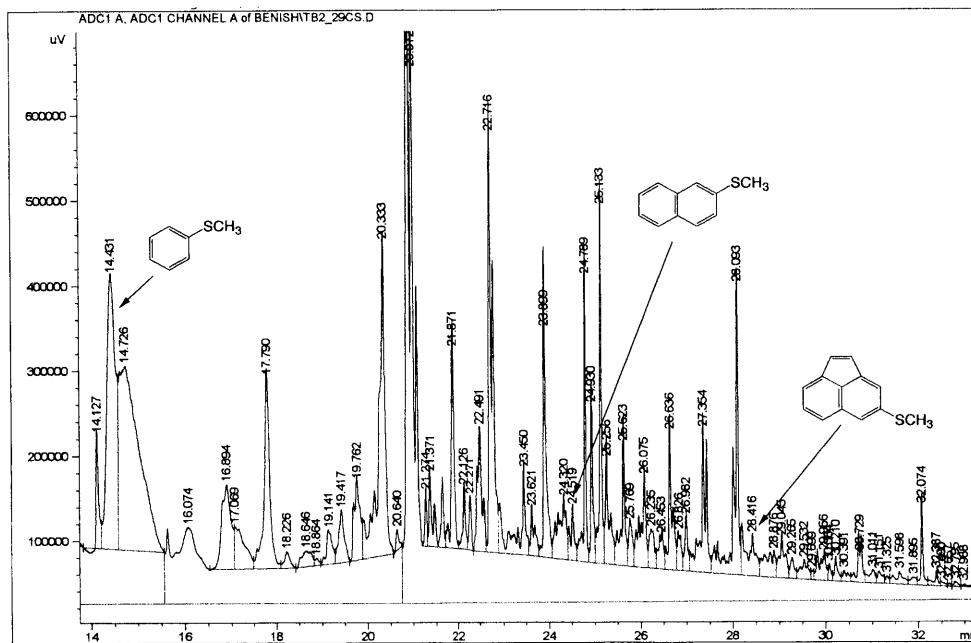


Figure 2.9 GC/SCD chromatogram of a flame sample.

Chapter 3

Results

Mole fractions for 55 compounds (including radicals) were measured in benzene $\phi=1.8$ and $\phi=2.0$ flames as a function of height above burner. They are plotted along with data from the $\phi=1.8$ flame analyzed by on-line mass spectrometry (Bittner and Howard, 1981), the $\phi=2.0$ flame analyzed by collection in a cold trap after sampling with a low-vacuum macroprobe (McKinnon, 1989), and a $\phi=1.8$ flame without argon measured by a similar radical scavenging technique (Hausmann, et al., 1992). Although the last of the three flames is not identical to those studied, it is the closest flame studied previously by radical scavenging, and is therefore presented.

Height above burner was taken to be the distance between the burner surface and the probe orifice and does not reflect the exact position in the flame where the sample was taken because of the acceleration of the sampled molecules to critical flow at the probe tip. Biordi, et al. (1974) and Stepowski, et al. (1981) calculated that the exact sampling point is approximately 2-3 orifice diameters upstream of the probe orifice. This may explain why the compounds sampled by McKinnon with a 1 mm orifice probe peak in concentration a little more than 1 mm beyond those measured in this study using a 0.7 mm orifice probe. However, the $\phi=1.8$ data by Bittner peak slightly beyond those of this study, which is unexpected considering that the same probe orifice size and flame conditions were used. The differences may be due to effects of the probes, though of the same design, which were manufactured years apart.

3.1 Mole Fractions of Stable Aromatics in Flames

3.1.2 SMALL CONDENSED PAH

The small, condensed PAH consist of those molecules having only closed rings up through mass 202 (Figure 3.1). The smallest ring structures typically seen in significant concentration in these flames include cyclopentadiene, benzene, and toluene. None were measured in this study, because the GC program allowed these volatile compounds to purge with the solvent. Bittner (1981) measured them in the $\phi=1.8$ flame, and the concentration profiles for benzene and toluene are presented in Figure 3.2 for later discussion.

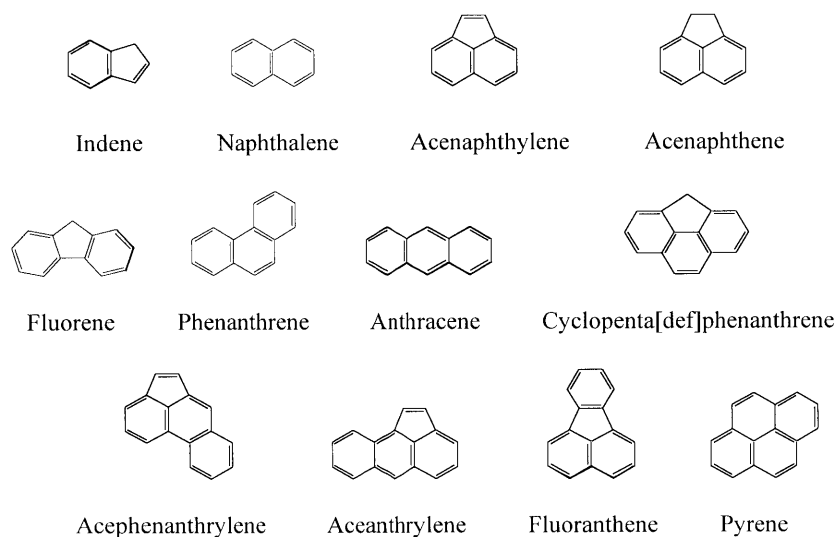


Figure 3.1 Structures of small condensed PAH

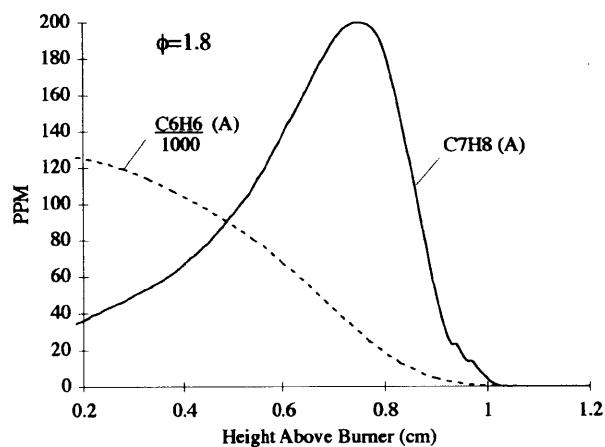


Figure 3.2 Benzene and toluene mole fractions in the $\phi=1.8$ flame. (Bittner and Howard, 1981)

The most prevalent PAH measured in this study were indene, naphthalene, and acenaphthylene, shown in Figure 3.3. In the $\phi=1.8$ flame, each peaked in concentration at approximately 7.5 mm. The naphthalene concentration peak was 3 times that measured by Bittner and Howard (1981) while acenaphthylene was 5 times greater. This suggests that the level of accuracy in the PAH measurements in the MB/MS system was rather poor, and that it decreased with molecular weight. In the $\phi=2.0$ flame, each of the compounds peaked in concentration around 9 mm. The peak indene concentration matched that of McKinnon (1989), but the naphthalene and

acenaphthylene measurements were two to three times higher. In fact, most of the compounds measured in this study appeared to be in significantly higher quantity than measured by either Bittner or McKinnon, though not by a consistent amount (which would have suggested a systematic error in this study). The reasons for these discrepancies have not been fully resolved.

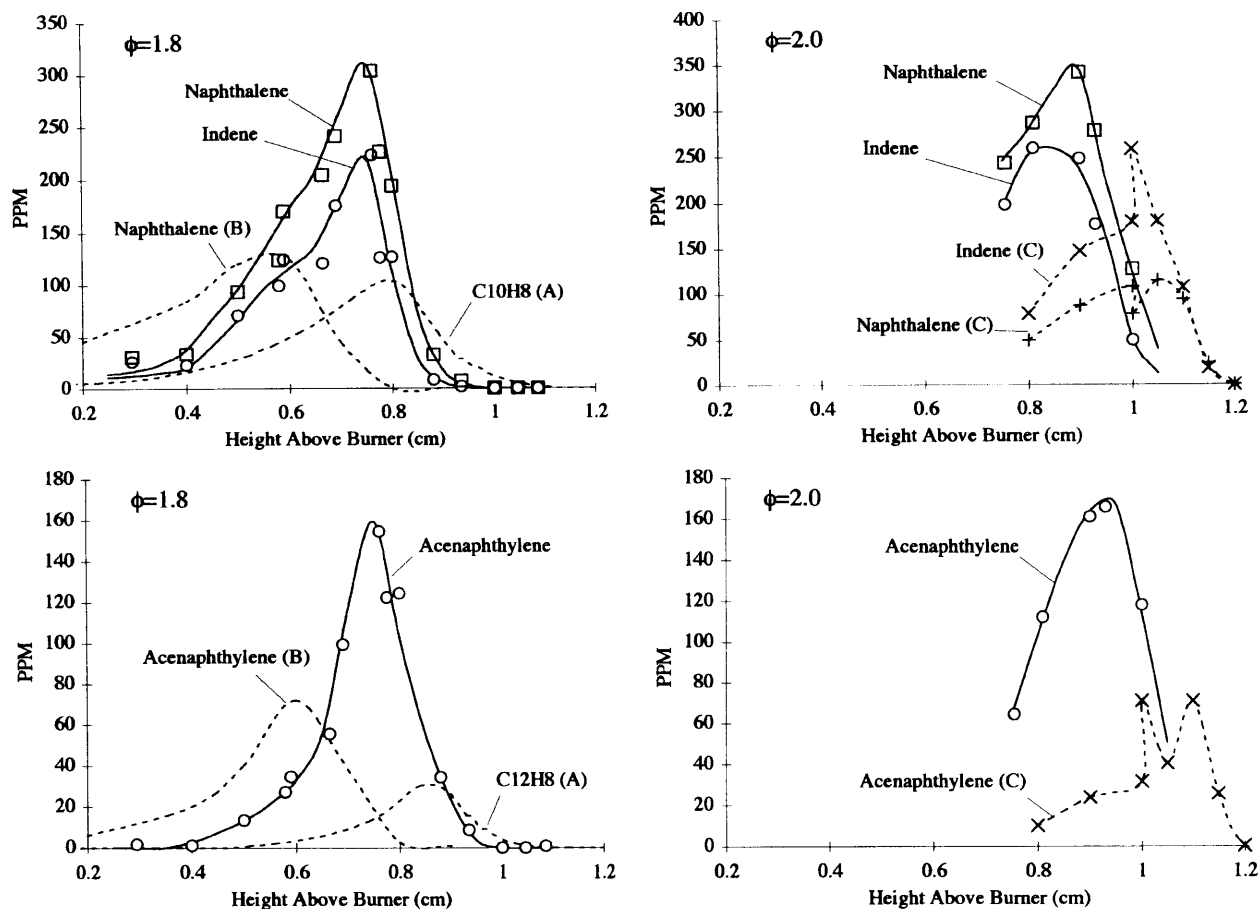


Figure 3.3 Prevalent PAH mole fractions in the $\phi=1.8$ and $\phi=2.0$ flames. (A=Bittner and Howard, 1981, B=Hausmann et al., 1992, C=McKinnon, 1989)

The remaining small condensed PAH measured in the flames are shown in Figure 3.4. Each peaks in concentration at approximately the same height in the flame as the previous compounds. The anthracene concentration is 15-20% of the concentration of its isomer, phenanthrene, which is consistent (relatively) with the measurements by McKinnon (1989), and can be easily explained by the relative stability of the two compounds stemming from their aromatic characters. Acephenanthrylene and Aceanthrylene show the same behavior, which is expected, since they are simply phenanthrene and anthracene with one added 5-membered ring. The other mass

$C_{16}H_{10}$ species, pyrene and fluoranthene are present in significantly higher concentrations. The sum of the $C_{16}H_{10}$ concentrations exceeds that measured by Bittner by a factor of 20. Acenaphthene could not be properly quantitated, but was estimated to peak at approximately 3 ppm in the $\phi=1.8$ flame and 2 ppm in the $\phi=2.0$ flame.

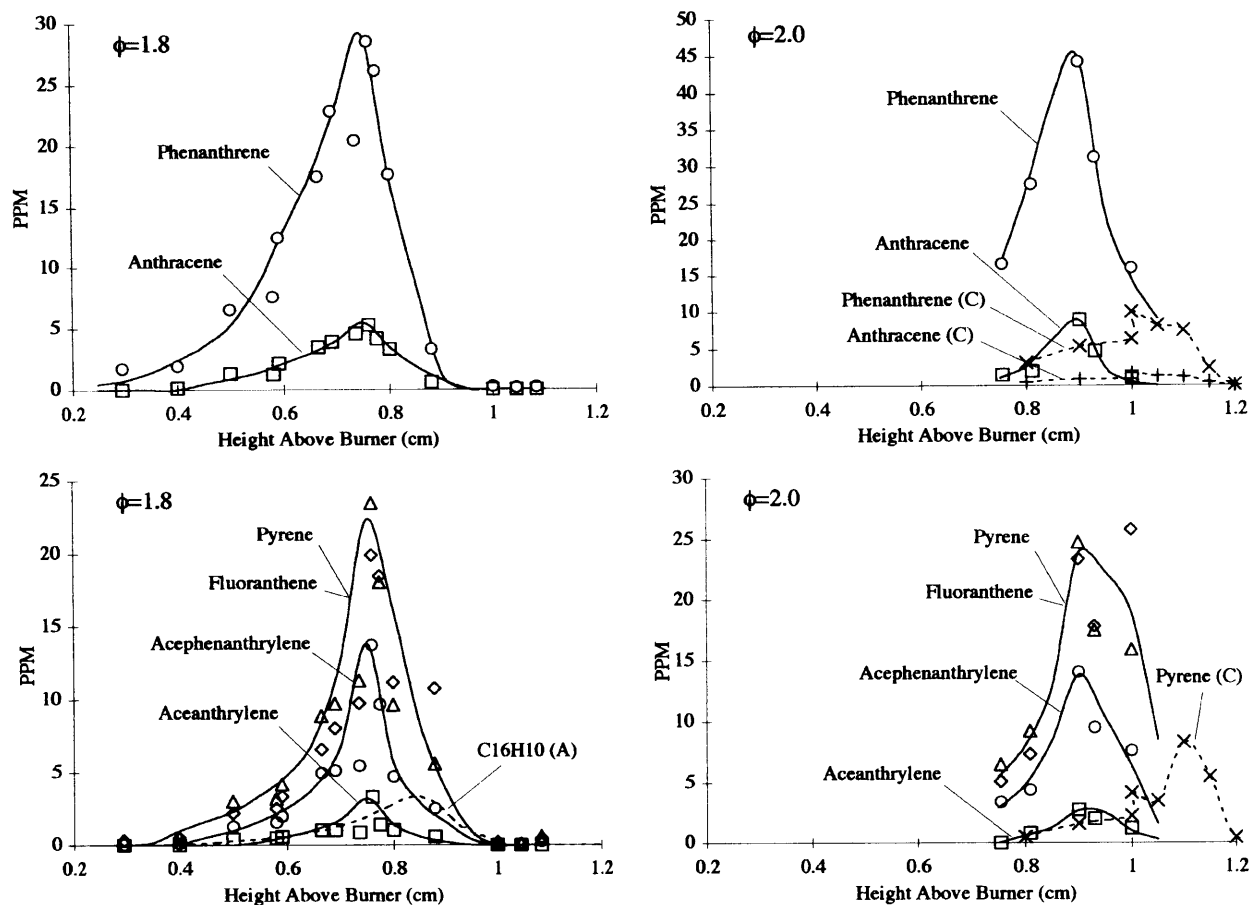


Figure 3.4 Small PAH mole fractions in the $\phi=1.8$ and $\phi=2.0$ flames.
(A=Bittner and Howard, 1981, C=McKinnon, 1989)

3.1.2 SUBSTITUTED AROMATICS

Although the condensed aromatics make up most of the PAH produced in these flames, substituted aromatics (Figure 3.5) are of particular interest as they may provide insights into the mechanisms of PAH growth.

The smallest of the compounds in this class are phenylacetylene and styrene (Figure 3.6), believed to be formed by the addition of acetylene or ethylene to benzene or the phenyl radical. The phenylacetylene concentration is approximately 10 times that of styrene in both of the $\phi=1.8$ and $\phi=2.0$ flames. Phenylacetylene peaks at the same height above burner as the small condensed PAH. Styrene appears to peak significantly earlier,

but there is more scatter in the styrene data. Both of these compare much closer to the Bittner and McKinnon data than any of the other compounds discussed thus far.

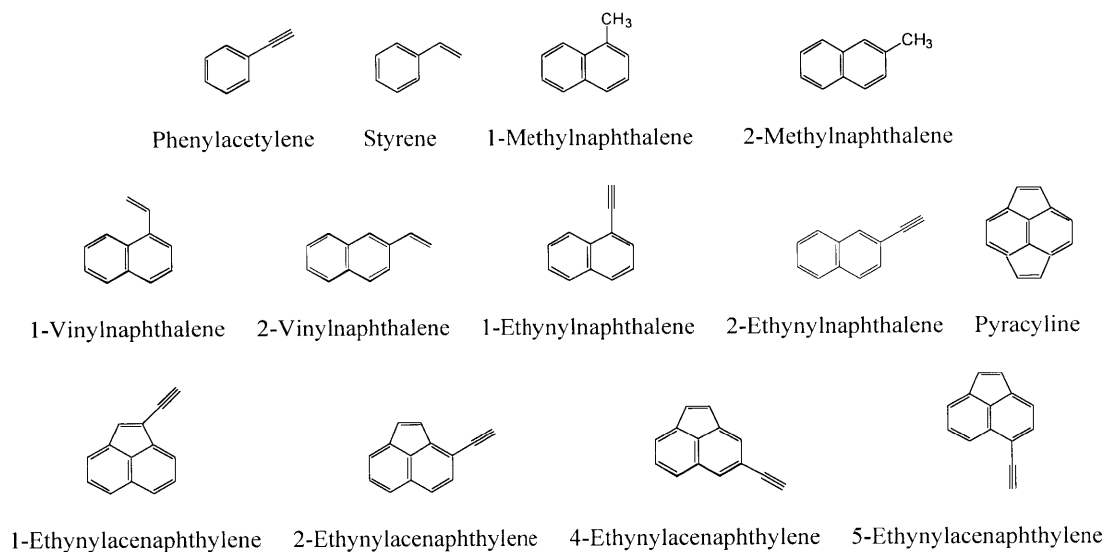


Figure 3.5 Structures of substituted PAH.

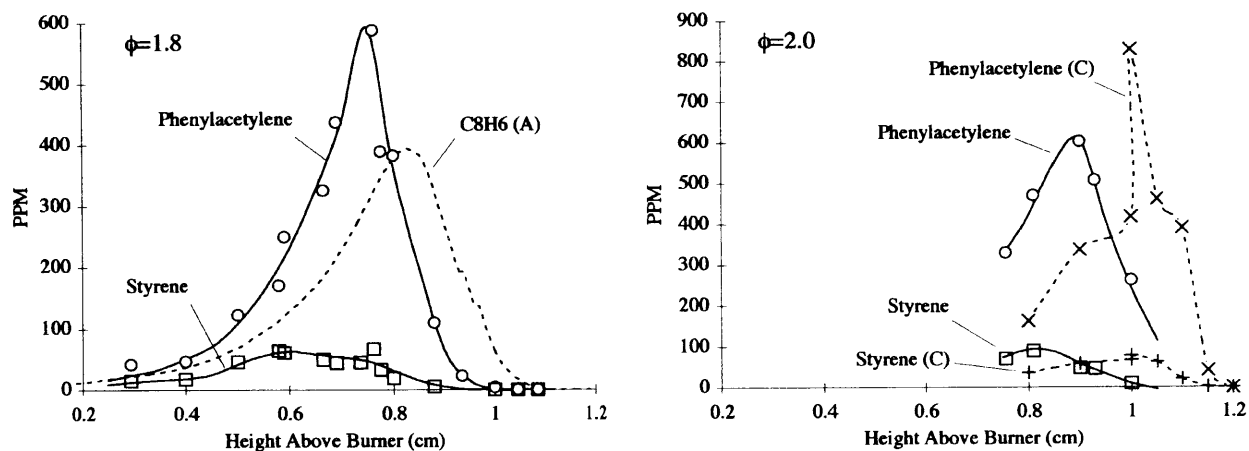


Figure 3.6 Phenylacetylene and styrene mole fractions in the $\phi=1.8$ and $\phi=2.0$ flames. (A=Bittner and Howard, 1981, C=McKinnon, 1989)

Similar compounds can be formed by the addition of small molecules to naphthalene. Reliable quantitation of 2-methylnaphthalene was not possible, because the peak partially co-eluted in the GC with another compound of mass 142, but using the best approximations it's concentration appeared to be 10-20% lower than that of 1-

methylnaphthalene, which is plotted in Figure 3.7. Although 2-vinylnaphthalene was easily detected, the other isomer of vinylnaphthalene was not seen, because either its concentration was below the detection limit (less than 0.1 ppm), or it co-eluted with another compound. The scatter in the methylnaphthalene and vinylnaphthalene data makes location of the peak concentrations difficult.

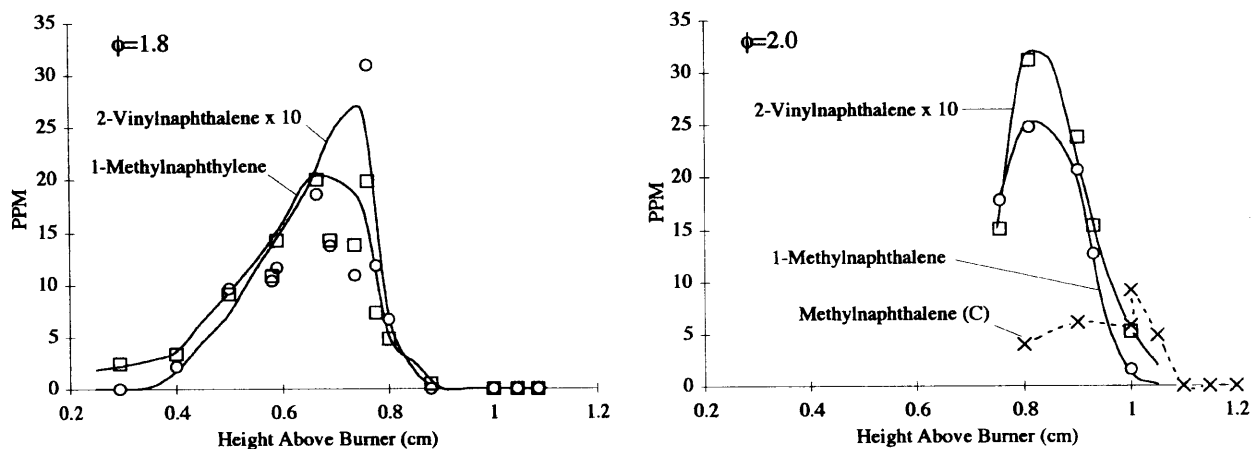


Figure 3.7 1-Methylnaphthalene and 2-vinylnaphthalene mole fractions in the $\phi=1.8$ and $\phi=2.0$ flames. (C=McKinnon, 1989)

Often an HP-5 column (5% phenylmethylsilicone) is used for PAH analysis by GC (McKinnon, 1989, Grieco, 1998), and was used initially in this study. With the HP-5 column, only 2 peaks were seen for the molecular ions of mass 152. One peak matched with a standard of acenaphthylene while the other was believed to be 2-ethynylnaphthalene. No standard was available for ethynylnaphthalene at the beginning of this study, so confirmation could not be made, but it was believed that the identity of the peak was less likely to be 1-ethynylnaphthylene as it could close in the flame to make acenaphthylene, one of the most prevalent PAH in the flames. A. Necula synthesized both isomers of ethynylnaphthalene and it was discovered that they co-elute on the HP-5 column. Upon switching to a more polar HP-50+ column, the two isomers separated well and four peaks of mass 152 were found in the flame samples (see Figure 3.8).

Both isomers of ethynylnaphthalene peak at the same height above burner as the small condensed PAH (including naphthalene and acenaphthylene). The concentration of 2-ethynylnaphthalene is three times higher than 1-ethynylnaphthalene (see Figure 3.9), presumably because the latter (or its radical precursor) closes to form the more stable acenaphthylene. The concentration of 2-vinylnaphthalene is within 30% of the concentration of 2-

ethylnaphthalene, which is significantly different that the relationship between phenylacetylene and styrene, suggesting that naphthalene chemistry is significantly different from benzene chemistry.

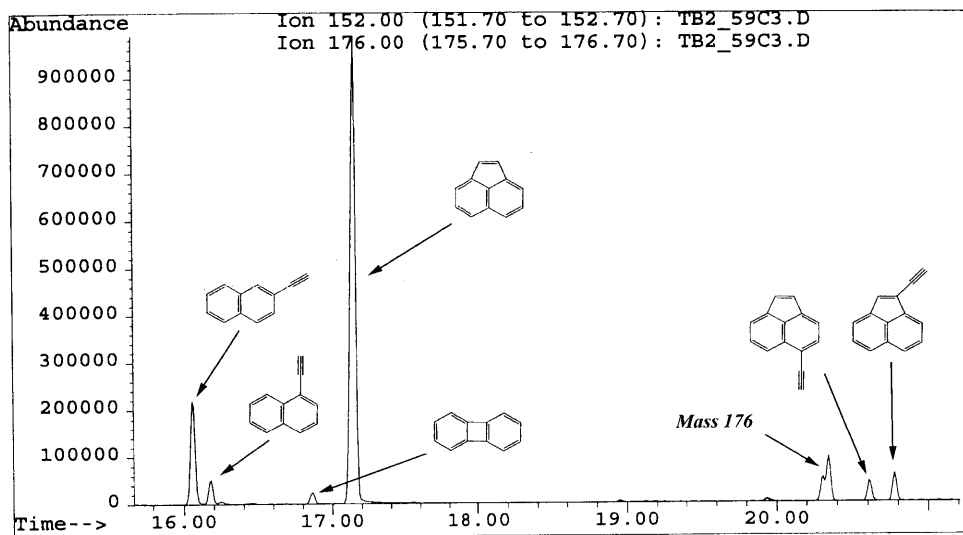


Figure 3.8 GC/MS chromatogram of a flame sample extracting molecular ions 152 and 176. ($\phi=1.8$, 7.75 mm, HP-50+ column)

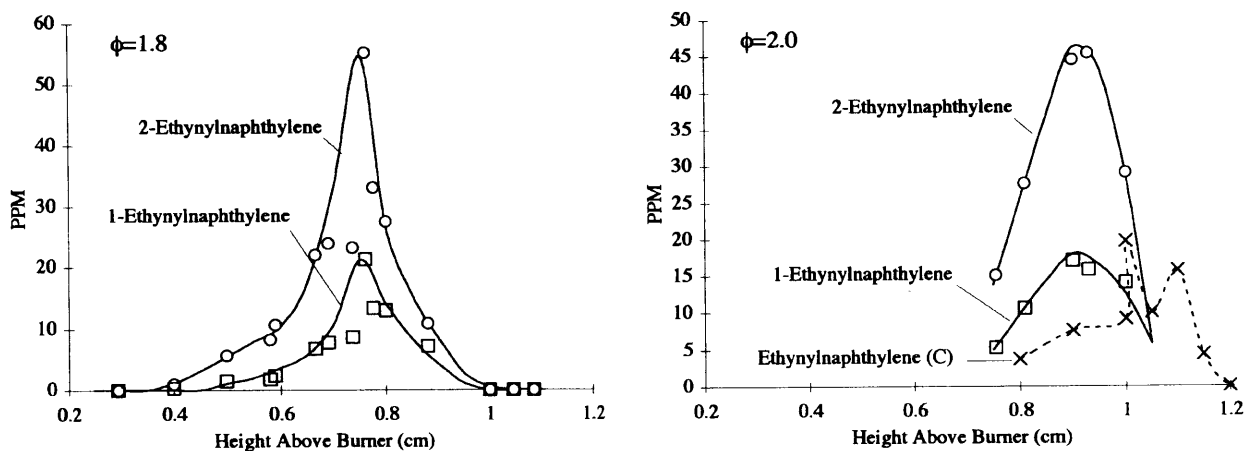


Figure 3.9 Ethylnaphthalene mole fractions in the $\phi=1.8$ and $\phi=2.0$ flames. (C=McKinnon, 1989)

Two of the four isomers of ethylnaphthalene were synthesized by A. Necula. They correlated by retention time to two of the peaks of mass 176 in the flame sample GC/MS chromatograms (see Figure 3.10). The remaining two mass 176 peaks, which partially co-elute on the HP-50+ column, are believed to be the remaining

two isomers (2- and 3-ethynylacenaphthylene), because of their close retention times and identical fragmentation patterns. Pyracylene, another PAH of mass 176, may be produced in the flames, but if it does exist in the flame samples, it is believed that it would not survive the high temperatures of the GC.

The concentration of 5-ethynylacenaphthylene exceeds that of 1-ethynylacenaphthylene by a small fraction, but the most prevalent isomer is believed to be one of the two unidentified isomers, which is possibly twice as prevalent as 1-ethynylacenaphthylene. The corresponding vinylacenaphthylenes (mass 178) were not found. The ratio of the peak concentrations of ethynylacenaphthylene (sum of all isomers) to acenaphthylene is approximately double that of ethynylacanthylene to naphthalene, again showing the differences in PAH chemistries, given acenaphthylene and naphthalene have the same number of potential active sites.

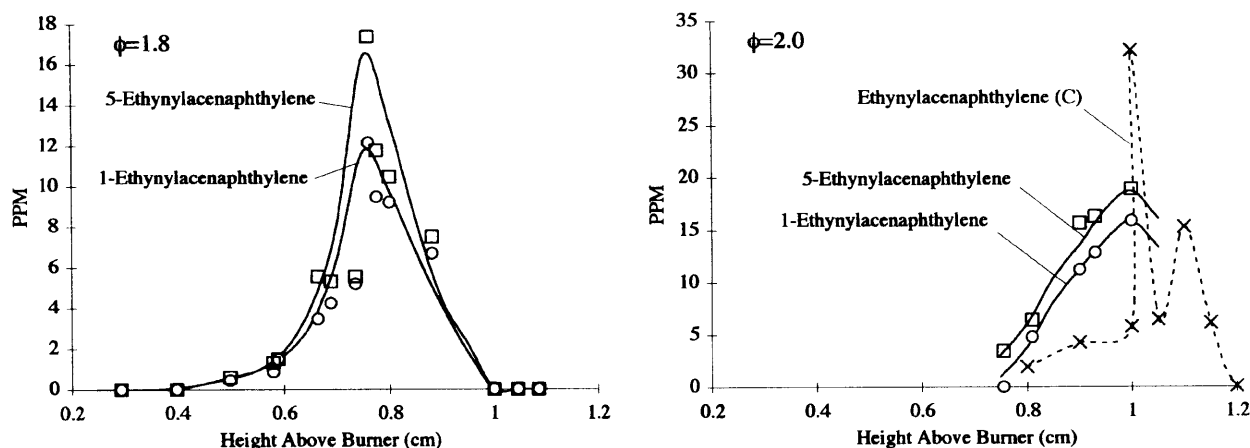


Figure 3.10 Ethynylacenaphthylene mole fractions in the $\phi=1.8$ and $\phi=2.0$ flames. (C=McKinnon, 1989)

3.1.3 BIARYLS

Biaryls are believed to be formed from reactions between aromatics and/or aromatic radicals (Figure 3.11).

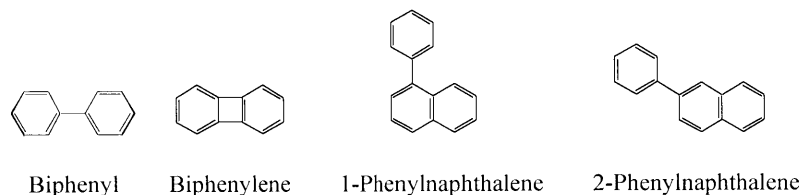


Figure 3.11 Structures of some biaryls.

The combination of two phenyl radicals (or a phenyl radical and a benzene molecule followed by loss of H atom) could lead to biphenyl, while dehydrogenation of biphenyl would produce biphenylene. Although

biphenylene looks like a highly strained compound, it is stable at least at room temperature, so it is reasonable that it could be formed in the flames. Biphenyl is one of the most prevalent PAH in these flames, presumably because the benzene concentration is so high. Biphenylene appears to peak after biphenyl, which is may be consistent with its being produced from biphenyl.

Reactions between phenyl and naphthyl radicals (or reactions between phenyl and naphthalene or naphthyl and benzene) could produce phenylnaphthalene. Phenylnaphthalene was not identified in the $\phi=2.0$ flame because it required *injection 3* (see section 2.5) which was not done for the $\phi=2.0$ flame samples. The concentration of the 2- isomer is nearly twice that of the 1- isomer. The 1-phenylnaphthalene isomer can close upon dehydrogenation to form fluoranthene. Possibly as a result, the isomer distribution of phenylnaphthalene is consistent with that of ethylnaphthalene, but not that of methylnaphthalene. Binaphthyl, which could be produced from two naphthyl radicals, was identified in a few samples, but its concentration was too small to quantitate.

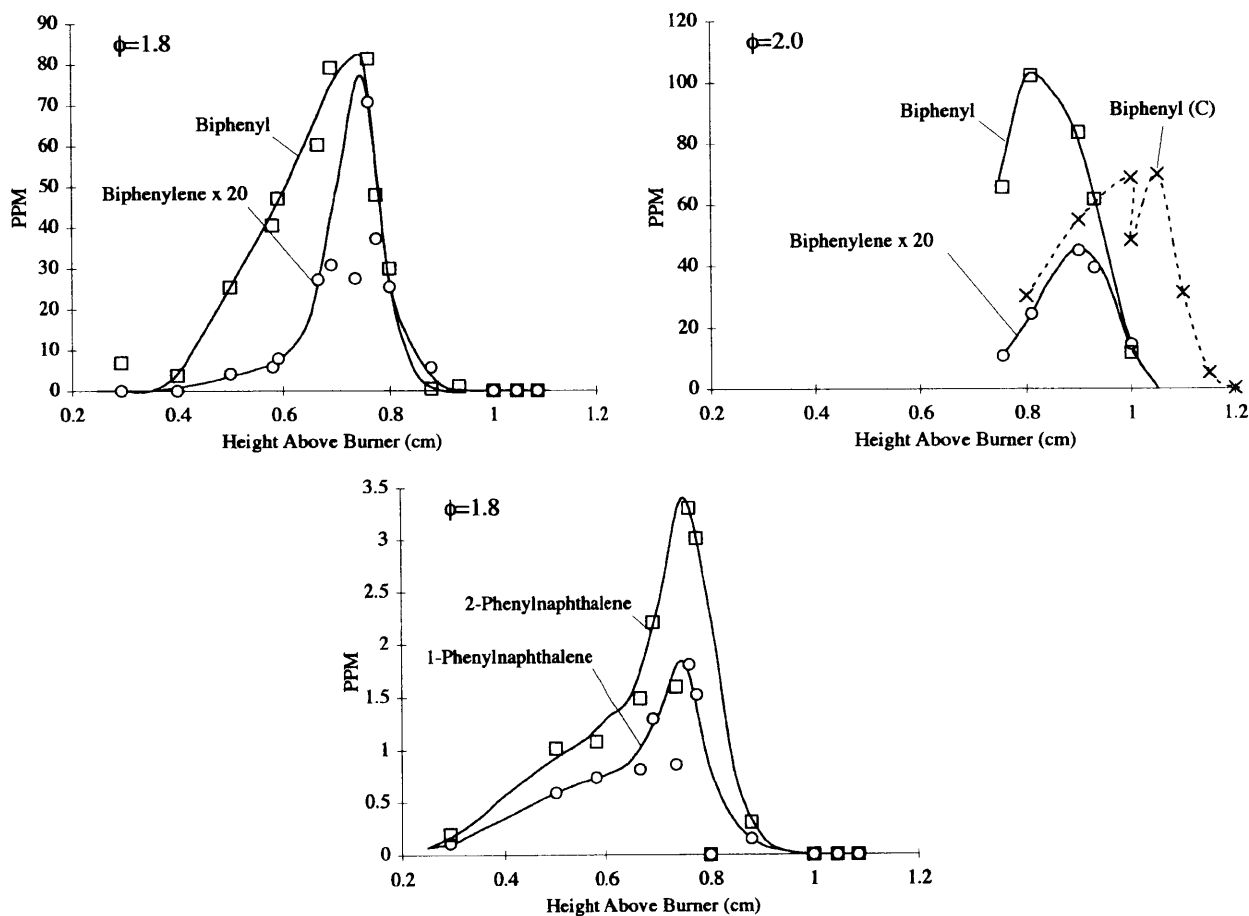


Figure 3.12 Biaryl mole fractions in the $\phi=1.8$ and $\phi=2.0$ flames.
(C=McKinnon, 1989)

3.1.4 LARGER PAH

Ten condensed PAH larger than pyrene were measured in the flames (Figure 3.13). The uncertainties in the measurements for these compounds are considerably higher than for the previous condensed PAH, because of the methods used to do the quantitations and the potential error associated with concentrating the sample solutions.

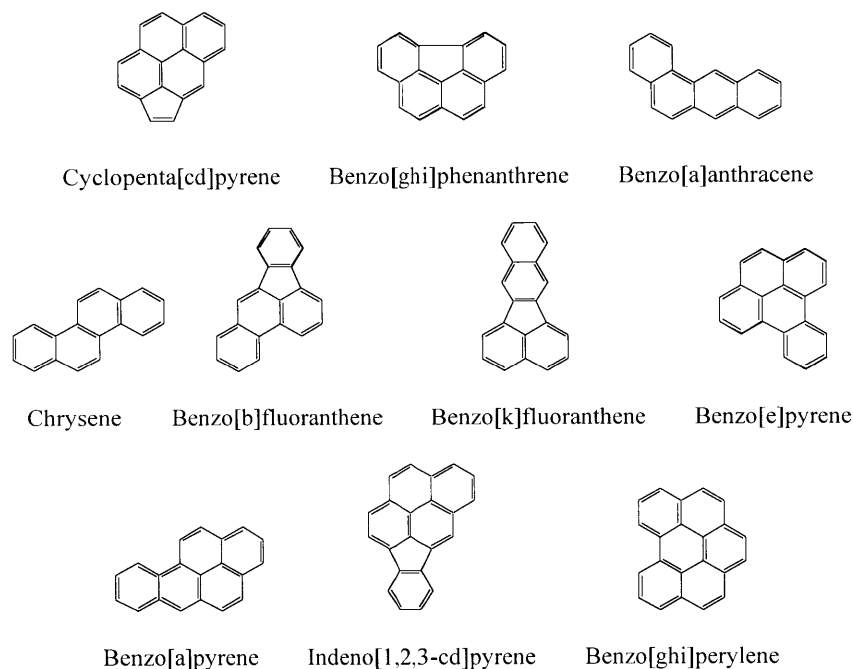


Figure 3-13 Structures of larger condensed PAH

The concentration profiles for the mass 226 and 228 compounds are shown in Figure 3.14. The peak concentrations for the mass 228 compounds have an additional amount of uncertainty, as they are defined by a single data point. However when comparing the two flames, the maximum concentrations of all of these compounds are practically equal, within experimental error. This observation is in contrast to the findings of Bittner and Howard (1981), who showed that the concentration of the total mass greater than 400 amu increases by two orders of magnitude when changing from the $\phi=1.8$ flame to the $\phi=2.0$ flame. Although the high molecular weight material (including soot) increases dramatically with equivalence ratio, the PAH detectable by GC do not change considerably.

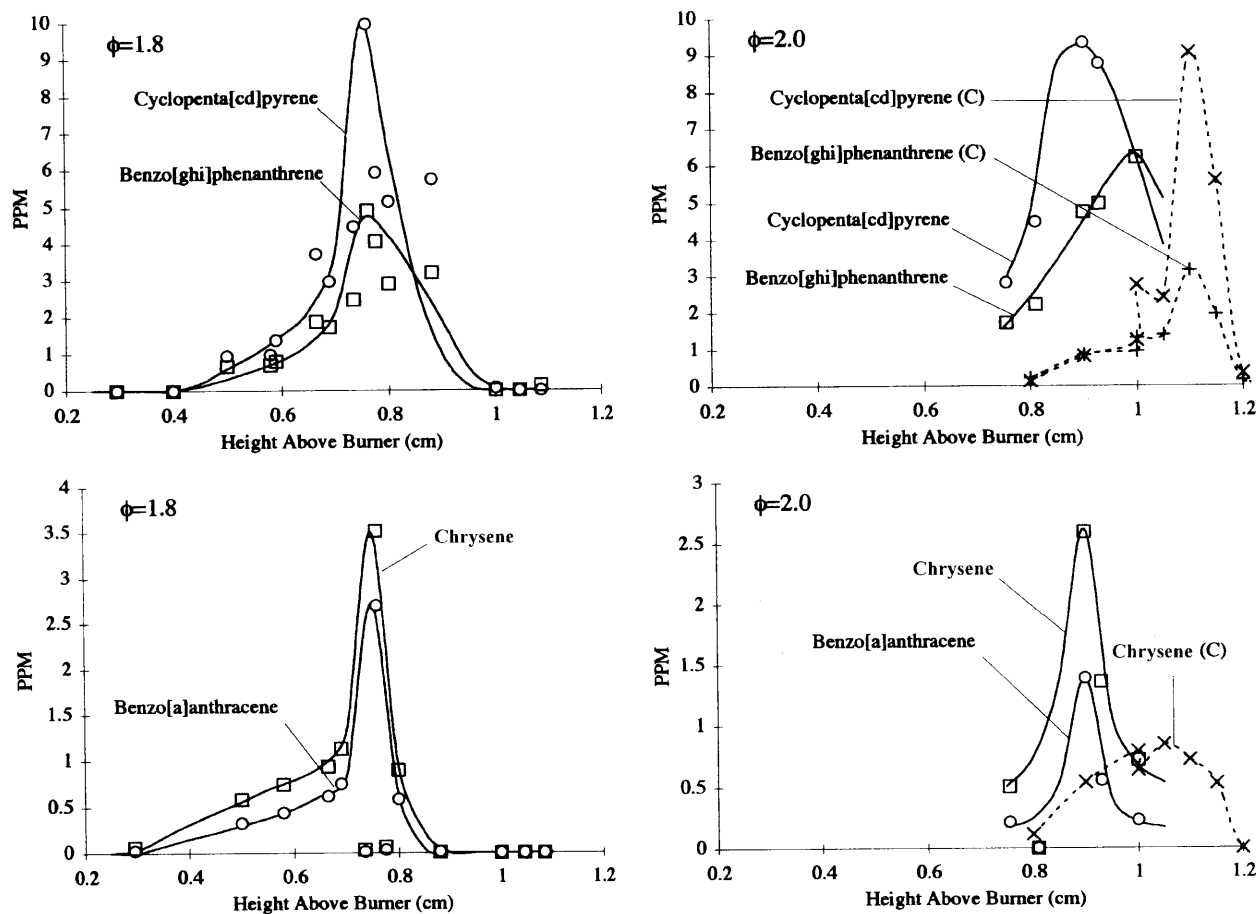


Figure 3.14 Mole fractions of the mass 226 and 228 compounds in the $\phi=1.8$ and $\phi=2.0$ flames. (C=McKinnon, 1989)

Several compounds of mass 252 were detected in the flames, but only 4 were identified (Figure 3.15).

Again, the overall differences between the $\phi=1.8$ and $\phi=2.0$ flames were not significant, but in this case, the $\phi=1.8$ data was obtained from *injection 3*, while the $\phi=2.0$ data could be extracted from *injection 2*, suggesting that both sets of data are reasonably accurate. Two compounds of mass 276 were identified, but were measured only in the $\phi=1.8$ flame. The flame data was analyzed for higher molecular weight material, including dibenzo[a]anthracene (mass 278) and coronene (mass 300), but none were found. PAH larger than mass 276 may have been too low in concentration to detect, they may have been insoluble in the sample solution, or they may have been eliminated by the GC. In fact, a standard solution containing significant amounts of coronene was repeatedly injected into the GC/MS, but coronene was detected in only 20% of the injections, suggesting that it was either pyrolyzing in the injector port or irreversibly adhering to the column.

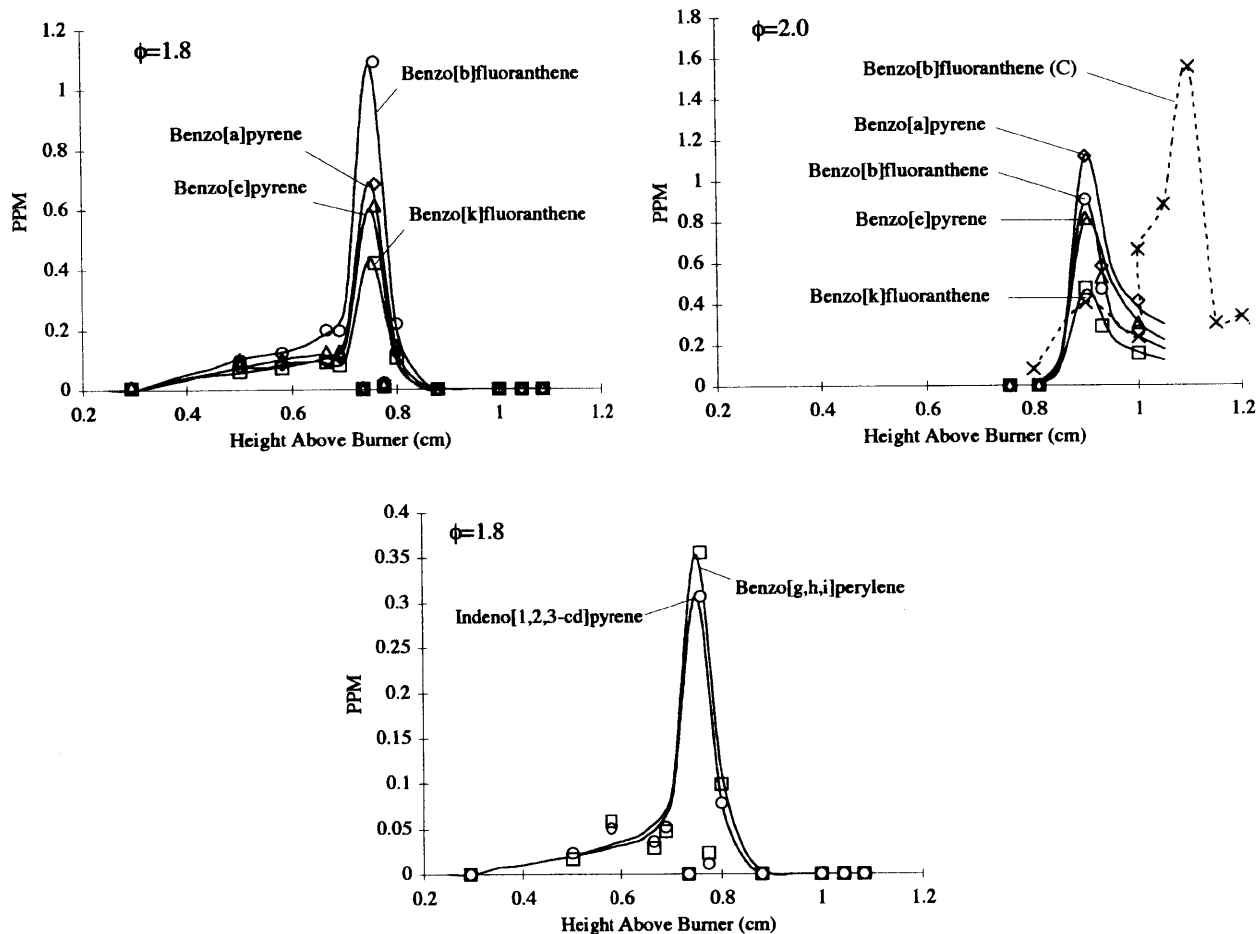


Figure 3.15 Mole fractions of the mass 252 and 276 compounds in the $\phi=1.8$ and $\phi=2.0$ flames. (C=McKinnon, 1989)

3.1.5 OXY-PAH

The incorporation of oxygen into PAH structures (Figure 3.16) is of interest because many of the resulting oxy-PAH have been shown to be particularly mutagenic (Durant et al., 1996). The most common oxygen-containing aromatics identified in these flames are those containing hydroxyl groups. The concentration profile of phenol matches that of Bittner closer than any of the compounds measured in this study (Figure 3.17), which fits the aforementioned trend, since phenol has the lowest molecular weight of all compounds measured. Phenol is also the most prevalent of all of the compounds measured in *both* of the flames, which is contrary to the data by McKinnon, who made special note that phenol was not present, even though he expected to find it. It is not clear why phenol

was not observed by McKinnon, but possible reasons could have been reaction or condensation upon sampling, evaporation while concentrating the sample solutions or use of a sub-optimal GC column and/or method.

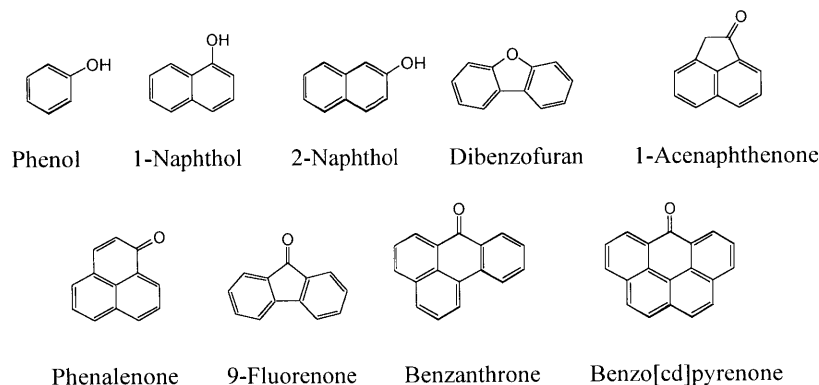
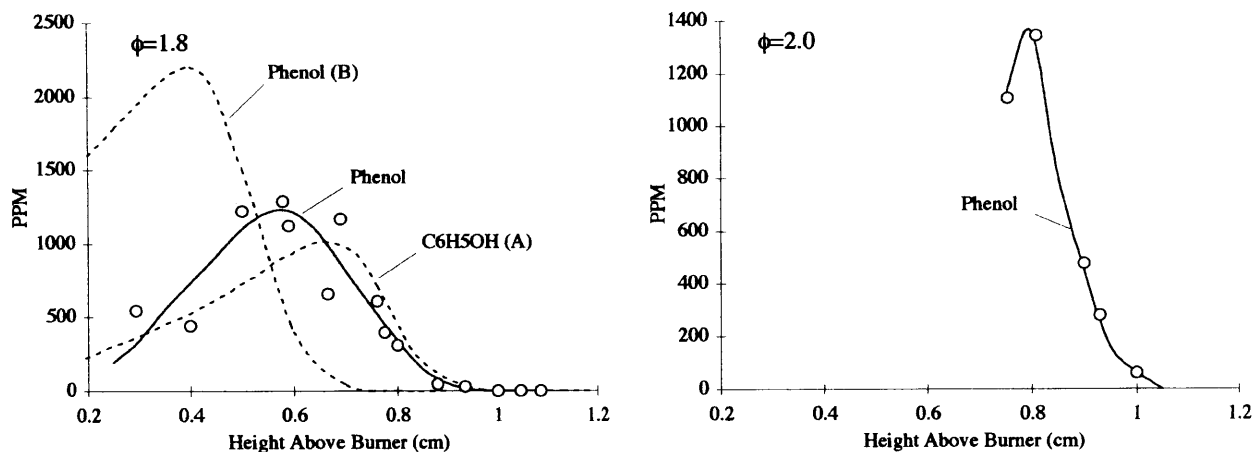


Figure 3.16 Structures of oxy-PAH



The naphthol concentration profiles are plotted in Figure 3.18. The scatter in the $\phi=1.8$ data does not allow for comparisons between the two isomers, but in the $\phi=2.0$ flame, 1-naphthol is 40% more prevalent than 2-naphthol, assuming that their response factors are equal. This observation is consistent with that seen for the isomers of methyl-naphthalene, suggesting that methyl-naphthalene and naphthol may be formed by similar reactions.

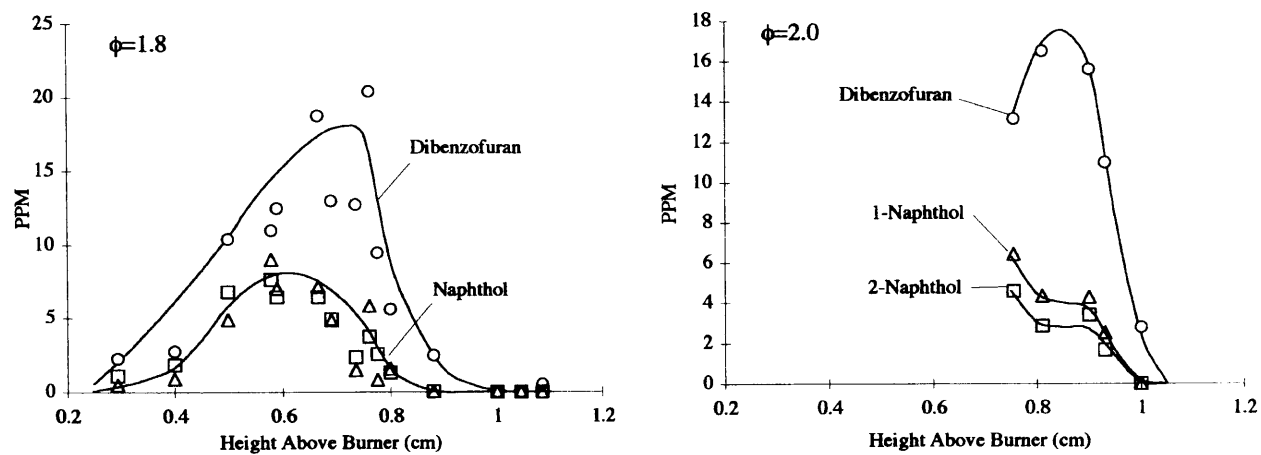


Figure 3.18 Naphthol and dibenzofuran mole fractions in the $\phi=1.8$ and $\phi=2.0$ flames.

The concentrations of the remaining oxy-PAH quantified in this study are shown in Figures 3.18 and 3.19. These are some of the oxy-PAH that are typically seen in flame samples and is in no way representative of the total number of oxy-PAH that can be identified in these flames.

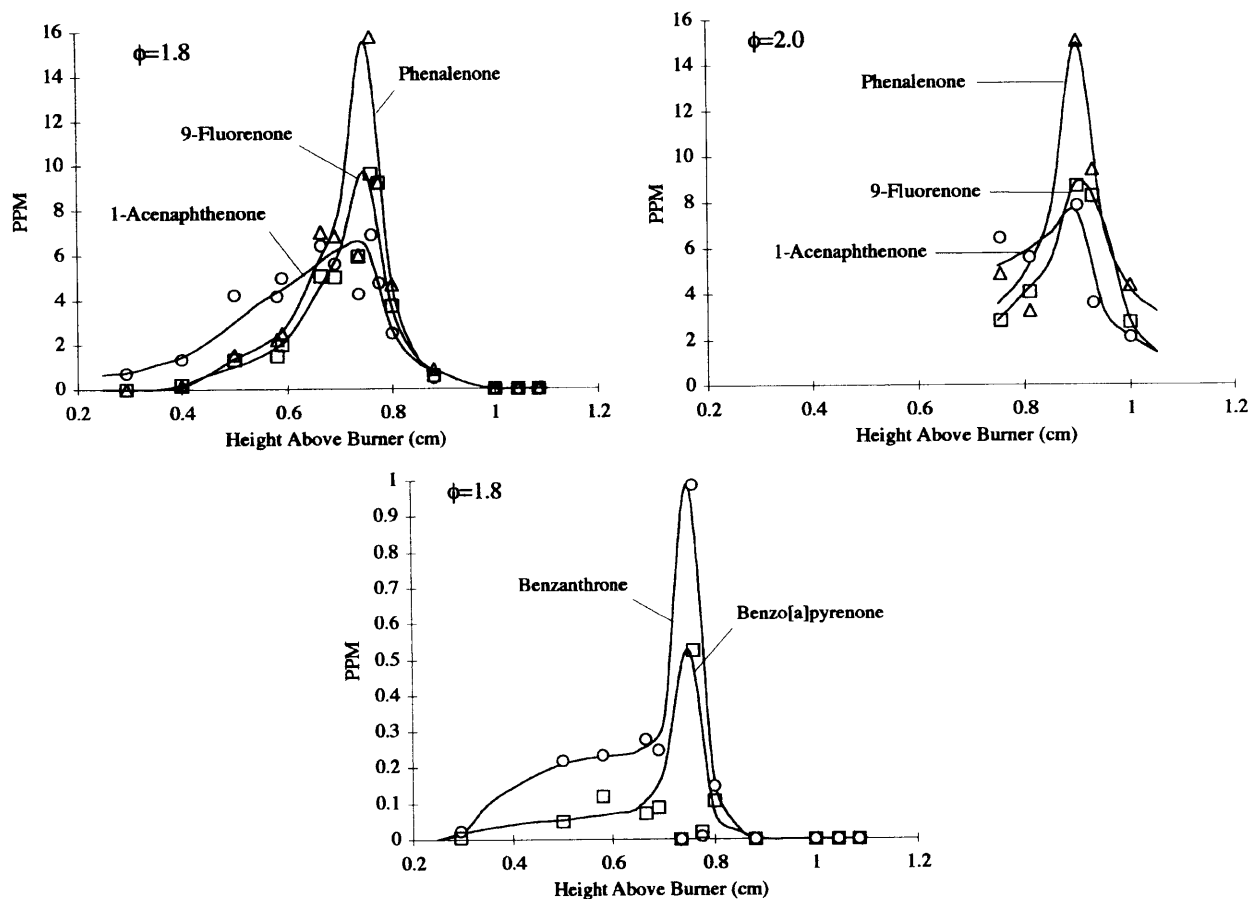


Figure 3.19 Oxy-PAH mole fractions in the $\phi=1.8$ and $\phi=2.0$ flames.

3.2 Mole Fractions of Aromatic Radicals in Flames

The flame concentrations of the radical species studied in this flame were calculated on the assumption (shown to be accurate by Hausmann et al., 1992) that each radical reacts with the scavenger to make a methylthio adduct. The methylthio-aromatic compounds can be located in a GC/MS chromatogram by extracting the major fragment ions. The fragment ion masses and their possible formation routes are: M (the molecular mass of the methylthio compound), M-15 (loss of CH_3), M-33 (transfer of the CH_3 group to an adjacent carbon with subsequent loss of SH), M-46 (transfer of H and loss of SCH_2), and M-59 (loss of C-SCH_3).

3.2.1 PHENYL AND BENZYL RADICALS

The scavenging products of phenyl, benzyl, and p-tolyl radicals are shown in Figure 3.20.

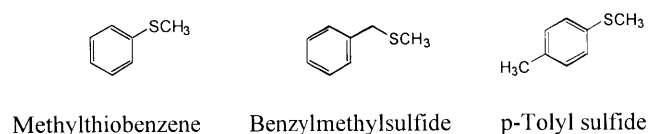


Figure 3.20 Structures of 1-ring methylthio compounds

Methylthiobenzene fragments in the mass spectrometer (Figure 3.21) into the 5 ions described above (masses 124, 109, 91, 78, and 65). P-tolyl fragments similarly, though the M-47 ion (loss of SCH₃) is much more prominent than the M-46 ion. The fragmentation pattern for benzylmethylsulfide is significantly different, because the methylthio group is not attached to the aromatic ring. The carbon-sulfur bond strength in benzylmethylsulfide is significantly lower than the others, resulting in a major mass fragment of 91 (loss of SCH₃).

The phenyl radical concentration in the flame peaks at the same point as the major PAH, and is more than twice as prevalent than that measured by Bittner and Howard (Figure 3.22), which is not surprising, as calibrating the on-line mass spectrometer for the radical is based solely on theory, since the radical can not be easily produced for experimental calibration. The benzyl radical peaks at the same point as phenyl (though the benzyl data is considerably more scattered), but the concentration is approximately 50 times less. P-tolyl sulfide was not found in any of the samples. One peak in the chromatograms matched the fragmentation pattern for p-tolyl sulfide, but the retention times were significantly different. The compound detected may be another isomer of a scavenged tolyl radical. The concentration of this unknown isomer was estimated to be approximately equal to that of the benzyl radical. Taking this into account, the total concentration of C₇H₇ calculated in this study was about 5 times less than that calculated by Bittner and Howard. This is the only compound studied where Bittner and Howard calculated higher concentrations than did this study.

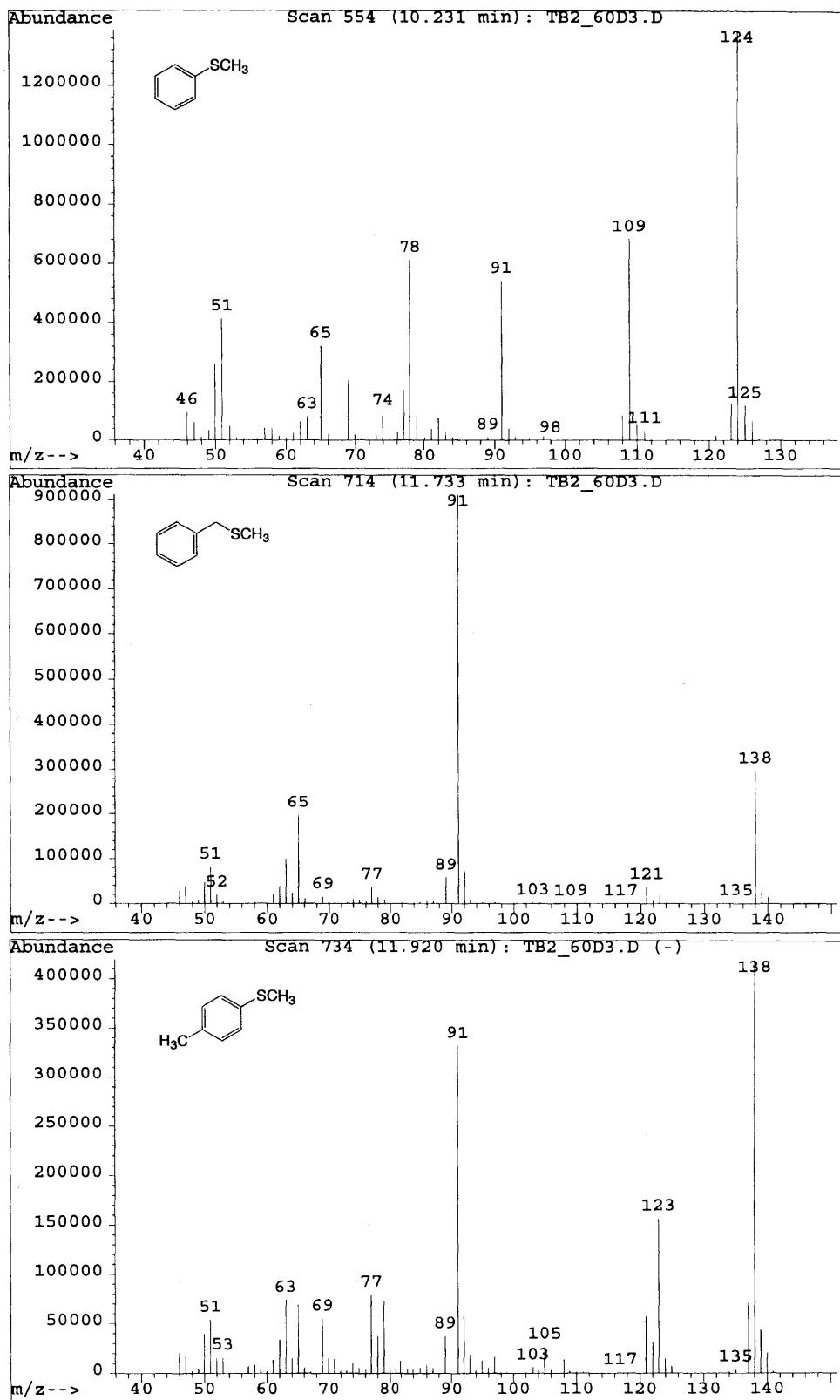


Figure 3.21 Mass spectra for 1-ring methylthio compounds: (top) methylthiobenzene, (middle) benzylmethylsulfide, (bottom) p-tolyl sulfide

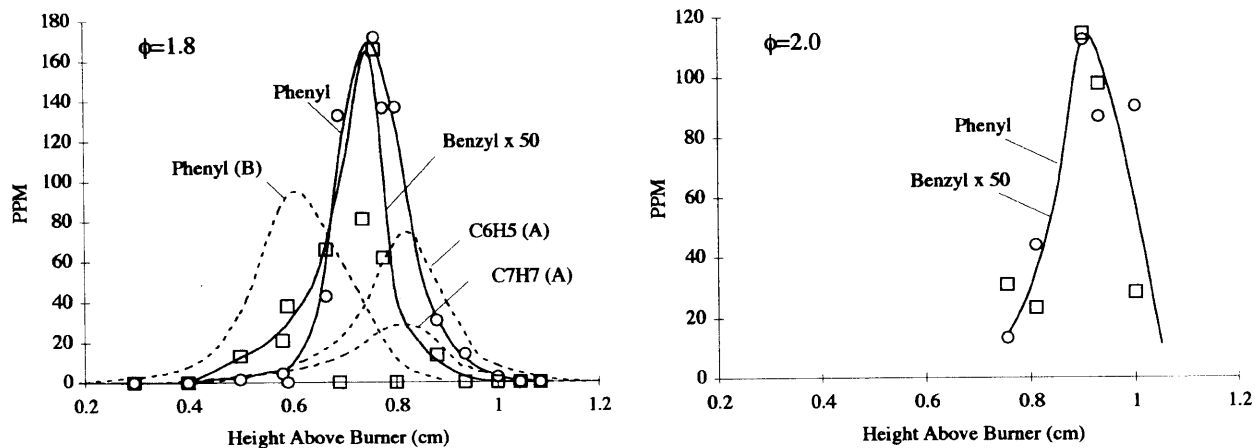


Figure 3.22 Phenyl and benzyl radical mole fractions in the $\phi=1.8$ and $\phi=2.0$ flames (A=Bittner and Howard, 1981, B=Hausmann et al., 1992)

3.2.2 NAPHTHYL RADICALS

There are eight sites on naphthalene that can support a σ radical, but by symmetry only two are different.

Therefore, two scavenging products are seen (Figure 3.23).

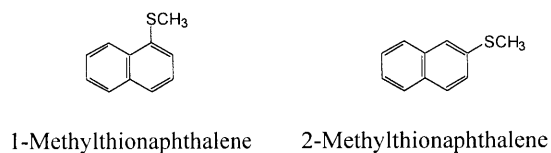


Figure 3.23 Structures of methylthionaphthalene

One of the compounds, 2-methylthionaphthalene was purchased from Sigma-Aldrich. The other was synthesized by A. Necula in an amount insufficient for accurate quantitation, so the calibration curve for the first was used for both compounds. The two isomers separated well on the HP-50+ column, which was critical, because the fragmentation patterns for the compounds (Figure 3.24) are nearly indistinguishable from each other.

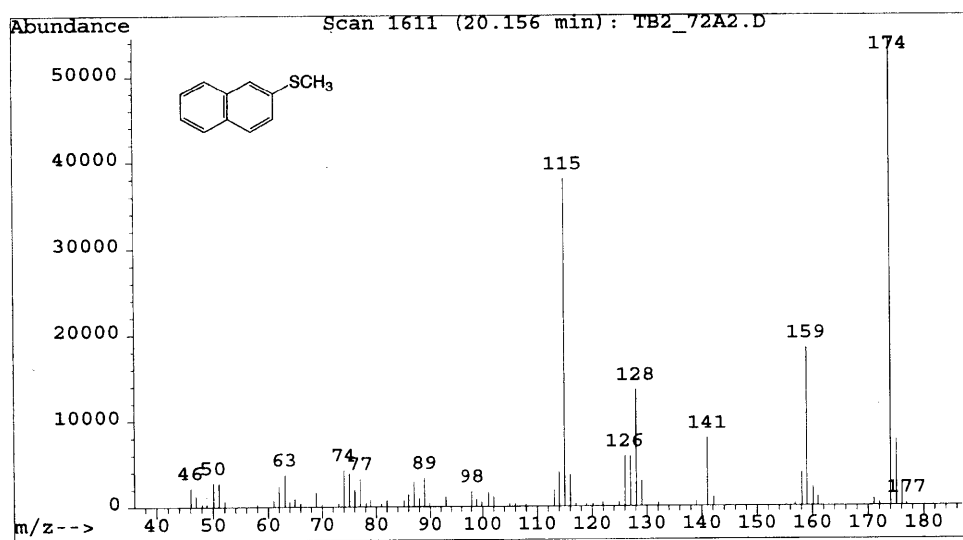


Figure 3.24 Mass spectra for the methylthionaphthalenes: (top) 1-methylthionaphthalene, (bottom) 2-methylthionaphthalene

The concentration profiles for the naphthyl radicals are shown in Figure 3.25. These are the only data that closely match those by Hausmann et al. The concentration of 2-naphthyl radical appears to be 30% higher than 1-naphthyl at all points in the flame. At most, only a small fraction of the difference may be attributed to calibration error.

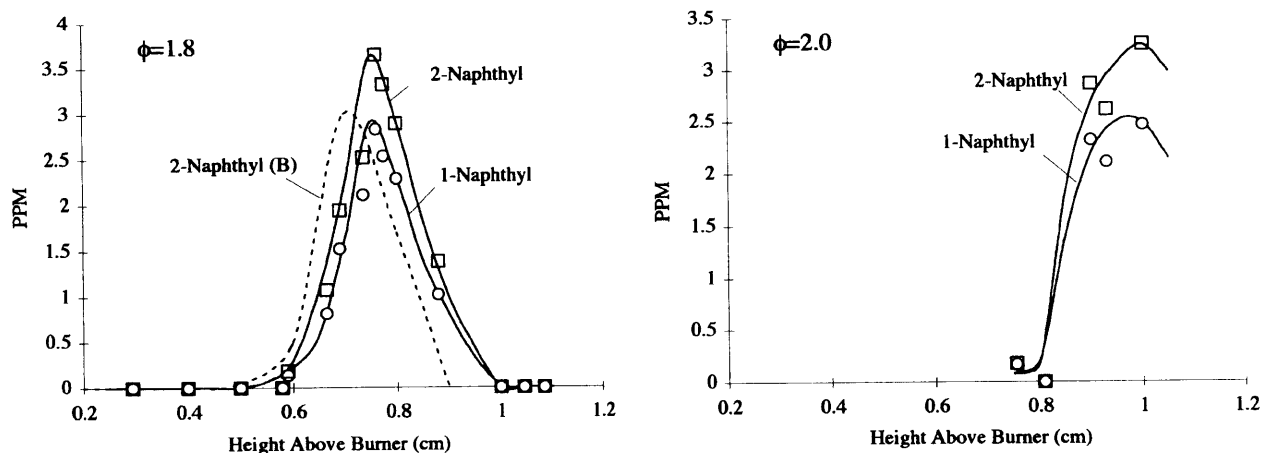


Figure 3.25 Naphthyl radical mole fractions in the $\phi=1.8$ and $\phi=2.0$ flames (B=Hausmann et al., 1992)

3.2.3 ACENAPHTHYL RADICALS

Acenaphthylene has the same number of carbons capable of having σ radical sites as naphthalene, but there are four different isomers for the scavenged radicals (Figure 3.26). Consequentially, four peaks are seen in the GC/MS chromatogram with the fragment ions expected for these molecules (masses 198, 183, 165, 152, and 139). The chromatogram with the 5 extracted ions is shown in Figure 3.27.

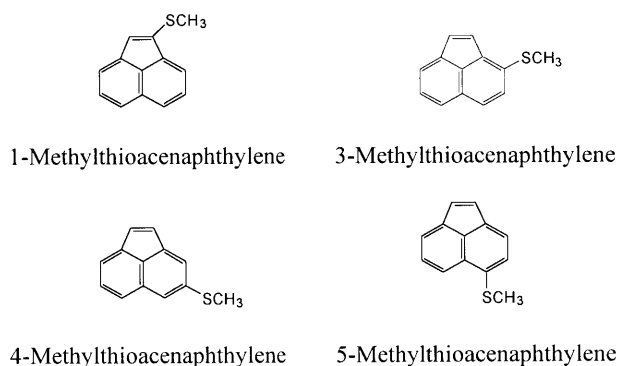


Figure 3.26 Structures of methylthioacenaphthylene

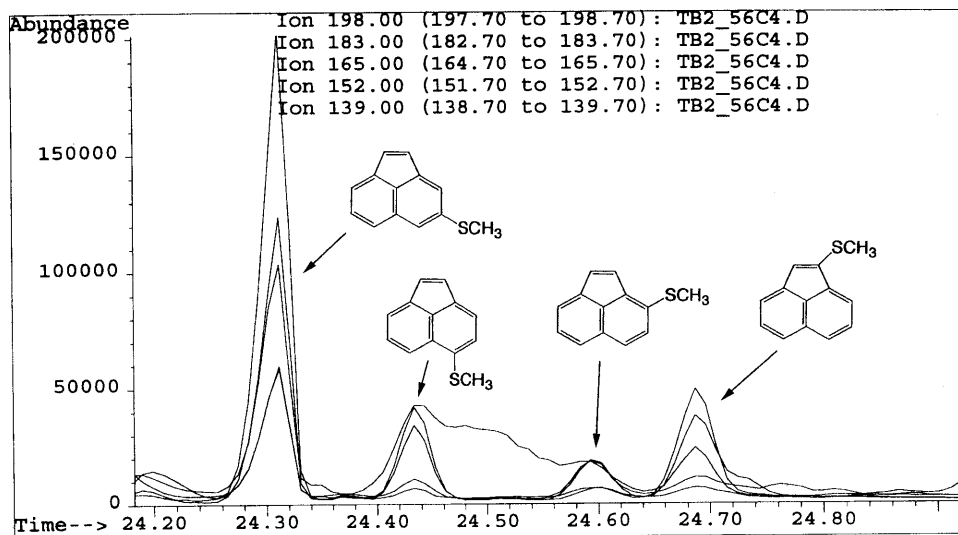


Figure 3.27 GC/MS chromatogram of the extracted fragment ions for methylthioacenaphthylene (HP-50+ column)

The four isomers were synthesized by A. Necula. Each had a significantly different fragmentation pattern (Figures 3.28 and 3.29), and each matched one of the GC/MS peaks both by retention time and fragmentation pattern.

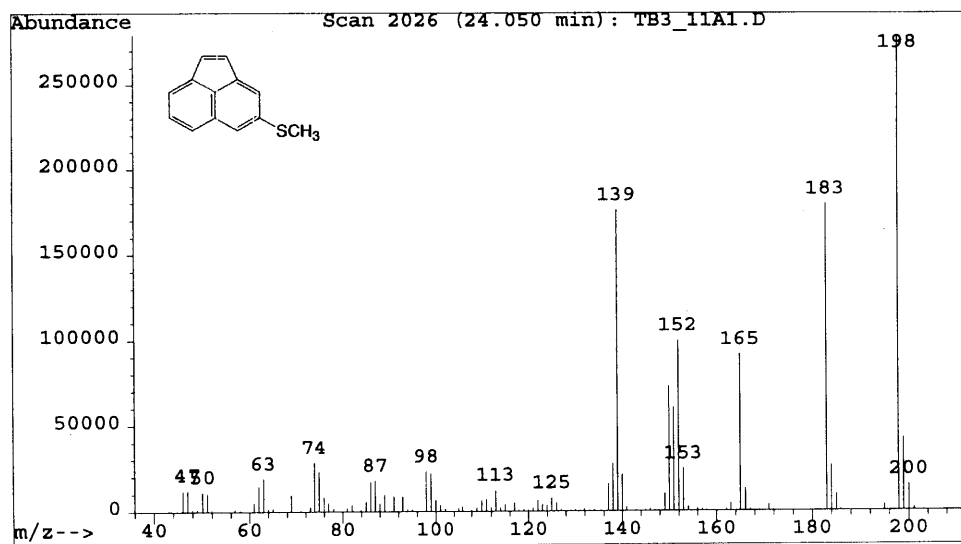


Figure 3.28 Mass spectrum for 4-methylthioacenaphthylene

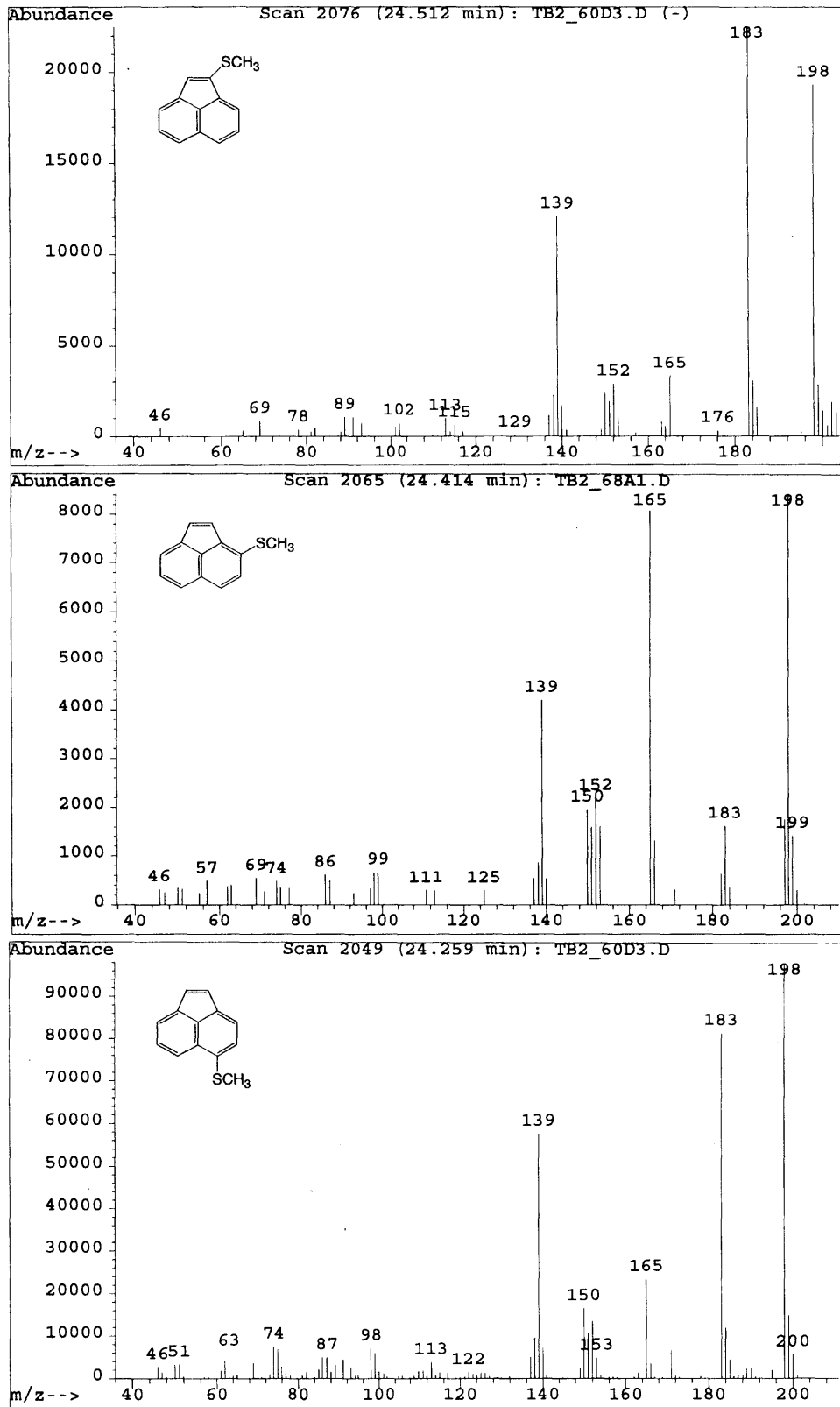


Figure 3.29 Mass spectra for 1-methylthioacenaphthylene (top), 3-methylthioacenaphthylene (middle), and 5-methylthioacenaphthylene (bottom)

Acenaphthyl radical was measured only in the $\phi=1.8$ flame, because it required data from *injection 3*, which was not available for the $\phi=2.0$ flame. The radical at the 4- position was over three times more prevalent than the radicals at the 1- and 5- position and nearly ten times more prevalent than the radical at the 3- position.

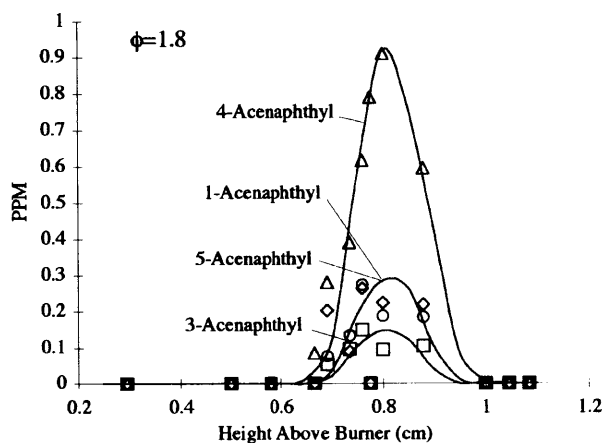


Figure 3.30 Acenaphthyl radical mole fractions in the $\phi=1.8$ flame

3.2.4 PYRENYL AND FLUORANTHENYL RADICALS

Four PAH of mass 202 were measured in the flames, so the number of possible scavenged radicals of mass 201 was large. Three different scavenging products were possible for pyrene, while five were possible for fluoranthene. Some of these structures are shown in Figure 3.31. Coincidentally, when the expected fragment ions for these compounds (masses 248, 233, 215, 202, and 189) were extracted from the chromatograms of the $\phi=1.8$ flame samples (again, using *injection 3*), one group of 5 small peaks followed by 3 larger peaks were found (Figure 3.32). The two groups were separated by 1 minute. Fluoranthene and pyrene, the most prevalent of the mass 202 species, were also separated by 1 minute with fluoranthene eluting first.

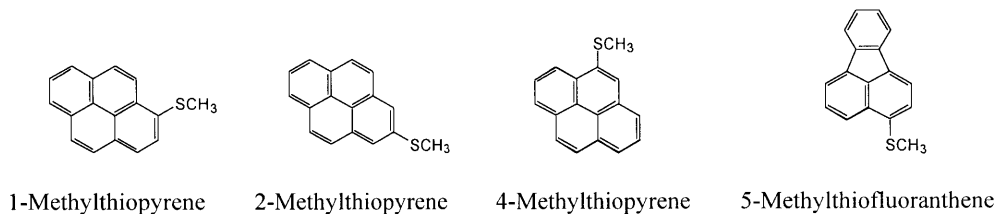


Figure 3.31 Structures of methylthiopyrene and methylthiofluoranthene

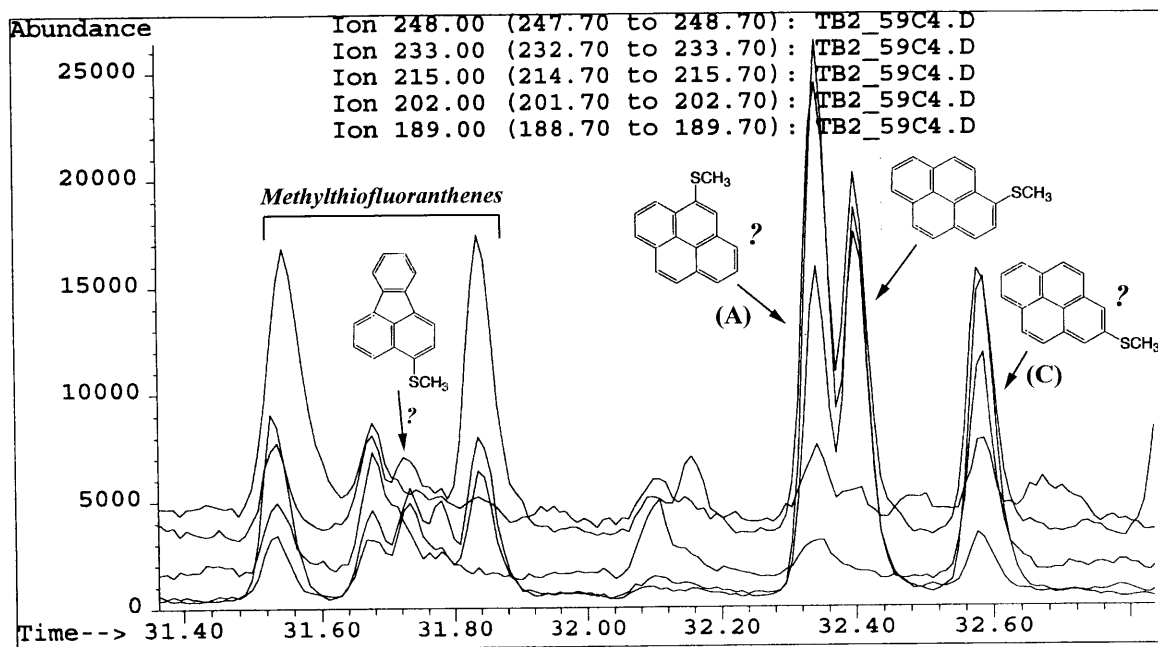


Figure 3.32 GC/MS chromatogram of the extracted fragment ions for methylthiopyrene and methylthiofluoranthene (HP-50+ column)

Two of the possible structures were synthesized by A. Necula: 5-methylthiofluoranthene and 1-methylthiopyrene. The first fell within the first group of peaks by retention time, but the peaks were not clean enough to make a match by fragmentation pattern. The second matched one of the peaks in the second group by both retention time and fragmentation pattern. The mass spectra of these two compounds as well as the remaining two peaks from the second group are shown in Figures 3.33 and 3.34. Attempts to estimate the structures of the two unknown compounds from their fragmentation patterns were unsuccessful, however polar compounds should preferentially adhere to the polar column and therefore elute later than less-polar compounds of similar structure. The sulfur atoms of 1-methylthiopyrene and 4-methylthiopyrene can easily hydrogen bond with an aromatic hydrogen, effectively reducing the polarity of the compounds, while the sulfur atom of 2-methylthiopyrene can not easily form a hydrogen bond within the molecule. So 2-methylthiopyrene is expected to elute later than the other isomers. The same logic can be applied to the elution order of the two isomers of methylthionaphthalene. For this reason, peak A in Figure 3.32 was assigned 4-methylthiopyrene, while 2-methylthiopyrene was assigned to peak C.

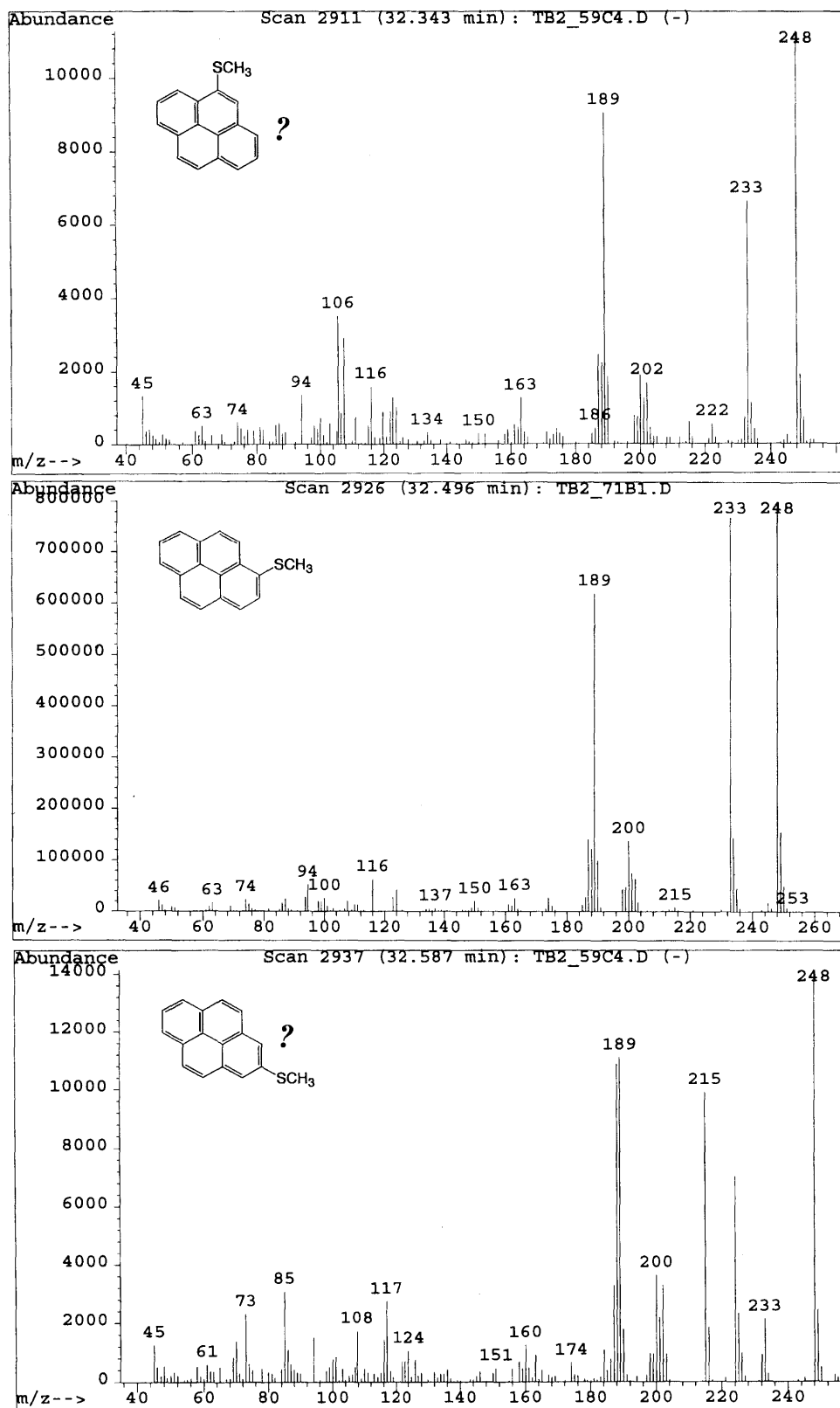


Figure 3.33 Mass spectra for the three isomers of methylthiopyrene: (top) peak A, (middle) 1-methylthiopyrene, (bottom) peak C

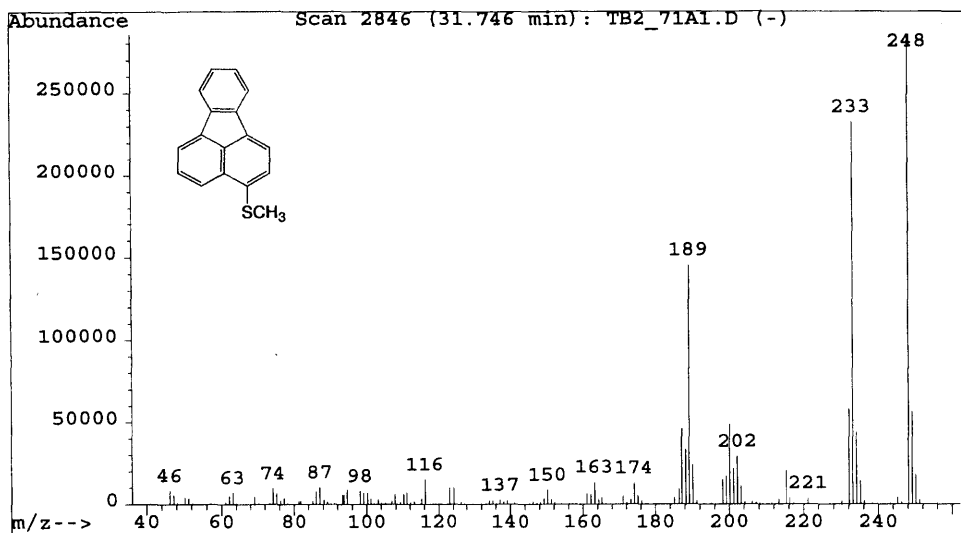


Figure 3.34 Mass spectra for 5-methylthiofluoranthene

Figure 3.35 shows the mole fractions of the individual pyrene radicals and the sum of the fluoranthene radicals as a function of height above burner. The individual fluoranthene radicals could not be plotted because the methylthiofluoranthene peaks in the GC/MS chromatogram were not very distinct. The total pyrenyl concentration exceeds that of fluoranthenyl by almost 100%, which is surprising since pyrene and fluoranthene have the same number of C-H bonds which can be broken to form radicals.

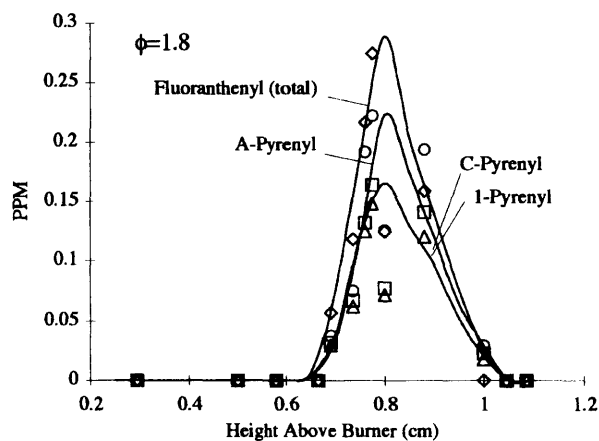


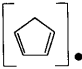
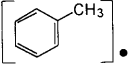
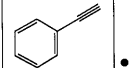
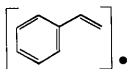
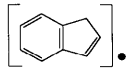
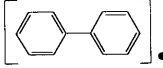
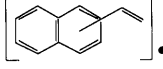
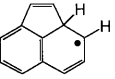
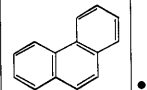
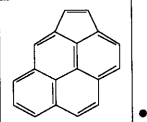
Figure 3.35 Pyrenyl and fluoranthenyl radical mole fractions in the $\phi=1.8$ flame

3.2.5 OTHER RADICALS DETECTED AND UNDETECTED

Several additional methylthio compounds were detected in the flames, but reliable assessments of structures could not be made, because standards were not available. Table 3.1 lists these compounds along with their retention times in the GC and their fragment ions. Because their identities could not be confirmed, estimated concentrations are not given. Included is one isomer of cyclopentadienyl, two isomers of tolyl (excluding benzyl and p-tolyl, which were discussed earlier), two isomers of ethynylbenzene radical and one isomer of the styrene radical. The styrene radical is of particular interest because one of the potential mechanisms for the formation of naphthalene from benzene includes styrene with one of the terminal vinyl hydrogens missing. It is possible that this is the isomer which is detected, but further work needs to be done to positively identify and quantitate it.

Indene radicals were seen in the benzene $\phi=1.8$ flame by Hausmann et al., but were not detected in this study. It is possible that the methylthio adduct co-eluted with one of the internal standards, which would have obscured the presence of any trace compounds. Another radical of interest is vinylnaphthalene, for the same reasons as for the styrene radical. So it is worth noting that no compound detected in this study had a fragmentation pattern remotely matching that expected for the methylthio adduct of vinylnaphthalene. Also, no radicals were detected that would be consistent with a π radical formed as an intermediate in a ring closure mechanism, which may simply indicate that they are too reactive to exist in detectable concentrations. No methylthio adduct of biphenyl was found, even though biphenyl is one of the most prevalent PAH. Only one peak in the GC/MS chromatograms matched the expected fragmentation pattern for methylthiophenanthrene, and it was not nearly as dominant as the peaks for methylthiopyrene. This is surprising because the peak flame concentration of pyrene is very close to that of phenanthrene, so it might have been expected that their radical concentrations would be similar. The largest potential methylthio-PAH detected was methylthiocyclopenta[cd]pyrene, but it was barely above the detection limit of the GC/MS, so although the correct mass fragments were seen together almost exclusively, well defined peaks were not available.

Table 3.1 Other Methylthio Compounds Detected

Radical Structure	Methylthio Adduct Mass Fragment Ions ^a	Retention Time (min)
	97, 112, 66	7.6
	91, 138, 102 123, 91, 138	10.2 12.9
	148, 115, 102, 89, 133 148, 133, 89	14.3 14.5
	150, 135, 91	15.7
	<i>Not seen</i>	<i>Not seen</i>
	<i>Not seen</i>	<i>Not seen</i>
	<i>Not seen</i>	<i>Not seen</i>
	<i>Not seen</i>	<i>Not seen</i>
	224, 165, 178	28.3
	272, 257, 213, 226	32.5

^ain order of prevalence (ion counts)

Chapter 4

Modeling and Discussion

Thermodynamic calculations of select PAH and PAH radicals were performed by a variety of techniques. These calculations were then added to one of the latest flame chemistry models and comparisons were made with the PAH and PAH radical data collected in this study to critically test the mechanisms within the model.

4.1 Thermodynamic Calculations

Many types of computational methods are available for determining the structures, thermodynamics, and other properties of molecules. Empirical methods, such as group additivity, use experimental data fitted to a set of parameters. Molecular mechanics methods, including MM3, treat the interactions between nuclei of the molecule in a semi-empirical manner using classical physics, but neglect electronic effects. Electronic structure methods utilize quantum mechanics and apply approximations in an effort to solve the Schrödinger equation. These types of calculations include semi-empirical methods, ab initio methods, and density functional methods.

Group additivity is an empirical method in which groups of atoms are assigned various property values based on how the atoms are bonded. The properties are then summed over the entire molecule and adjusted for factors such as free rotors and symmetry. Although there are some theoretical considerations in this method, the values of the group properties have been obtained by fitting the method to a large number of experimental values. Group additivity is simple enough that the calculations can be performed by hand, but the program THERM (Ritter and Bozzelli, 1991) calculates enthalpies, entropies, and heat capacities for a number of temperatures and requires a negligible amount of computer time. This method may be accurate for compounds close to those used to fit the group parameters, but for other compounds, the results can be quite poor.

Semi-empirical electronic structure methods, including AM1, use parameters fitted from experimental data to approximate solutions to the Schrödinger equation. AM1 calculations do not take a great deal of computational time and they are useful for making qualitative observations of reaction systems. They can be reasonably accurate for the types of molecules used in the parameterization, but are often poor for others (Foresman and Frisch, 1996).

Ab initio methods do not use any experimental data, so they are not limited by parameter sets. They use only the laws of quantum mechanics and a variety of mathematical approximations that allow the equations to be solved in a reasonable amount of time. Ab initio methods are computationally intensive, and the accuracy of any properties obtained is strongly dependent on the level of approximation. The simplest ab initio method, Hartree Fock, does not include a complete treatment of the interaction of electrons, so this calculation may not be suitable for calculating properties such as bond dissociation energies. A number of methods have been developed in order to correct for the inadequacies of Hartree Fock, but these add significantly more computational complexity. As a result, some of the molecules of interest in this study may be too large to be computed by these ab initio methods at an appropriate level of accuracy within a reasonable amount of time.

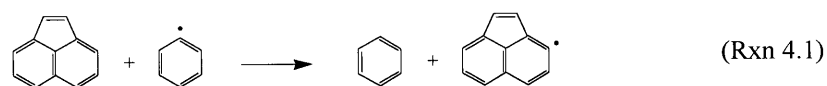
Density functional methods (DFT's) are similar to ab initio methods, but they include electron interaction by utilizing functionals which partition the electronic energy into components, including the kinetic, Coulomb, and exchange-correlation contributions to the energy, which are all computed individually. As a result, a greater accuracy can be obtained with DFT's than for Hartree Fock with a comparable amount of computation time. Various functionals have been developed to estimate the electron spin densities. The functional used in the following calculations, BLYP, is a combination of a method developed by Becke and another developed by Lee, Yang, and Parr, and includes consideration of both the electron densities and their gradients. Ab initio and density functional methods also require a basis set, such as 6-31G*, which mathematically approximates the molecular orbitals. The double-zeta-valence-polarization (DZVP) basis set uses two contracted Gaussian functions to represent each of the valence orbitals.

4.1.1 HEATS OF FORMATION AND H-DISSOCIATION

Thermodynamic calculations were carried out on select PAH using both group additivity and electronic structure methods. Estimations of enthalpies, entropies and heat capacities were first calculated by group additivity using the program THERM (Ritter and Bozzelli, 1991). The heats of formation calculated by group additivity match experimental data well for the small species considered, but this method does not appear to be suitable for the larger species (Table 4.1). AM1 calculations were performed on the same molecules using the MNDO94 package of UNICHEM. Although the geometry optimization procedure of AM1 gives a reasonable starting point for higher

level calculations, the thermodynamic quantities obtained from AM1 are no better than those obtained from the simpler group additivity method.

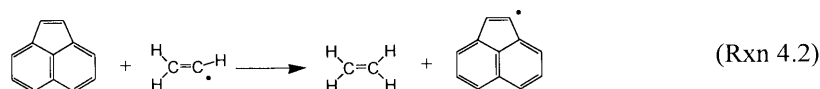
Density functional theory calculations were carried out with the DGAuss package within UniChem¹. The BLYP functional was used in conjunction with the DZVP basis set. Molecular geometries were first optimized using moderate convergence criteria. The final geometry was optimized using tight convergence criteria (gradient convergence threshold $< 5 \times 10^{-4}$, electron density convergence $< 1 \times 10^{-5}$, total energy accuracy $< 1 \times 10^{-7}$) and high numerical accuracy (SCF=23, gradient=29) before calculating the vibrational frequencies. The SCF energy (the amount of energy released by bringing each atom of a molecule from infinity to the final geometry) calculated at the final geometry was then added to the zero-point vibrational energy (the vibrational energy of the molecule at 0 K) and the enthalpy correction at 298 K. However, this energy, calculated in hartrees (1hartree = 627.51 kcal/mol), is not equivalent to the heat of formation, but can be used to evaluate reaction enthalpies. The heat of formation ($\Delta H_{f,298}^{\circ}$) of the molecule of interest can then be backed out if the $\Delta H_{f,298}^{\circ}$ of the other compounds involved in the reaction are known. This calculation works best when the reaction considered is *isodesmic*, maintaining the same overall number and types of bonds (Foresman and Frisch, 1996) as in Rxn. 4.1.



In this case, the $\Delta H_{f,298}^{\circ}$ for the acenaphthyl radical can be calculated from the heat of the reaction and the experimental $\Delta H_{f,298}^{\circ}$ of acenaphthylene, benzene and the phenyl radical (Table 4.1). The experimental values have been obtained from the most recent version of the NIST database (<http://webbook.nist.gov>). Experimental values were not available for cyclopenta[def]phenanthrene or cyclopenta[cd]pyrene. Even if the DFT method is highly accurate, the resulting heats of formation and bond dissociation energies can be only as accurate as the experimental values involved in their calculation.

In some cases the radical site of interest may be better represented by a different reaction. Similar computations were therefore performed, but replacing benzene and phenyl with ethylene and vinyl (Rxn 4.2). This had the effect of lowering the heats of formation by approximately 1 kcal/mol, which is within the error of the experimental values for vinyl and phenyl. For the sake of consistency, all further calculations will use the values obtained from Rxn 4.1.

¹ UniChem and DGAuss are trademarks of Oxford Molecular Group, PLC.



The vibrational frequencies calculated by the DFT method lead directly to the heat capacities and entropies for the molecules, which are calculated by UniChem. The dependence of the enthalpies and entropies on temperature are tabulated in Appendix D along with the SCF and zero-point energies for each molecule considered in this study. The entropies calculated by UniChem have been adjusted lower by $R[\ln(\sigma)]$, where R is the gas constant and σ is the symmetry number for the molecule. The C-H bond dissociation energy ($\Delta H_{\text{diss},298}^{\circ}$) for each radical site was calculated from the $\Delta H_{f,298}$ for the radical, its parent PAH, and the hydrogen atom.

Table 4.1 Standard Heats of Formation and H-Dissociation Energies

Compound ^a	$\Delta H_{f,298}^{\circ}$ Experimental kcal/mol	$\Delta H_{f,298}^{\circ}$ Group Add. kcal/mol	$\Delta H_{f,298}^{\circ}$ AM1 kcal/mol	$\Delta H_{f,298}^{\circ}$ BLYP kcal/mol	$\Delta H_{\text{diss},298}^{\circ}$ BLYP ^b kcal/mol
Hydrogen Atom	52.10311 Chase (1998)				
Ethylene	12.5399 Chase (1998)	12.52	16.471		
Vinyl	71.5 ± 1.2 Tsang (1996)	70.42	60.456		111.063 (Experimental)
Benzene	19.82 ± 0.12 Prosen et al. (1945)	19.80	22.026		
Phenyl	81.0 ± 1.9 Tsang (1996)	81.35	73.146		113.283 (Experimental)
Toluene	11.95 ± 0.15 Prosen et al. (1945)	11.81	14.411		
Benzyl	49.5 ± 1.0 Tsang (1996)	49.51	38.556	49.957	89.627
Naphthalene	35.99 ± 0.26 Coleman and Pilcher (1966)	36.32	40.583		
1-Naphthyl		96.37	88.778	96.946	113.059
2-Naphthyl		96.87	88.756	97.195	113.308
Acenaphthylene	61.7 ± 1.4 Boyd et al. (1965)	54.66	80.745		
1-Acenaphthyl		112.56	138.102	126.726	117.129
3-Acenaphthyl		114.71	130.469	122.476	112.879
4-Acenaphthyl		116.21	128.463	122.734	113.137
5-Acenaphthyl		114.71	130.044	123.212	113.615
Pyrene	53.94 ± 0.31 Smith et al. (1980)	62.76	67.359		
1-Pyrenyl		122.81	118.581	115.241	113.404
2-Pyrenyl		124.31	109.617	115.152	113.315
4-Pyrenyl		122.81	117.579	115.048	113.211
Cyclopentaphenanthrene		51.72	76.526		
4-Cyclopentaphenanthrene		86.62	119.291		81.438
Cyclopenta[cd]pyrene		79.64	109.424		
4-Cyclopenta[cd]pyrene		135.54	162.253		117.297

^aNumbering schemes for these PAH are shown in Appendix D; ^bunless otherwise noted

Except for the calculation of the properties of the methyl and methylene-type radicals, the reaction enthalpies of the isodesmic reactions are no more than a few kcal/mol. This suggests that good estimations of $\Delta H_{f,298}$ are obtained for the radicals, within the error of the experimental values. Although no study was conducted to estimate the uncertainties in the calculations, the bond dissociation energies to form the aryl radicals are believed to be accurate to within 0.3 kcal/mol *relative to each other*. The uncertainties in the bond energies of the non-aryl bonds relative to the aryl bonds are estimated to be 1-2 kcal/mol.

The bond dissociation energies for all of the aryl σ radicals are roughly equivalent, with less than 1 kcal/mol differences between all of the sites listed. This finding is in agreement with Cioslowski et al. (1996), who by way of similar DFT methods found evidence that the unpaired σ electrons had virtually no interaction with the π structure of the PAH. The loss of hydrogen deforms the ring structures, increasing the bond angle at the radical site by approximately 6° for *each* of the aryl radicals studied (from 122.5° to 128.2° for the 4-position of acenaphthylene – see Figure 4.1), again suggesting that the size of the overall structure does not affect the local radical site. It must be noted that sterically hindered sites, such as “bay regions”, were not analyzed and may show significantly different behavior.

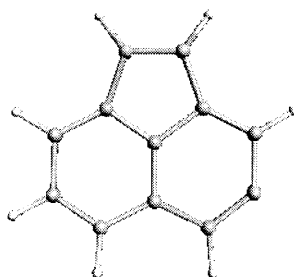


Figure 4.1 Optimized geometry of 4-acenaphthyl radical from BLYP/DZVP calculations

The thermodynamics of the benzyl radical was calculated as in the above method, but using three different pairs of isodesmic partners: benzene/phenyl, ethylene/vinyl, and ethane/ethyl. The differences between the calculations of heat of formation of benzyl and its experimental value are +0.5, -0.6, and -1.4 kcal/mol respectively. The validity of using the benzene/phenyl reaction (Rxn. 4.2) is affirmed as it performs best even for this bond type.

The benzyl radical is planar, with the radical site aligned with the aromatic π structure. The stability gained by this alignment makes the methyl C-H bond in toluene 15 kcal/mol weaker than that of ethane. The methylene group of cyclopenta[def]phenanthrene shows similar behavior, though its C-H bond energy is 8 kcal/mol weaker

than that of toluene, presumably because of greater interaction with the π system, and is in close agreement with the estimation by Howard (1990). The methylene C-H bond in cyclopenta[def]phenanthrene is nearly 1% longer than the aryl C-H bonds (1.106 vs. 1.097 Å), consistent with a weaker bond strength.

The vinyl-type C-H bonds on the five-membered ring of acenaphthylene were calculated to be 5 kcal/mol stronger than the aryl C-H bonds, which was surprising, because the C-H bond energy for ethylene is 2 kcal/mol lower than that for benzene. It was initially believed that the radical site of 1-acenaphthyl would behave more like the vinyl radical, however, when ethylene loses a hydrogen, the hydrogen adjacent to the radical site adjusts by almost 15° to fill in the void, while the loss of a hydrogen from the 5-membered ring of acenaphthylene results in only a 4° adjustment (as calculated by the DFT method). The C-C bonds in the 5-membered ring are relatively restricted, and upon radical generation any increase in the internal bond angle at the radical site adds more strain to the rest of the ring (which is already significantly strained), so the radical on the 5-membered ring is less stable than the vinyl radical. Consequentially, the bond lengths of the C-H bonds on the 5-membered ring are 0.003 Å shorter than those of the aryl C-H bonds.

The energy required to remove a hydrogen from cyclopenta[cd]pyrene to form 4-cyclopenta[cd]pyrenyl radical (having a radical site on the 5-membered ring of cyclopenta[cd]pyrene) was within 0.2 kcal/mol of the C-H bond energies of the 5-membered ring of acenaphthylene. This agreement suggests that the C-H bond energies are similar and that, like the aryl radicals, the σ radicals on vinyl-type 5-membered rings of PAH are not affected by the size of the molecule.

4.1.2 EQUILIBRIUM CALCULATIONS

The first step of the PAH growth process is generally believed to be reversible hydrogen abstraction from the PAH to produce a PAH radical. Most of the abstraction is believed to be caused by hydrogen atoms, which are the most prevalent radicals in the flames studied (Rxn 4.3).



Although the PAH growth region in the flame is considered to be far from equilibrium, it is interesting to determine just how far these particular species are from equilibrium. Also, if PAH and their radicals could be taken to be in equilibrium with hydrogen in an empirical sense, the flame kinetic model would be drastically simplified. To investigate this, the Gibbs free energy (ΔG_{rxn}) of Rxn 4.3 was calculated at 1800 K. This temperature was chosen

because it is the temperature at the flame position where most of the PAH were observed to peak in the $\phi=1.8$ flame by Bittner (1981). The ΔG 's for the PAH and PAH radicals were extracted from the BLYP/DZVP calculation output of enthalpy and entropy, while the temperature dependence of enthalpy and entropy for H \cdot and H₂ were taken from experimental measurements from the NIST database.

The equilibrium constant for Rxn 4.3 was then computed by Eqn. 4.1:

$$K = \frac{[\text{PAH}\cdot][\text{H}_2]}{[\text{PAH}][\text{H}\cdot]} = e^{-\Delta G_{\text{rxn}}/RT} \quad (\text{Eqn 4.1})$$

where T = temperature (1800 K) and R = the gas constant. Experimental mole fractions for H (.00238) and H₂ (.0727) were also taken from the data of Bittner at the approximate point where the PAH peak *in his measurements* (0.86 cm height above burner). The equilibrium concentrations of the PAH radicals relative to their parent PAH were calculated, along with the actual relative *peak* concentrations taken from the $\phi=1.8$ data of this study, and the results are presented in Tables 4.2, 4.3, and 4.4. The relative prevalence of each radical calculated from equilibrium and experimental data is also listed. The uncertainty in this calculation is estimated to be a factor of 3, because the temperature and concentration gradients are very high in this region of the flame, and the actual sampling position due to distortions by the probe is not well defined. In addition, this calculation does not take into account the disagreement in the location of the peak concentrations measured by Bittner and this study, as the reason for the difference has not been identified. Finally, the uncertainty in the estimation of the entropy, which contributes strongly to the free energy at flame temperatures, is not known.

The experimentally measured flame concentrations of naphthyl radical (Table 4.2) are approximately 10% of the equilibrium concentrations. As expected, kinetics dominate over the thermodynamics of this reaction in the PAH formation and consumption region of the flame. Since there are 2 sets of 4 identical C-H bonds in naphthalene, at equilibrium conditions, each *individual* site would have a 2-3% probability of being a radical. The dissociation energy for the beta C-H bond is calculated to be 0.3 kcal/mol lower than that of the alpha site, giving rise to a higher equilibrium concentration of the beta radical. Although these values are within the calculation uncertainties, they are consistent with arylation kinetics studies, in which the 1-position of naphthalene was found to form weaker bonds with arenes, and subsequent computations of C-H bond strengths (Chen et al., 1989). However, the experimental data shows that the 2-naphthyl radical is more prevalent in the flames. The disagreement suggests

different formation and/or destruction kinetics for the two radicals; either 1-naphthyl is formed preferentially, or 2-naphthyl is consumed preferentially.

Table 4.2 Naphthalene/Hydrogen Equilibrium

Compound [X]	Calculated Equilibrium [X]/[C ₁₀ H ₈], 1800K	Experimental Peak [X]/[C ₁₀ H ₈]	Calculated Equilib. Relative Mole Frac.	Experimental Peak Relative Mole Frac.
1-Naphthyl	11.3%	0.94%	1	1
2-Naphthyl	10.2%	1.17%	0.90	1.25

The overall calculated equilibrium concentrations of the pyrene radicals are significantly closer to the measured flame concentrations (Table 4.3) than the naphthyl radicals, relative to their parent PAH. The potential mechanisms for the formation and destruction of these compounds are too numerous to speculate on the reason(s) for the difference. Also, the uncertainty in the experimental measurement of the pyrenyl radicals is almost a factor of 2, though it is likely that the values presented are at the low end of the uncertainty range. As in naphthalene, when considering symmetry effects, each individual peripheral carbon has a 2-3% probability of hosting a σ radical site at equilibrium, demonstrating the similarity of the aryl bonds even at high temperature. The differences between the isomers based on the calculations may not be significant (when including symmetry considerations), because there is some question as to the reliability of the entropy calculations for these large compounds.

Table 4.3 Pyrene/Hydrogen Equilibrium

Compound [X]	Calculated Equilibrium [X]/[C ₁₆ H ₁₀], 1800K	Experimental Peak [X]/[C ₁₆ H ₁₀]	Calculated Equilib. Relative Mole Frac.	Experimental Peak Relative Mole Frac.
1-Pyrenyl	8.61%	2.51%	1.00	1.00
2-Pyrenyl	5.69%	2.51%	0.66	1.00
4-Pyrenyl	11.4%	3.39%	1.32	1.35

Some of the acenaphthylene radicals appear to be further from equilibrium conditions (Table 4.4) than the other radicals discussed. Again, in equilibrium conditions, each aryl site has a 2-3% chance of being a radical, but for the sites on the 5-membered ring, this value drops by nearly a factor of 4, which is a result of the higher C-H bond energies only. The experimental concentrations of the 1- and 4-acenaphthyl radicals are approximately 10% of the equilibrium concentrations, which agrees with the naphthyl data. Therefore, it appears that the 3- and 5-acenaphthyl radicals may be involved in unique reactions that keep their concentrations low. Coincidentally, the

closure of the 5-membered ring after the addition of acetylene to 1-naphthyl would form an intermediate π radical at the 3- position that could move to the 5- position by resonance.

Table 4.4 Acenaphthylene/Hydrogen Equilibrium

Compound [X]	Calculated Equilibrium [X]/[C ₁₂ H ₈], 1800K	Experimental Peak [X]/[C ₁₂ H ₈]	Calculated Equilib. Relative Mole Frac.	Experimental Peak Relative Mole Frac.
1-Acenaphthyl	1.43%	0.18%	1.00	1.00
3-Acenaphthyl	5.44%	0.09%	3.80	0.52
4-Acenaphthyl	5.62%	0.58%	3.93	3.23
5-Acenaphthyl	4.71%	0.18%	3.29	1.00

4.2 Flame Model

The flame model developed by Richter et al (1999) and predecessors, which has been tested extensively against the $\phi=1.8$ benzene/oxygen flame by Bittner and Howard (1981), was utilized to compare model predictions with the data from this study.

4.2.1 BASE CASE MODEL

The fullerene formation and soot growth reactions in the model were made inactive, as the $\phi=1.8$ flame produces negligible quantities of both. Acenaphthene, the four acenaphthyl radicals, and the four ethynylacenaphthylenes were added to the species list, and the following reactions were added to account for their formation (Table 4.5):

Table 4.5 Added Reactions for Base Case Kinetic Model

Reaction	A (cm ³ mol ⁻¹ s ⁻¹)	n	Ea (cal/mol)
Acenaphthylene + H = X-Acenaphthyl + H ₂	2.50 x 10 ¹⁴	0.0	16000
Acenaphthylene + OH = X-Acenaphthyl + H ₂ O	2.10 x 10 ¹³	0.0	4600
X-Acenaphthyl + C ₂ H ₂ = X-Ethynylacenaphthylene + H	3.98 x 10 ¹³	0.0	10100
1-Naphthyl + C ₂ H ₄ = Acenaphthene + H	2.51 x 10 ¹²	0.0	6200
C ₅ H ₅ + C ₅ H ₅ = C ₁₀ H ₈ + 2H (A-factor increased 50%)	3.00 x 10 ¹²	0.0	4000

where X = 1, 3, 4, 5 and reaction rate coefficient $k=AT^n e^{-E_a/RT}$

The rate coefficients for the hydrogen abstractions by H and OH were taken from Kiefer et al. (1985) and Madronich and Felder (1985) respectively and applied to formation of all aromatic radicals in the model, including the newly added acenaphthylene radicals. The rate coefficient found for the reaction $phenyl + C_2H_2 \leftrightarrow phenylacetylene + H$ by Fahr and Stein (1988) was used for all acetylene addition reactions to PAH in the model, including the reaction in Table 4.5, because it is the only available experimental rate coefficient for acetylene addition to aromatic radicals at high temperatures. The application of these reactions to all PAH in the model appears to be valid, given the findings in Section 1.2 that PAH aryl C-H bonds are very similar. Less appropriate is the use of the same acetylene addition rate coefficient for the reaction $1-naphthyl + C_2H_2 \leftrightarrow acenaphthylene + H$, which includes a ring closure that has an unknown effect on the rate of reaction, but no better model reaction is currently available. A similar questionable rate constant was used for the addition of ethylene to naphthyl to form acenaphthene (Fahr and Stein, 1988). Finally, the pre-exponential factor for cyclopentadienyl combination to form naphthalene, which is the dominant naphthalene formation pathway in the model, was increased by 50% to bring the computed naphthalene concentration up to the experimental level, as this was the starting point for analyzing the mechanism. The increase was well within the uncertainty in the rate of this reaction (Richter et al., 1999).

Computations were performed with PREMIX (Kee, et al., 1997), using the experimental temperature profile from Bittner and Howard (1981). The thermodynamics properties for the added species were computed by group additivity using THERM (Ritter and Bozzelli, 1991). Transport parameters were taken from the calculations for compounds of similar size and structure to the added species.

The experimental and model-calculated mole fractions for several species are shown in Figure 4.2. Naphthalene and indene peak concentrations match the experimental values well, though the model depicts slower rates of consumption for both. The model predicts the naphthyl radicals to peak at concentrations approximately half of those measured, but it does correctly predict that 1-naphthyl is less prevalent, most likely because 1-naphthyl has an additional consumption pathway through acenaphthylene. The 1-naphthyl concentration peaks at the same point as the naphthalene concentration, which is consistent with experimental results, but the predicted 2-naphthyl peak is shifted significantly downstream. The differences between the model and experimental results for the naphthyl radicals are magnified for the ethylnaphthalenes, which is to be expected since they are formed directly from the radicals.

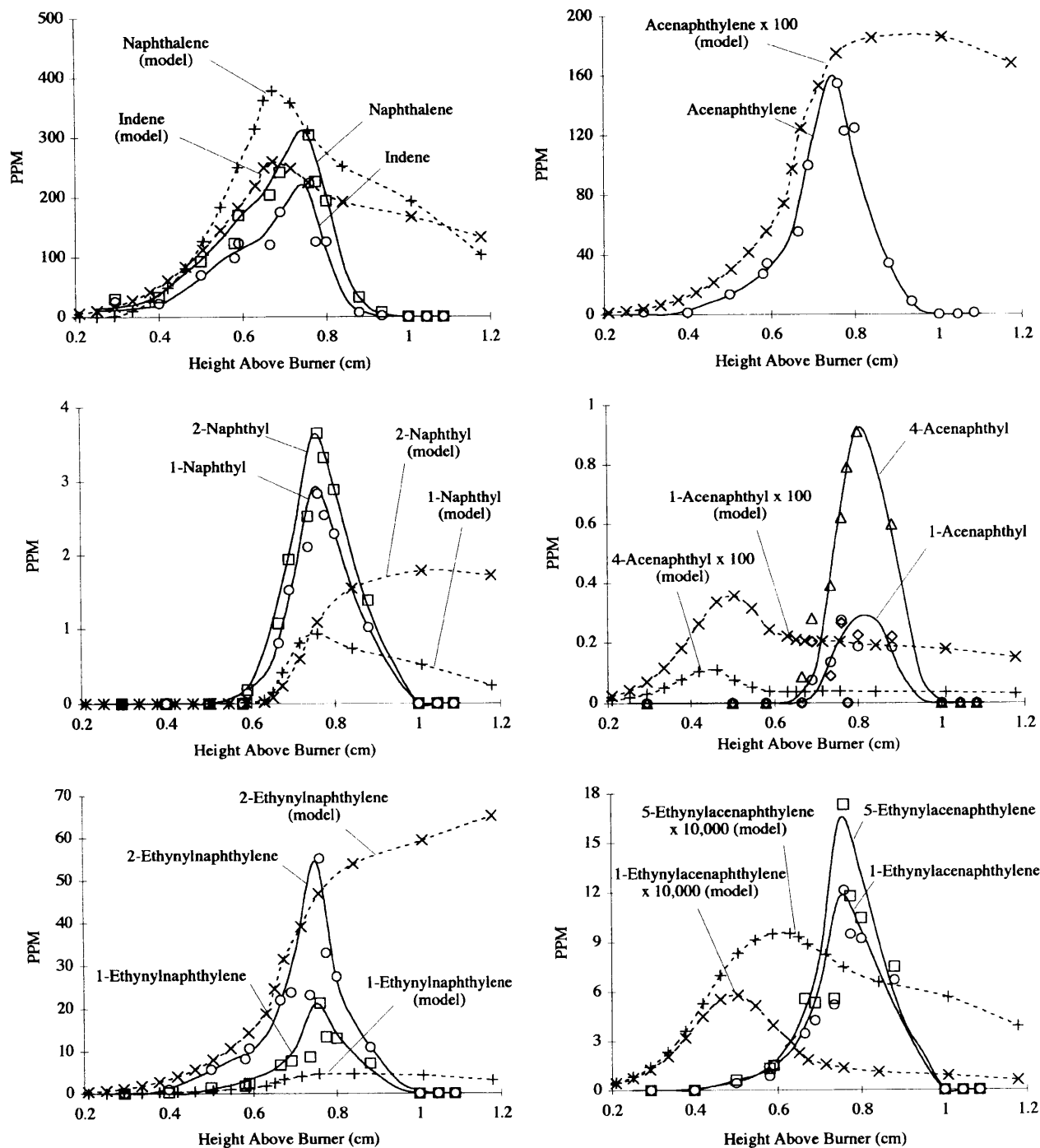


Figure 4.2 Base case model results for naphthalene, acenaphthylene, and related species.

In the base case model, the acenaphthylene concentration is two orders of magnitude lower than the experimental results. As a sensitivity test, the rate constant for acetylene addition to naphthyl was increased by a factor of 10, and the peak acenaphthylene concentration increased by a factor of 4. Similarly, dividing the activation

energy for this reaction by half resulted in a 6-fold increase in the peak acenaphthylene concentration. However, these drastic changes could not bring the acenaphthylene prediction within an order of magnitude of the experimental observations. This suggests that there is another dominant pathway to acenaphthylene. Hausmann et al. (1992) also postulated that another acenaphthylene formation mechanism exists at low positions in their benzene flame, because acenaphthylene was seen to form before the 1-naphthyl radical. One potential mechanism is through PAH isomerization, which has been found to readily occur between species such as fluoranthene and acephenanthrylene (Scott and Roelofs, 1987). Wiersum and Jenneskens (1993) found that the flash-vacuum pyrolysis of biphenylene at 900° C produced acenaphthylene in almost 100% yield. Brown et al. (1994) suggested that this rearrangement occurs by formation of a biphenyl diradical, which then undergoes ring contractions to form acenaphthylene. A recent unpublished study found that similar pyrolysis of biphenyl and pyrolysis of 2-bromobiphenyl (a precursor to the biphenyl-2-yl radical) also produce acenaphthylene in high yield (Scott, 1999). Therefore, a pathway is proposed for the formation of acenaphthylene by combination of phenyl radicals (Figure 4.3), which is similar to the combination of cyclopentadienyl radicals to make naphthalene, found in this model to be the predominant naphthalene formation pathway. A second similar mechanism could involve a reaction between a phenyl radical and benzene. Since the aromatic system must be temporarily destroyed in this second pathway, the energy barrier is much higher than for the radical combination reaction, but the concentration of benzene far exceeds that of the phenyl radical, so the overall rate may be significant.

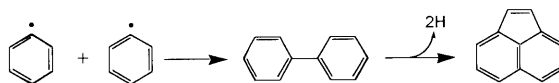


Figure 4.3 Acenaphthylene formation via biphenyl

In a separate computation, the rate coefficients in the model were adjusted by QRRK methods to be applicable at atmospheric pressure, and the model was used to study the ethylene jet-stirred/plug flow reactor (JSR/PFR) data collected by Marr (1993). In this case, the acenaphthylene concentration was within a factor of 2 of the experimental value, while the naphthalene concentration was predicted to be up to a factor of 3 too low (Richter, 1999), which suggests that the acenaphthylene formation chemistry is already adequate for the ethylene system. A possible reason for the disparity between the model's performance in the two systems is the greater concentration of benzene and phenyl radicals in the benzene flame, which may force the pathway in Figure 4.3 to become dominant.

The low prediction of acenaphthylene translates into low predictions for the acenaphthyl radicals and the ethynylacenaphthylenes (Figure 4.2). The differences among the radicals and ethynyl species must be due to the thermodynamics calculated from group additivity, as the same reactions and rate coefficients apply to each. Interestingly, each of these species peak significantly earlier than acenaphthylene, even though they are formed as *products* of reactions with acenaphthylene. Although this behavior is not mirrored in the experimental data, it is a good example of how the chemical mechanism can have unpredicted results. This observation casts doubts on the interpretation of Hausmann et al. (1992), who concluded that PAH radical species must be products of their parent species rather than precursors because the radical concentration profiles were found to peak downstream of the stable species. Acenaphthene was also underpredicted, but by 7 orders of magnitude.

The phenanthrene concentration is within a factor of 3 of the experimental value and the relative relationship with anthracene is predicted correctly, though like most species, the consumption of each is too slow (Figure 4.4), either because PAH oxidation is not adequately modeled or because the PAH are consumed to form larger hydrocarbons via pathways not considered in the model (e.g., radical reactive coagulation). The concentrations of fluoranthene and pyrene are far lower than the experimental measurements from this study, though they are in good agreement with the data from Bittner and Howard (1981), which was used predominantly in the development of this model. This may suggest the existence of pathways for the formation of pyrene and fluoranthene other than those in the model.

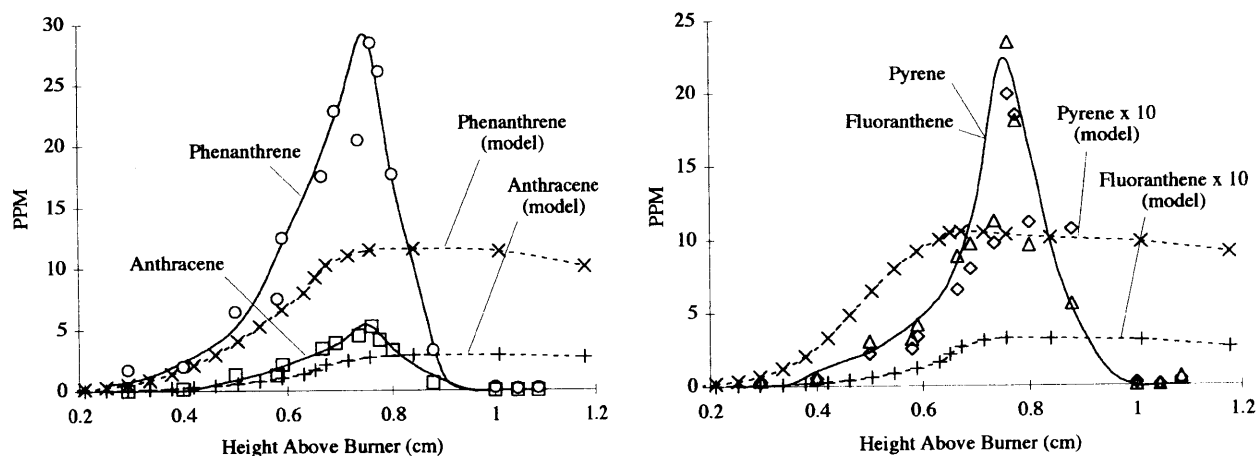


Figure 4.4 Base case model results for the mass 178 and mass 202 species.

4.3.2 MODIFIED MODEL

The reactions added to the base case model are listed in Table 4.6. The rate coefficient for the combination of cyclopentadienyl radicals to form naphthalene was used for the combination of phenyl radicals to make both acenaphthylene and acenaphthene. A pathway between acenaphthylene and acenaphthene was added, with the rate coefficient for the dehydrogenation of 1,3-cyclohexadiene to make benzene (Orchard and Thrush, 1974). Finally, the formation of fluoranthene by acetylene addition to 1-ethynylacenaphthylene was added, using the same rate coefficients for the formation of other 6-membered rings within the model.

Table 4.6 Modifications to the Base Case Model

Reaction	A (cm ³ mol ⁻¹ s ⁻¹)	n	Ea (cal/mol)
C ₆ H ₅ + C ₆ H ₅ = Acenaphthylene + 2H	3.00 x 10 ¹²	0.0	4000
C ₆ H ₅ + C ₆ H ₅ = Acenaphthene	3.00 x 10 ¹²	0.0	4000
Acenaphthene = Acenaphthylene + H ₂	4.70 x 10 ¹³	0.0	61660
1-Ethynylacenaphthylene + H = 1-Ethynyl-2-acenaphthyl + H ₂	2.50 x 10 ¹⁴	0.0	16000
1-Ethynylacenaphthylene + OH = 1-Ethynyl-2-acenaphthyl + H ₂ O	2.10 x 10 ¹³	0.0	4600
1-Ethynyl-2-acenaphthyl + C ₂ H ₂ = Fluorethenyl	3.98 x 10 ¹³	0.0	10100
Fluorethenyl + H = Fluoranthene	5.00 x 10 ¹³	0.0	0

Next, thermodynamic properties derived from DFT calculations for naphthalene, acenaphthylene, and the naphthyl and acenaphthyl radicals replaced the corresponding group additivity values. This change had a dramatic effect on some of the species. Table 4.7 separates some of the effects of adding the above reactions to the model from the effects of changing the thermodynamic calculation method. Some of the species profiles calculated by the modified model with DFT-generated thermodynamics are plotted in Figures 4.5 and 4.6.

Table 4.7 Effect of Thermodynamics on Model Predictions

Compound	<i>Peak Mole Fractions from Model Calculations (PPM)</i>		
	Base Case Model (Group Additivity)	Modified Model (Group Additivity)	Modified Model (Density Functional Theory)
Naphthalene	3.8 x 10 ⁻⁴	2.9 x 10 ⁻⁴	2.3 x 10 ⁻⁴
Acenaphthylene	1.8 x 10 ⁻⁶	7.0 x 10 ⁻⁶	4.5 x 10 ⁻⁶
1-Naphthyl	9.3 x 10 ⁻⁷	9.8 x 10 ⁻⁷	8.3 x 10 ⁻⁷
1-Acenaphthyl	3.6 x 10 ⁻⁹	2.1 x 10 ⁻⁸	5.4 x 10 ⁻⁷

The addition of the phenyl combination pathway increases the acenaphthylene concentration by nearly a factor of 4 and does not significantly affect the concentrations of either phenyl or biphenyl. But changing to the DFT-generated thermodynamics lowers the acenaphthylene concentration by 35%. The pathway through biphenyl appears to dominate the formation of acenaphthylene, though the concentration of acenaphthylene is still over a factor of 10 too low. An inaccurate prediction of acenaphthylene is to be expected considering that the rate constant for the rearrangement of biphenyl to acenaphthylene is not known, and that the formation of acenaphthylene from reactions between phenyl radicals and benzene was not considered. The increase in the acenaphthylene concentration causes the peak concentrations of the acenaphthylene radicals to increase dramatically, and the DFT-generated thermodynamics cause an additional order-of-magnitude increase, but also force the radical concentrations to remain high in the post-flame region (Figure 4.5), which is due in part to an inadequate prediction of the consumption of acenaphthylene.

The concentrations of the ethynylacenaphthylenes are much higher than in the base case, which is expected as they are formed directly from the acenaphthyl radicals, though much of the 1-ethynylacenaphthylene is consumed in the formation of fluoranthene. An unexpected outcome of the changes is a sharpening of the peaks for indene, naphthalene, and the naphthyl radicals. Acenaphthene concentration is increased by over 4 orders of magnitude over the base case, though the result is still not close to the experimental measurements. The fluoranthene concentration is increased by a factor of 2 because of the added formation pathway, while the pyrene concentration actually decreases slightly (Figure 4.6).

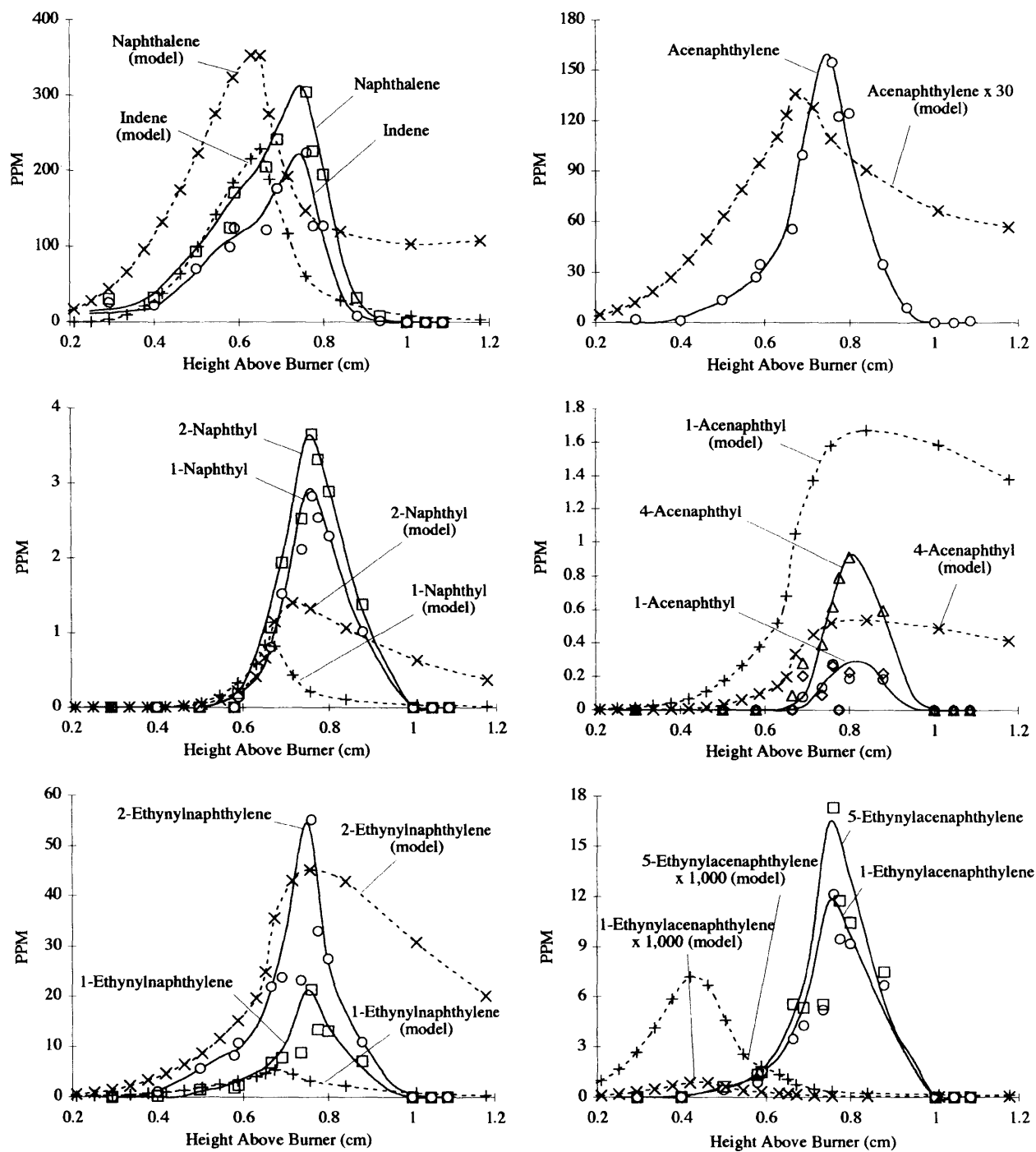


Figure 4.5 Modified model results for naphthalene, acenaphthylene, and related species.

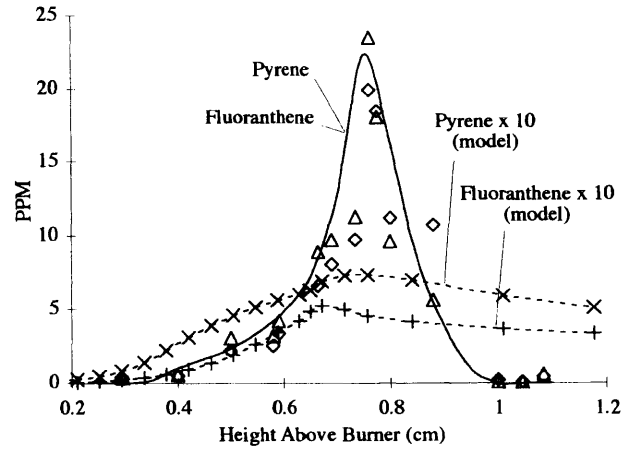


Figure 4.6 Modified model results for the mass 202 species.

Chapter 5

Soot Surface Growth

The formation of soot in flames has been divided into two distinct stages. The first, which occurs close to the flame front, includes an inception and nucleation process thought to involve reactions of heavy PAH molecules leading to particulate species (McKinnon and Howard, 1992). The next stage, which continues into the post-flame (often yellow) portion of the flame, involves growth by coagulation of the particles along with mass addition from molecular reactants, whose identity is an open question.

Though PAH have been widely accepted as the soot inception reactants, they are neglected in many growth models in response to the belief that acetylene alone dominates mass growth (Bockhorn, 1994). Soot growth by C_2H_2 was promoted by Harris and Weiner (1983a) after studying several C_2H_4 -air flat flames. They concluded that only acetylene satisfies the essential requirements for a soot growth reactant and proposed a simple model in which soot mass growth rate is proportional to soot surface area and C_2H_2 concentration. PAH were not measured and were not believed to be in high enough concentrations to be counted as possible soot growth reactants.

In contrast to the simple C_2H_2 model above, PAH have been found to be important soot growth reactants in ethylene combustion in a plug flow reactor (Lam et al., 1989, 1991), in the same system with naphthalene injection (Marr et al., 1992, 1994) and in C_6H_6/O_2 flames (McKinnon and Howard, 1992). Smedley et al. (1992) reached a similar conclusion based on measurements in two ethylene-air flames studied by Harris and Weiner (1989). Furthermore, rate coefficients deduced by fitting the simple C_2H_2 -soot mechanism to data (Harris and Weiner, 1983b) are larger than would be expected for C_2H_2 addition chemistry, consistent with there possibly being a significant contribution of PAH within the C_2H_2 rate coefficient (Howard, 1990). In view of these observations, reassessment of the original basis for the simple C_2H_2 -soot growth mechanism is warranted. To that end, the present study was designed to measure PAH concentrations in the particular flames from which Harris and Weiner (1983a) first formulated their acetylene model and to evaluate the contributions of both PAH and C_2H_2 to soot mass growth in these flames.

5.1 Microprobe Sampling of an Atmospheric Ethylene Flame

Premixed C₂H₄-air flat flames at 1 atm, shielded by an annular N₂ stream, were stabilized on a 5 cm diameter porous plug burner (Figure 5.1). A water-cooled plate ~35 mm above the burner surface helped stabilize the flame and protect the sampling apparatus. The feed rate to the burner was 8.65 l/min (STP) with C/O=0.70 and 0.79 (ϕ =2.1 and 2.4). The flame conditions were the same as used by Harris and Weiner (1983a), though the burner diameter was 1 cm smaller.

The flames were sampled isokinetically at a rate of ~0.60 L/min (STP) by a water-cooled quartz probe with a 1 mm orifice diameter. Flame products at 10 mm, 17 mm, and 25 mm above the burner were collected on cartridge filters (Balston DFU 9933-05), which have been shown to collect the majority of soot and PAH (Marr, 1993). After sampling for 45 min, the filter, probe interior, and connecting lines were washed with dichloromethane (DCM) and the resulting solutions were filtered through a 0.2 mm syringe filter to remove insolubles. The mass of material extracted from the soot and soluble in DCM, denoted " Σ PAH," was measured by weighing a portion of each solution and allowing the DCM to evaporate.

To verify that the extractable material was composed primarily of PAH, each sample was concentrated under nitrogen, exchanged into DMSO, and injected into an HPLC-DAD with a C18 Reverse Phase Vydac Column. Peak areas were converted to concentrations for select PAH by calibration with a 16 PAH standard. By observing species which had similar UV spectra, the calibrations were extended to approximate concentrations of most of the remaining identified PAH.

Soot samples were collected from the flames using the same sampling apparatus, but with the massive cartridge filter replaced by a lighter 0.22 mm flat Teflon filter to permit accurate weighing of the collected soot. The filter, probe, and connecting lines were washed with DCM to remove all soot, and each solution was filtered through a second 0.22 mm filter. The material on the filter was dried in a dessicator and weighed, and the result was used to calculate the soot concentration in the flame. Soot particle sizes were measured with a TUPCON 002B high resolution electron microscope, operated at 200 keV. Soot from the filter was dispersed in toluene using intense ultrasonic agitation, and a drop of the suspension was evaporated on holey carbon film supported on a 200 mesh copper grid.

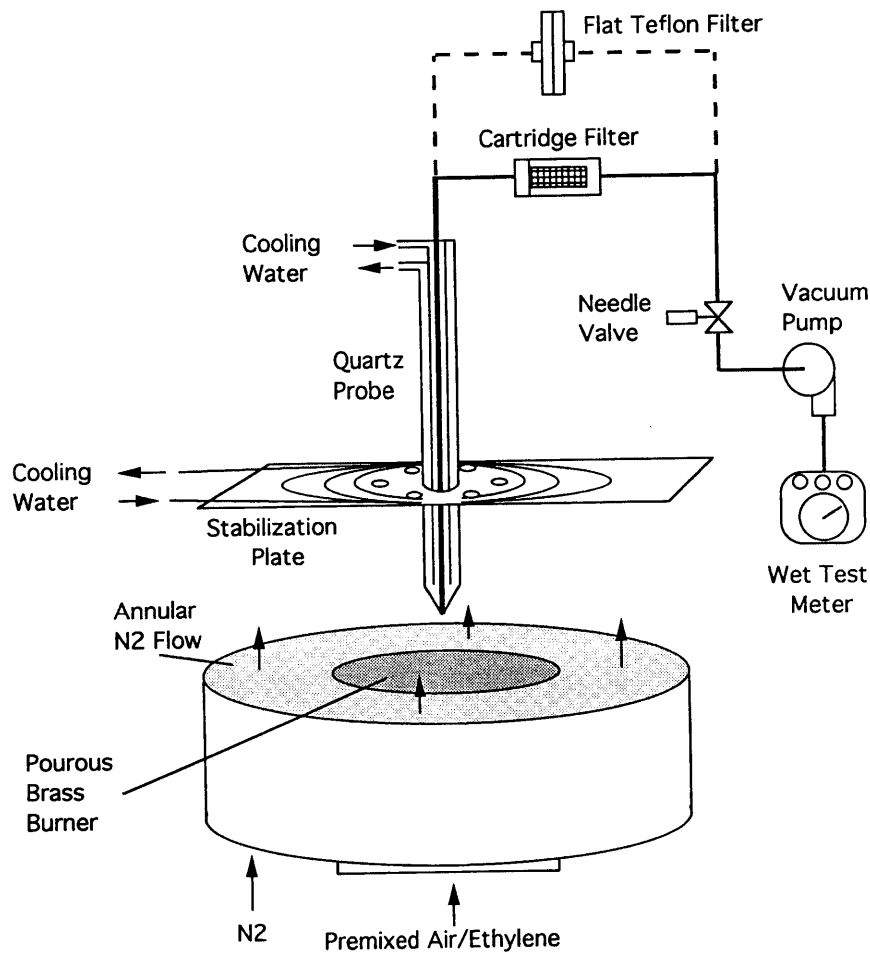


Figure 5.1 Atmospheric flame burner and sampling apparatus

5.2 Results

Soot concentration profiles for the $C/O=0.79$ flame are compared in Fig. 1 to the previous results (Harris and Weiner, 1983a), which were obtained by light absorption measurements and are 3-times higher than the present measurements throughout the post-flame region. Choi et al. (1995) recently reported optically measured soot concentrations to exceed gravimetric measurements by a factor of 2. However, the present results are in excellent agreement with interpolated values from optical measurements of Feitelberg (1993) in similar C_2H_4 flames at $C/O=0.77$ and 0.80, and therefore are employed in this study. The amount of soot retrieved from the $C/O=0.70$ flames was insufficient to make accurate weighings, so the previous soot concentration measurements (Harris and Weiner, 1983a), reduced by a factor of 3 as for the $C/O=0.79$ case, are used here.

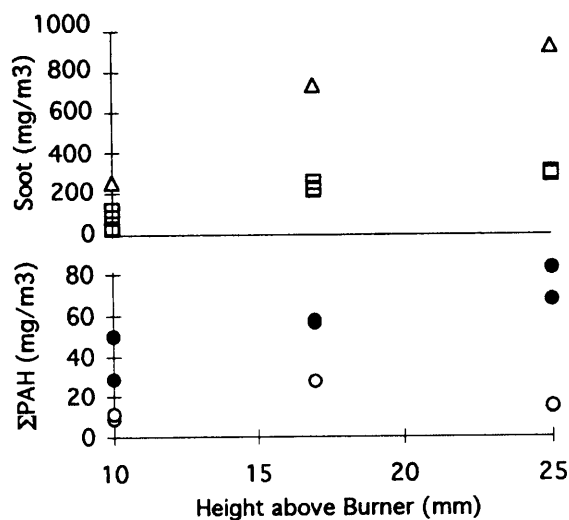


Figure 5.2 Soot and Σ PAH concentrations at different positions in flame. C/O = 0.79 (□, ●, ○); 0.70 (○). Data source: present study (□, Δ, ●); Harris and Weiner, 1983a (Δ).

Twenty-six PAH were individually identified by HPLC from the extracted solutions (Figure 5.3) and are shown in Table 5.1. These species account for 49% of the Σ PAH mass. Whether the discrepancy is due solely to high molecular weight PAH not seen by HPLC or in part to inaccuracies in the calibration assumptions is not known. Fourteen of the identified PAH, accounting for an estimated 70% by mass of the identified species, contain in their periphery 5-membered rings.

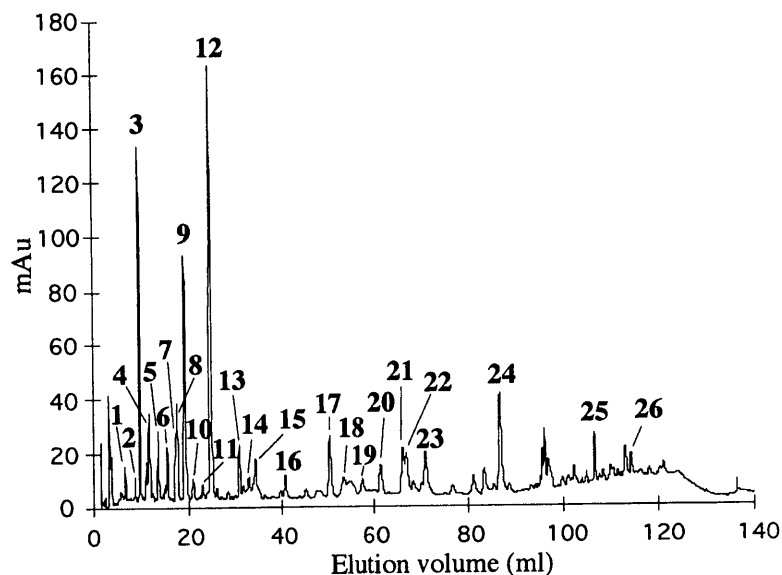
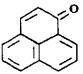
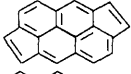
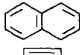
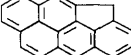
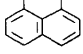
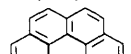
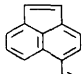
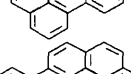
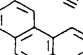
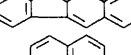
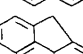
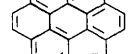
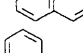
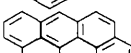
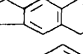
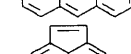
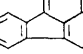
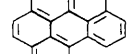
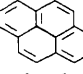
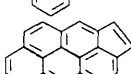
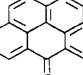
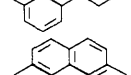
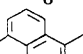
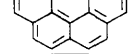
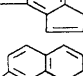
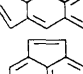


Figure 5.3 HPLC chromatogram of soot extract at 368 nm wavelength (C/O=0.70, 10 mm).

Table 5.1 Identified flame compounds and their estimated mass fractions of total PAH.

Structure	Formula	Mass	Name	Mass % of ΣPAH	Structure	Formula	Mass	Name	Mass % of ΣPAH
	C ₁₃ H ₈ O	180	Phenalenone	NA		C ₂₀ H ₁₀	250	Dicyclopenta [cd,jk]pyrene	1.1 ^c
	C ₁₀ H ₈	128	Naphthalene	2.9		C ₂₁ H ₁₂	264	Benzo[a]pyrene w/CH2 bridge	0.6 ^e
	C ₁₂ H ₈	152	Acenaphthylene	12.5		C ₂₂ H ₁₂	276	Benzo[ghi] perylene	1.3
	C ₁₄ H ₈	176	Ethynyl- acenaphthylene	4.0 ^a		C ₂₂ H ₁₂	276	Indeno[1,2,3- cd]pyrene	0.4
	C ₁₄ H ₁₀	178	Phenanthrene	1.2		C ₂₃ H ₁₂	288	Benzo[ghi] perylene w/CH2 bridge	0.2 ^f
	C ₁₅ H ₁₀	190	Cyclopenta[def] phenanthrene	0.5 ^b		C ₂₂ H ₁₂	276	Anthanthrene	0.6 ^g
	C ₁₆ H ₁₀	202	Acephen- anthrylene	0.5 ^c		C ₂₄ H ₁₂	300	Cyclopenta[fg] benzo[ghi] perylene	1.2 ^f
	C ₁₆ H ₁₀	202	Fluoranthene	2.8		C ₂₄ H ₁₂	300	Cyclopenta[cd] benzo[ghi] perylene	0.8 ^g
	C ₁₆ H ₁₀	202	Pyrene	4.1		C ₂₄ H ₁₂	300	Coronene	0.8 ^h
	C ₁₉ H ₁₀ O	254	6H-Benzo[cd] pyren-6-one	NA		C ₂₆ H ₁₂	324	Cyclopenta- coronene	1.8 ^h
	C ₁₈ H ₁₀	226	Cyclopentaace- phenanthrylene	0.4 ^d		C ₃₀ H ₁₄	374	Naphtho[8,1,2- acb]coronene	0.6 ^f
	C ₁₈ H ₁₀	226	Cyclopenta[cd] pyrene	9.4 ^c		C ₃₂ H ₁₄	398	Ovalene	0.05 ^h
	C ₂₀ H ₁₀	250	Dicyclopenta [cd,mn]pyrene	1.1 ^c					
	C ₂₀ H ₁₀	250	Dicyclopenta [cd,fg]pyrene	0.4 ^c					

Quantitation done using calibration for ^a Acenaphthylene, ^b Phenanthrene, ^c Fluoranthene, ^d Pyrene, ^e Benzo[a]pyrene, ^f Benzo[ghi]perylene, ^g Indeno[1,2,3-cd]pyrene, ^h Dibenzo[ah]anthracene. NA = Identified but not quantified.

Additional measurements and properties obtained from other studies are given in Table 5.2. Flame temperatures and C₂H₂ concentrations for the C/O=0.79 flame were obtained by interpolation of measurements in similar C/O=0.77 and 0.80 flames (Feitelberg, 1993). An average temperature and C₂H₂ concentration for the C/O=0.70 flame were obtained from data of Bönig et al (1990). In both flames, the total number of moles in the region studied was assumed to be 50% larger than the feed value.

Table 5.2 Additional measurements and calculated values.

	10 mm	17 mm	25 mm
C/O = 0.79			
Temperature (K)	1750	1700	1660
Soot particle diameter (nm)	9.2	13	25
Soot number density (cm ⁻³)	1x10 ¹¹	1x10 ¹¹	2x10 ¹⁰
C ₂ H ₂ mole fraction	0.032	0.028	0.026
C/O = 0.70			
Temperature (K)	1700	1700	1700
Soot particle diameter (nm)	4.8	7.4	14
Soot number density (cm ⁻³)	1x10 ¹¹	1x10 ¹¹	2x10 ¹⁰
C ₂ H ₂ mole fraction	0.013	0.013	0.013

Σ PAH was taken to have an average molecular weight of 200 g/mol, based on the molecular weights and mass fractions of the identified compounds, and an average collision diameter of 0.74 nm (Pope, 1988). Soot particles were approximated as spheres of density 1.8 g/cm³. Soot number densities for the C/O=0.79 flame were calculated from the total mass collected and the average diameter of soot particles from electron micrographs (Table 5.2). The same number densities were assumed to apply also to the C/O=0.70 flame in accordance with the observed invariance of number density with C/O ratio (Haynes et al., 1980).

For each measured point in the post-flame region, soot and Σ PAH concentrations were plotted (Figure 5.2), and the mass growth rates were found by approximating derivatives at each point. Soot and Σ PAH balances were then calculated as follows, assuming (see reaction mechanism in Fig 5.4) PAH growth is the net of C₂H₂ addition to PAH and PAH addition to soot, and soot growth results from addition of C₂H₂ and PAH, ignoring oxidation in view of the fuel-rich post-flame conditions:

$$R_{\text{soot}} = Z_{\text{acet-soot}}\gamma_{\text{acet-soot}}m_{\text{acet}} + Z_{\text{PAH-soot}}\gamma_{\text{PAH-soot}}m_{\text{PAH}} \quad (\text{Eqn. 5.1})$$

$$R_{\Sigma\text{PAH}} = Z_{\text{acet-PAH}}\gamma_{\text{acet-PAH}}m_{\text{acet}} - Z_{\text{PAH-soot}}\gamma_{\text{PAH-soot}}m_{\text{PAH}} \quad (\text{Eqn. 5.2})$$

where R = mass growth rate (g cm⁻³s⁻¹), Z = collision rate calculated from kinetic theory, γ = collision efficiency, and m=molecular mass. Eqn 5.1 and Eqn. 5.2 permit two of the three collision efficiencies to be computed from the

data and known properties. Solving for $\gamma_{\text{PAH-soot}}$ and $\gamma_{\text{acet-soot}}$ in terms of $\beta = \gamma_{\text{acet-PAH}} / \gamma_{\text{acet-soot}}$, and then computing the fraction of the soot mass growth contributed by PAH addition, i.e., $(R_{\text{soot}})_{\text{PAH}} / R_{\text{soot}}$, gives:

$$\gamma_{\text{PAH-soot}} = r_1(\beta - r_2 r_3) / (\beta + r_3) \quad (\text{Eqn. 5.3})$$

$$\gamma_{\text{acet-soot}} = r_4(1 + r_2) / (\beta + r_3) \quad (\text{Eqn. 5.4})$$

$$(R_{\text{soot}})_{\text{PAH}} / R_{\text{soot}} = (\beta - r_2 r_3) / (\beta + r_3) \quad (\text{Eqn. 5.5})$$

where $r_1 = R_{\text{soot}} / Z_{\text{PAH-soot}} m_{\text{PAH}}$, $r_2 = R_{\text{PAH}} / R_{\text{soot}}$, $r_3 = Z_{\text{acet-soot}} / Z_{\text{acet-PAH}}$, and $r_4 = R_{\text{soot}} / Z_{\text{acet-PAH}} m_{\text{acet}}$.

Although $\gamma_{\text{acet-PAH}}$ and $\gamma_{\text{acet-soot}}$ are not well known, their ratio can be approximated closely enough as follows to permit solution of the above equations. Based on observed reaction rates and the various C-H bond energies involved, the reactions involve radicals, and the predominant radical centers or active sites are edge carbons of PAH gaseous molecules or condensed layers (Howard, 1990). The collision efficiency is approximately proportional to the fraction of radical carbons within PAH or soot. For a given temperature and gas composition, this fraction depends on the H/C ratio, i.e., the fraction of carbons that can become active by loss of an H atom, and the types of C-H bonds present. The H/C ratio decreases from near unity for the smallest PAH to 0.4 for the largest PAH identified here (Table 5.1), and from around 0.3 to 0.5 for young soot to ~0.1 for older soot having undergone annealing accompanied by dehydrogenation during longer residence times in the flame. Also, the distribution of C-H bond types, which include those of carbon atoms in 5- and 6-membered rings, trends toward smaller fractions of the more reactive types as the H/C ratio decreases. Therefore the progression to larger PAH and to soot of increasing particle size and age in the flame is accompanied by a decreasing reactivity for carbon addition to the material.

The decrease in reactivity is well known in the case of soot growth (Harris and Weiner, 1983a, Haynes and Wagner, 1982, Bockhorn and Schäfer, 1994, Woods and Haynes, 1994). The trend for soot meets the trend for PAH at the transition from soot precursors to nascent soot particles, the material at the transition being incipient soot. An overall decrease in reactivity during the transition can be expected to result initially from radical recombination and addition and, then, in the incipient soot, intramolecular condensation involving dehydrogenation, cross-linking, and ring formation. Accordingly the reactivity of the soot precursors presumably exceeds that of the

nascent soot particles. Furthermore, $\gamma_{\text{acet-PAH}}$ exceeds the value for soot precursors since the former represents all PAH, among which the soot precursors make up the least reactive fraction. Also, once soot growth is under way, $\gamma_{\text{acet-soot}}$ is always smaller than the value for nascent soot particles. Therefore, the overall reactivities represented by $\gamma_{\text{acet-PAH}}$ and $\gamma_{\text{acet-soot}}$ will differ more than do the reactivities of the soot precursors and the nascent soot particles. Thus $\gamma_{\text{acet-PAH}} / \gamma_{\text{acet-soot}}$ can be assumed to be considerably larger than unity during soot growth, and from Figure 5.4 we conclude that most of the soot growth occurs by PAH addition.

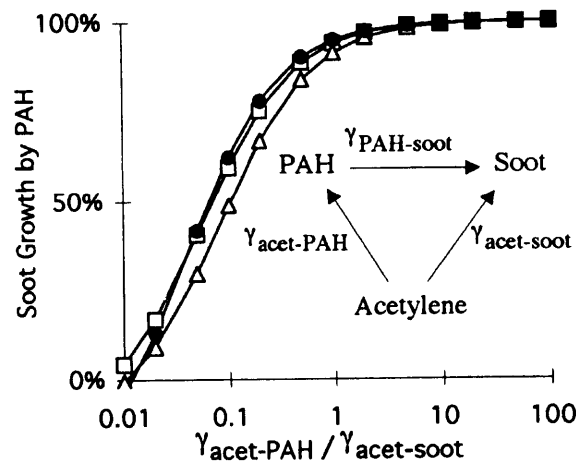


Figure 5.4 Effect of the relative reactivity of soot and Σ PAH on the calculated soot growth contribution by Σ PAH. C/O=0.79. (\square) 10 mm, (Δ) 17 mm, (\bullet) 25 mm.

To calculate representative collision efficiencies, $\gamma_{\text{acet-PAH}} / \gamma_{\text{acet-soot}}$ was set to 1, an underestimation given the above discussion. The collision efficiencies obtained, shown in Figure 5.5, are within the range of values found previously (McKinnon and Howard, 1992, Lam et al., 1989, Marr et al., 1994, Howard, 1990) when the contributions of both C_2H_2 and PAH are taken into account ($\gamma_{\text{acet-soot}} = 1 \times 10^{-5}$ to 7×10^{-4} , $\gamma_{\text{PAH-soot}} = 0.1$ to 0.5). The collision efficiency for PAH with soot is of order 5000 times that for acetylene with soot, presumably reflecting the radical character of many PAH under flame conditions. The relatively high reactivity as well as substantial concentration of PAH in the present flames are reflected by the $\sim 95\%$ or higher contribution of Σ PAH to soot growth in both flames. If the soot concentrations reported by Harris and Weiner (1983a) for the C/O=0.70 flame were used without the factor of 3 reduction described above, both collision efficiencies for this case would roughly double, and the soot growth contribution by PAH would decrease $\sim 5\%$.

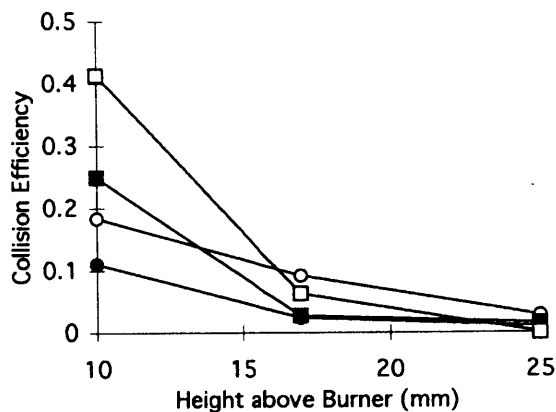


Figure 5.5 Collision efficiencies at different distances from burner.
 $\gamma_{\text{acetylene-soot}} \times 10^4$: (\square) C/O=0.70, (\circ) C/O=0.79.
 $\gamma_{\text{PAH-soot}}$: (\blacksquare) C/O=0.70, (\bullet) C/O=0.79.

Both $\gamma_{\text{acet-soot}}$ and $\gamma_{\text{PAH-soot}}$ drop $\sim 90\%$ through the region studied. This is not inconsistent with the hypothesis that reactivity is controlled by the number of radical sites on PAH and soot, which is expected to decrease significantly as temperature, concentrations of H-abstrating radicals such as H atom, and H/C ratio of the soot all decrease in the post-flame region (Howard, 1990, Mauss et al., 1994). Current experimental work is focusing on this issue.

5.3 Discussion

The present results support the earlier plug flow reactor findings (Lam et al, 1989, 1991, Marr et al, 1992, 1994) regarding the important role of PAH in soot growth and at the same time extend the range of conditions under which this behavior has been observed. The following evidence indicates the behavior may also be important under still other, quite different flame conditions.

Extensive recent studies of soot formation in premixed C_2H_2 -air flat flames at pressures up to 100 bar (Böhm et al., 1992) exhibit features which, combined with the present results, are consistent with an even stronger dominance of PAH over C_2H_2 as a soot-growth reactant than is seen at atmospheric pressure. Data shown in Figure 5.6 reveal, as pointed out by Böhm et al. (1992), that the fraction of the carbon fed which is found as C_2H_2 in the flame decreases with increasing pressure, while the fraction found as ΣPAH changes relatively little. The $\Sigma\text{PAH}/\text{C}_2\text{H}_2$ mass ratio is 100 times larger at 70 bar than at 1 bar where, according to the present study, ΣPAH is already

dominant over C_2H_2 as the soot growth reactant. Therefore, essentially all of the soot growth at the higher pressures would be expected to occur by PAH addition.

Soot mass growth in diffusion flames has recently been modeled along with the gas phase chemistry assuming the growth reaction to be first order in acetylene concentration [C_2H_2] (Lindstedt, 1994). Several different assumptions about the dependence of growth rate on soot surface area were tested by comparing model predictions against experimental data. The best fit was obtained when the growth rate (r_s) was assumed to be independent of soot surface area (Lindstedt, 1994), consistent with other observations from premixed flames (Wieschnowsky et al., 1988) and diffusion flames (Delichatsios, 1994), and proportional to the soot particle number concentration (n_s). The growth rate coefficient, defined as $k = r_s / n_s [C_2H_2]$, was found to be $10^{-12} \text{ m}^3 \text{ s}^{-1} \exp(-12100 / (T/K))$.

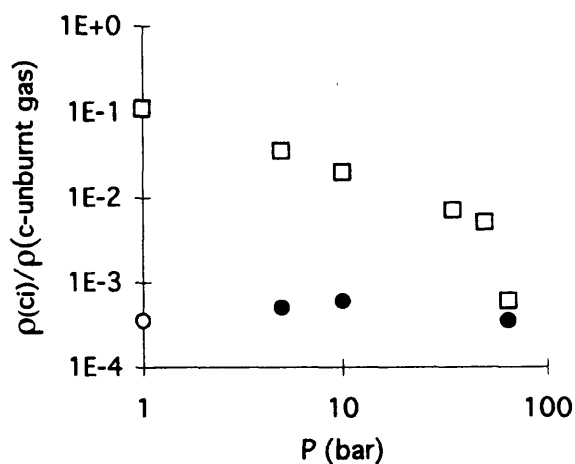


Figure 5.6 Carbon densities of (\square) acetylene and (\bullet , \circ) Σ PAH for premixed C_2H_4 -air flat flames at different pressures. Data: (\circ) present study, distance from burner = 10 mm, $C/O = 0.70$, $v_{unburnt \text{ gas}} = 7 \text{ cm/s}$, $T \sim 1700 \text{ K}$; (\bullet , \square) Böhm et al. (1992), $C/O = 0.68$, $v_{unburnt \text{ gas}} = 6 \text{ cm/s}$, $1600 \leq T_{10\text{mm}} [\text{K}] \leq 1750$.

From simple kinetic theory, k can be shown to correspond to a collision efficiency of

$\gamma_{\text{acet-soot}} = k(2\mu/\pi RT)^{1/2} / \sigma^2$, where σ and μ are the collision diameter and reduced mass for C_2H_2 -soot collisions. At 1700 K, this $\gamma_{\text{acet-soot}}$ decreases from 2 to 10^{-3} as the effective soot particle diameter increases from 1 nm, the smallest particle included in the model fitting (Lindstedt, 1994), to 20 nm, typical of the end of growth. The collision efficiency in principle cannot exceed unity, and should be some factors of 10 less than unity for C_2H_2 addition to a radical site in the possible structures of a 1 nm soot particle. Therefore, the assumed growth of soot by C_2H_2 alone

is clearly an empirical representation of a growth process whose true rate exceeds the fundamental limit of the assumed mechanism. If C_2H_2 is the carbon source for soot growth, a mechanism is required that gives a faster rate of removal of carbon from C_2H_2 than can be achieved with C_2H_2 -soot collisions. Such a mechanism is C_2H_2 addition to PAH, followed by PAH addition to soot (Figure 5.5). Agreement of this mechanism with the data represented by the above k can also be seen from the strong increase in $\gamma_{\text{acet-soot}}$ with decreasing particle size, consistent with the above reasoning that $\gamma_{\text{acet-PAH}}$ exceeds $\gamma_{\text{acet-soot}}$ and hence, from Figure 5.4, consistent with most of the soot mass growth actually coming from PAH addition.

Chapter 6

Conclusions and Recommendations

Low-pressure, fuel-rich premixed benzene flames have been studied by molecular-beam type probe sampling and radical scavenging with dimethyl disulfide, with an emphasis on detailed quantitation of PAH and PAH radicals. Fifty-five compounds were measured throughout the PAH formation and consumption region of the flames, many of which have not previously been equivocally measured in these flames, including 1- and 2-ethylnaphthalene, biphenylene, 1- and 5-ethynylacenaphthylene, and the acenaphthyl, fluoranthenyl, and pyrenyl radicals. Chromatographic separation of some of these compounds required the use of a more polar column than is typically used for PAH analysis. Particular care must be taken in handling flame samples to prevent evaporation and condensation of the compounds of interest, which can drastically affect the quantitation and later interpretations of the data.

PAH analysis by this radical scavenging technique showed that PAH are in significantly higher concentrations in the benzene $\phi=1.8$ flame than were measured by MB/MS studies by Bittner and Howard (1981), presumably because of difficulties in calibrating an MB/MS system for PAH. The observed difference scales with the size of the PAH and ranges from 20% to a factor of 10.

The inventory of PAH less than 300 amu does not change significantly by increasing the equivalence ratio past the sooting limit of the flame, even though the concentration of high molecular weight species (>800 amu) increases by two orders of magnitude. If PAH are the precursors to soot inception, then increasing the sooting potential of a flame speeds up both the formation and consumption pathways of PAH by the same amounts.

Vinyl-PAH radicals that could be produced by acetylene addition to PAH were not detected, nor were π radicals resulting from ring closures. But this observation does not exclude their importance in PAH growth pathways, as they may be too reactive to exist in detectable concentrations.

Acenaphthylene appears to be formed by the addition of C_2H_2 to the 1-naphthyl radical, which is supported by the relative concentrations observed for the naphthyl radical isomers and the ethylnaphthalenes. The formation of acenaphthylene is the easiest explanation for the preferential consumption of the 1-naphthyl species, and is

verified by kinetic modeling of this mechanism. However, the model also suggests that another acenaphthylene formation pathway is necessary in the benzene flame to account for the high concentrations of acenaphthylene. A reaction between two phenyl radicals (or a reaction between phenyl and benzene) and subsequent rearrangement has been postulated as the dominant pathway for the formation of acenaphthylene in the benzene flames. The occurrence of phenyl-phenyl reactions is supported by the high concentration of biphenyl in the flames, while the rearrangement of biphenyl and biphenylene into acenaphthylene has been seen to occur readily at temperatures as low as 1100° C and 900° C respectively.

Ab initio density function calculations show that the aryl C-H bond dissociation energies around the periphery of PAH are roughly the same as those for benzene, regardless of the size of the PAH. The σ radicals created by hydrogen abstractions from PAH are unaffected by the resonance π structures of the PAH. This adds credibility to the application of the hydrogen abstraction and acetylene addition rate coefficients, experimentally measured only for benzene, to the rest of the PAH inventory. The vinyl-type C-H bonds in the five-membered rings of PAH are 4-kcal/mol stronger than their aryl counterparts. The high bond dissociation energy of these vinyl groups may be a result of the inability of the already strained C-C bonds of the 5-membered ring to relax upon loss of the hydrogen, unlike what is observed in the vinyl groups of linear hydrocarbons, or to a lesser extent, the less-strained six-membered rings of PAH. The C-H bonds of the methylene-type 5-membered ring of cyclopenta[def]phenanthrene are 32 kcal/mol weaker than the aryl C-H bonds due in part to stabilization by the adjacent π system.

The concentrations of the PAH radicals measured in this study are 5% to 30% of the values predicted by an assumption of equilibrium with H and H₂ at the point in the flame where PAH concentrations are at their maxima. This suggests that kinetic mechanisms dominate over thermodynamics in the PAH growth and consumption region of the flame, but that thermodynamic considerations can be significant. Thermodynamics predicts that the percentage of PAH that contain a radical site depends almost exclusively on the number of C-H bonds on the periphery of the each molecule. At least in the early stages of the flame, this prediction can be significantly incorrect, presumably because of kinetic effects.

PAH have been measured in the ethylene-air flames studied by Harris and Weiner (1983a) when they concluded that acetylene is the only significant reactant in soot growth. PAH were found in sufficiently high concentrations that their contribution to soot growth appears to be important. Therefore PAH should be considered

reactants in soot growth models. The observed mass growth rates of the total PAH and soot are consistent with a simple mechanism in which both C_2H_2 and PAH react with soot, and C_2H_2 also reacts with PAH. The PAH-soot reaction occurs with a collision efficiency of order 5000-times larger than the C_2H_2 -soot value, and contributes 95% or more of the soot mass growth. The relatively high PAH-soot reactivity presumably reflects the radical character of the reaction.

Recommendations

A variety of sampling techniques has produced widely varied measurements of PAH in flames. To improve the quality of some of the measurements from this study, particularly those of the PAH radicals for which quantitation was not straight-forward and for compounds that experience solubility problems, further analytical methods must be developed. These methods may include chromatographic pre-separation to remove the sulfur-containing scavenged radicals from the rest of the PAH, or detection by methods other than MS, including an improved method of equimolar sulfur detection. Additional methylthio-PAH must be synthesized to unequivocally identify PAH radicals other than those discussed in this study.

The differences seen between the measurements of radicals by Hausmann et al. (1992) and this study can be resolved by re-examining the two slightly different flames, but using the same sampling apparatus.

While the rate coefficients for hydrogen abstraction and acetylene addition to benzene can be reasonably applied to PAH, the kinetics of ring closures are very poorly understood. Transition state methods may add insight into the rates of these reactions. Transition state computations may also help to determine the rate of phenyl-phenyl and phenyl-benzene reactions and rearrangement to form acenaphthylene, though the actual rearrangement mechanism is still speculative. Experimentally, the overall rate of reaction may be estimated by the pyrolysis or shock-tube study of phenyl-producing compounds, such as bromobenzene, and the potential intermediate species in the mechanism, biphenyl and biphenylene.

Further ab initio calculations may be useful to draw conclusions regarding the reactivity of PAH. These should include study of the bay region on molecules like phenanthrene, where steric effects may be influential. Also of interest are π radicals generated by hydrogen abstraction, such as indenyl in comparison to π radicals formed by ring closures and destruction of the aromaticity of the benzene ring.

Appendices

Appendix A: Radical Scavenging with Dibromomethane	103
Appendix B: Tabulated Mole Fraction Data	110
Appendix C: Detailed Sampling Procedure	113
Appendix D: Tabulated Thermodynamic Data from DFT Calculations	118

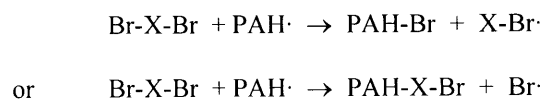
Appendix A: Radical Scavenging with Dibromomethane

Initially, dibromomethane (CH_2Br_2) was used as the radical scavenger in the flame sampling system, because it was believed to be less hazardous and less offensive than DMDS, and had other admirable properties, which are listed below. Initial tests showed dibromomethane to be a poor substitute for DMDS, but the results of these tests are presented for future reference.

A.1 SELECTION CRITERIA

The first criterion for a compound useful in radical scavenging is that the scavenging products must be easy to identify and quantitate. Bromine is particularly useful as an adduct in this regard. Bromine exists as two isotopes in approximately equal parts of masses 79 and 81. Therefore, a bromine-containing compound will typically be seen on a mass spectrum as two equal peaks, separated by two mass numbers. As a result, it is easy to pick out a brominated compound in low concentrations out of a sea of dominating and co-eluting compounds in a GC/MS spectrum. In Figure A.1, bromonaphthalene shows ions at masses 206 and 208. By tracking these mass numbers through the chromatogram, the two isomers of bromonaphthalene can be easily found at the points where these two masses peak together.

Radical scavenging requires that the radical of interest breaks a bond in the scavenger, and one of the two scavenger fragments adds to the radical. So in order to be assured that the scavenged PAH will contain at least one bromine atom, the scavenger must contain at least two bromine atoms:



The scavenger must react and stabilize PAH radicals, but not react with stable PAH. The bond within the scavenger must be significantly weaker than that created in forming a brominated PAH from a radical to ensure scavenging, but it can not be so weak to be reactive with stable PAH, as is the case for Br_2 (Table A.1). The

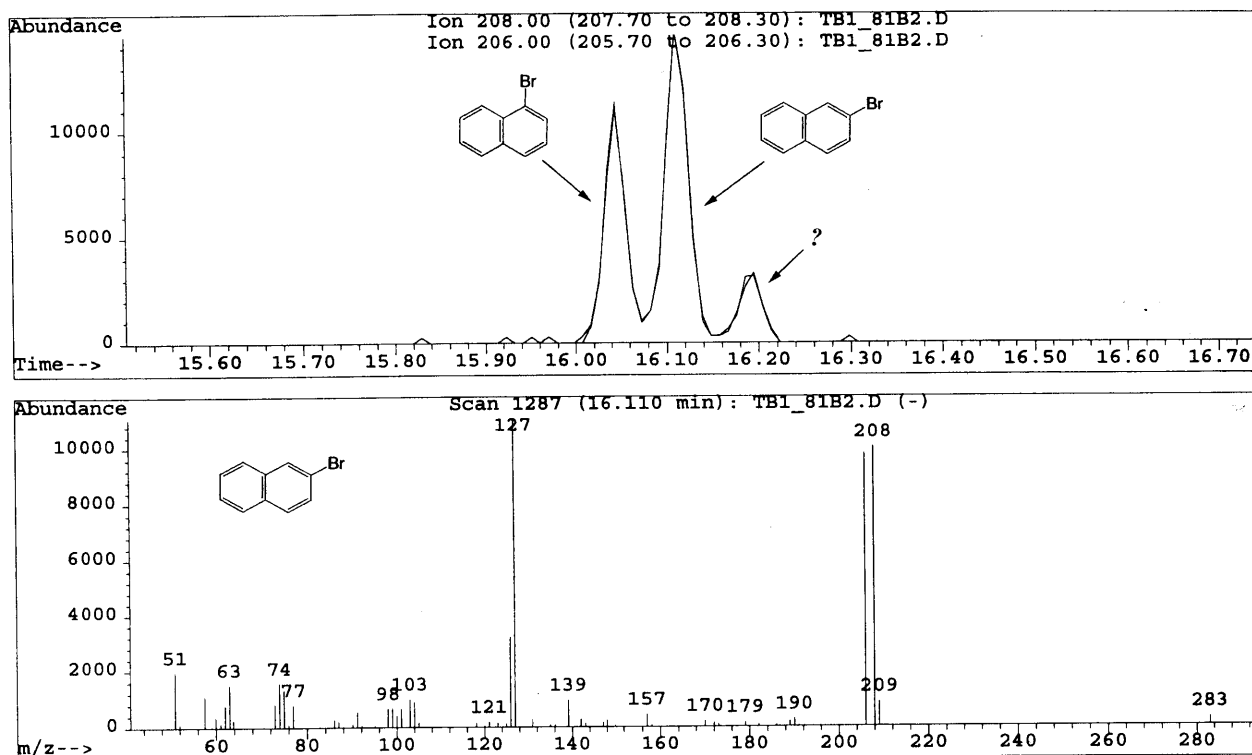


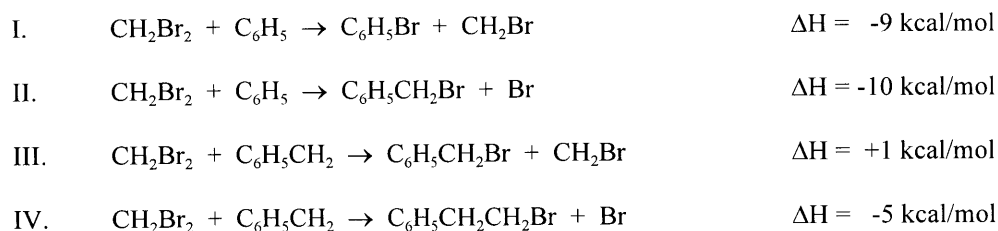
Figure A.1 GC/MS chromatogram of bromonaphthalene and mass spectrum of 1-bromonaphthalene.

thermodynamically feasible scavenging compounds containing bromine, which were commercially available, were those with a carbon center surrounded by halogens and hydrogen. Compounds of this type, which had the physical properties necessary for use, included CH_2Br_2 , CHBr_3 , CClFBr_2 , CHClBr_2 , CFBr_3 , $\text{C}_2\text{F}_4\text{Br}_2$, and $\text{C}_2\text{H}_2\text{Br}_4$. With the small amount of data available to compare the reactivities of these compounds (including reaction rates), the scavenger choice was based on minimizing reaction enthalpies for the scavenging reaction and maximizing enthalpies for side reactions.

Table A.1 Selected Bond Dissociation Energies (Weast, 1985)

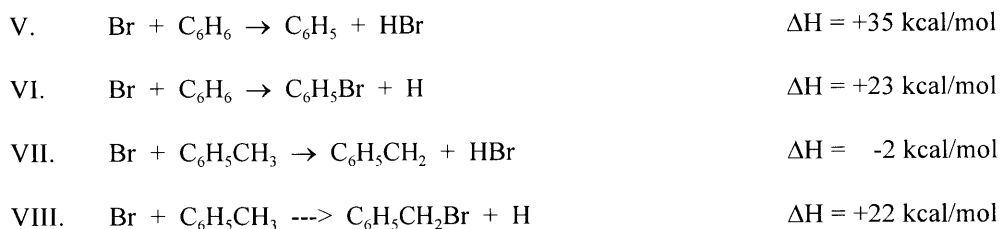
Bond	H_{diss} (kJ/mol)	Bond	H_{diss} (kJ/mol)	Bond	H_{diss} (kJ/mol)
H-C ₆ H ₅	461	Br-C ₆ H ₅	337	Br-CF ₃	295
H-CH ₂ C ₆ H ₅	368	Br-H	366	Br-CHBr ₂	250
H-CHBr ₂	434	Br-CH ₃	293	Br-Br	193

Dibromomethane can react with PAH radicals in essentially two ways. Thermodynamics suggested that the primary scavenging products would be bromomethyl adducts (reactions II and IV):

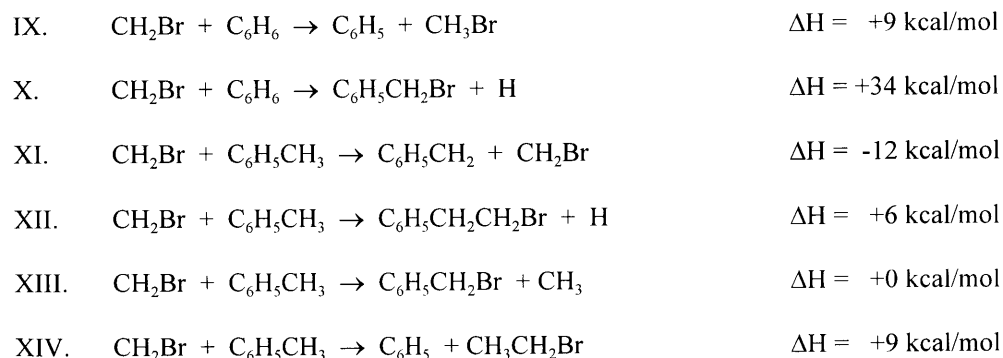


Since the scavenger was not symmetrical around the bond that was broken, there were two products possible for any radical reacting with the scavenger, complicating the analysis. For example, bromomethylbenzene could be produced from either phenyl radical (reaction II) or benzyl radical (reaction III).

The remaining bromine atoms could readily add to multiple bond aliphatic regions of PAH, so each substituted PAH would need to be examined for the possibility that it's precursor was such a molecule. Bromine may also abstract hydrogen from stable species, although it was thermodynamically likely only for compounds with weak C-H bonds:



Remaining bromomethyl radicals can react in a similar manner, but should be more reactive than bromine radicals:



The physical properties of CH_2Br_2 were within tolerances, with a melting point of -52°C (Weast, 1985) and a boiling point of 97°C (-35°C at 1 torr). CH_2Br_2 condensed at liquid nitrogen temperatures and vacuum pressures as a solid and became liquid at room temperature. Since it was similar in structure to the solvent used, CH_2Cl_2 , it was compatible with the solvent and was a good solvent itself for PAH. CH_2Br_2 was available in liquid form from Aldrich Chemical Co. in 99+% purity at reasonable cost. Also, the expected scavenged products, phenyl bromide, benzyl bromide, 1- and 2-bromonaphthalene, 1- and 2-bromomethylnaphthalene, and 1-bromopyrene, were available as standards for GC/MS analysis.

When dibromomethane was used as a scavenger in a benzene/oxygen $\phi=1.95$ flames, the brominated adducts for the following molecules were detected by GC/MS (estimated structures from fragmentation patterns): benzene, toluene (2 isomers), phenol (2 isomers), ethynylbenzene (2 isomers), indene (2 isomers), naphthalene (2 isomers), methyl naphthalene (3 isomers), acenaphthylene (3 isomers), fluorine, and pyrene (3 isomers). A number of additional molecules containing bromine were also detected, but not identified.

A.2 ADDUCT ADDITION FROM A NON-SYMMETRICAL SCAVENGER

It was important to determine which part of the scavenger was adding to radical sites in order to differentiate between radicals such as phenyl and benzyl (reactions II and III). For this, the scavenger CH_2Br_2 was replaced by CD_2Br_2 . In this case, a $\text{C}_6\text{H}_5\text{CH}_2\text{Br}$ product would appear different from a $\text{C}_6\text{H}_5\text{CD}_2\text{Br}$ product, being separated by two mass numbers. Table A.2 shows which precursors could be attributed to each scavenged product using each of these two scavengers. Only one sample was taken due to the high cost of CD_2Br_2 .

Table A.2 Scavenged Products of Standard and Deuterated Dibromomethane

Scavenger	Product	Radical Precursors	Side-Reaction Precursors
CH_2Br_2	$\text{C}_6\text{H}_5\text{Br}$	C_6H_5	C_6H_6
	$\text{C}_6\text{H}_5\text{CH}_2\text{Br}$	C_6H_5 , $\text{C}_6\text{H}_5\text{CH}_2$	C_6H_6 , $\text{C}_6\text{H}_5\text{CH}_3$
CD_2Br_2	$\text{C}_6\text{H}_5\text{Br}$	C_6H_5	C_6H_6
	$\text{C}_6\text{H}_5\text{CH}_2\text{Br}$	$\text{C}_6\text{H}_5\text{CH}_2$	$\text{C}_6\text{H}_5\text{CH}_3$
	$\text{C}_6\text{H}_5\text{CD}_2\text{Br}$	C_6H_5	C_6H_6

If CH_2Br was adding significantly to PAH (relative to bromine) when using CH_2Br_2 as a scavenger, then substituting CD_2Br_2 should have caused a significant decrease in the concentrations of PAH containing CH_2Br . Table A.3 demonstrates that a decrease was observed in both bromo-PAH and bromomethyl-PAH when the deuterated scavenger was used. The change in bromo-PAH was possibly a result of sampling or analysis error. The greater change seen in bromomethyl-PAH suggested that some addition of the CH_2Br portion of the scavenger may have occurred, but the large amount of error in this study did not allow for any conclusive statement.

Table A.3 Relative Amounts of Brominated PAH Using Different Scavengers
(Benzene/ O_2 /Ar Flame, $\phi=1.95$, 9mm)

Product	CH_2Br_2	CD_2Br_2	Change
$\text{C}_6\text{H}_5\text{Br}$	100.0	69.1	-31%
$\text{C}_6\text{H}_5\text{CH}_2\text{Br}$	47.0	20.1	-57%
1- $\text{C}_{10}\text{H}_7\text{Br}$	2.9	2.0	-30%
1- $\text{C}_{10}\text{H}_7\text{CH}_2\text{Br}$	74.4	16.9	-77%
2- $\text{C}_{10}\text{H}_7\text{Br}$	2.8	2.3	-19%
2- $\text{C}_{10}\text{H}_7\text{CH}_2\text{Br}$	28.8	19.2	-33%

Most strikingly, however, $\text{C}_6\text{H}_5\text{CD}_2\text{Br}$ was not detected when using CD_2Br_2 as a scavenger even though $\text{C}_6\text{H}_5\text{CH}_2\text{Br}$ was present at a significant level. This strongly suggests that bromination of PAH overwhelmingly resulted from addition of Br, not CD_2Br , and that reactions I, III, and IX - XIV probably did not produce significant amounts of brominated PAH.

A.3 EXTENT OF SIDE REACTIONS

Initially, CH_2Br_2 was added along with a few PAH in dichloromethane solvent. No reactions were observed over a period of a few weeks. But this did not rule out the possibility of reactions with PAH when radical initiators were present. To quantify the extent of "side reactions" (reactions V - XIV), deuterated naphthalene (C_{10}D_8) was added to the vacuum system along with the scavenger while sampling flames. Since this compound was not present in the flame (Benzene/ O_2 /Ar, $\phi=1.95$), the amount of hydrogen abstraction from naphthalene was determined as the percentage of C_{10}D_8 that became brominated. $\text{C}_{10}\text{D}_7\text{CH}_2\text{Br}$ was not found in any samples, again suggesting that reactions IX - XIV were not important. Table A.4 shows the amounts of brominated species found

in the flame samples referenced to their precursor PAH. The percentages shown are ratios of the concentrations of the listed species as determined by GC/MS peak areas and calibration standards.

Table A.4 Calculation of Side Reactions of CH_2Br_2
(Benzene/ O_2 /Ar Flame, $\phi=1.95$, 9mm)

Height above Burner	6.58 mm	7.65 mm	7.97 mm	8.75 mm	8.80 mm	8.85 mm	9.08 mm
1- $\text{C}_{10}\text{H}_7\text{Br}$ / C_{10}H_8	0.01%	0.03%	0.07%	0.11%	0.13%	0.25%	0.08%
2- $\text{C}_{10}\text{H}_7\text{Br}$ / C_{10}H_8	0.01%	0.02%	0.09%	0.08%	0.08%	0.14%	0.08%
1- $\text{C}_{10}\text{D}_7\text{Br}$ / C_{10}D_8	0.00%	0.08%	0.08%	0.11%	0.42%	0.37%	0.21%
2- $\text{C}_{10}\text{D}_7\text{Br}$ / C_{10}D_8	0.00%	0.01%	0.03%	0.02%	0.04%	0.07%	0.09%
By comparing these values, the percentages of brominated naphthalene that appeared to come from the <i>side reactions only</i> were calculated:							
1- $\text{C}_{10}\text{H}_7\text{Br}$	0%	256%	108%	97%	312%	151%	275%
2- $\text{C}_{10}\text{H}_7\text{Br}$	0%	30%	37%	22%	51%	53%	117%

It appeared that all of the 1- $\text{C}_{10}\text{H}_7\text{Br}$ in the flame samples was a product of the reaction between bromine radicals and naphthalene, and was not representative of naphthyl radical. At least a large fraction of 2- $\text{C}_{10}\text{H}_7\text{Br}$ appeared to result from side reactions as well. It was not clear why side reactions were less prevalent for the second isomer of $\text{C}_{10}\text{H}_7\text{Br}$. From this data, dibromomethane was deemed to be a poor candidate for scavenging radicals.

A.4 COMPARISON WITH DMDS

Mole fractions for phenyl radical calculated from the later use of DMDS were compared with measurements of bromobenzene (believed to be the main scavenging product of phenyl) in this study. The calculated mole fractions from bromobenzene should be indicative of the scavenging efficiency of CH_2Br_2 plus the contribution of side-reactions. Phenyl concentrations were calculated to be 50 times lower when using CH_2Br_2 instead of DMDS, and naphthyl concentrations were 10 times lower, even considering that the effect of side reactions added to the calculated concentrations (See Figure A.2). Therefore, the scavenging efficiency of CH_2Br_2 was incredibly low.

Though CH_2Br_2 was not useful for quantitation of PAH radical profiles in a flame, it was considered that it may be used to predict trends for radicals that may be difficult to find with another scavenger. In fact the concentrations calculated when using CH_2Br_2 did peak at the correct positions in the flame. Although this observation was surprising given the results obtained in Section A.3, no definitive statement about the usefulness of CH_2Br_2 could be made without further study, and further experimentation could not be justified.

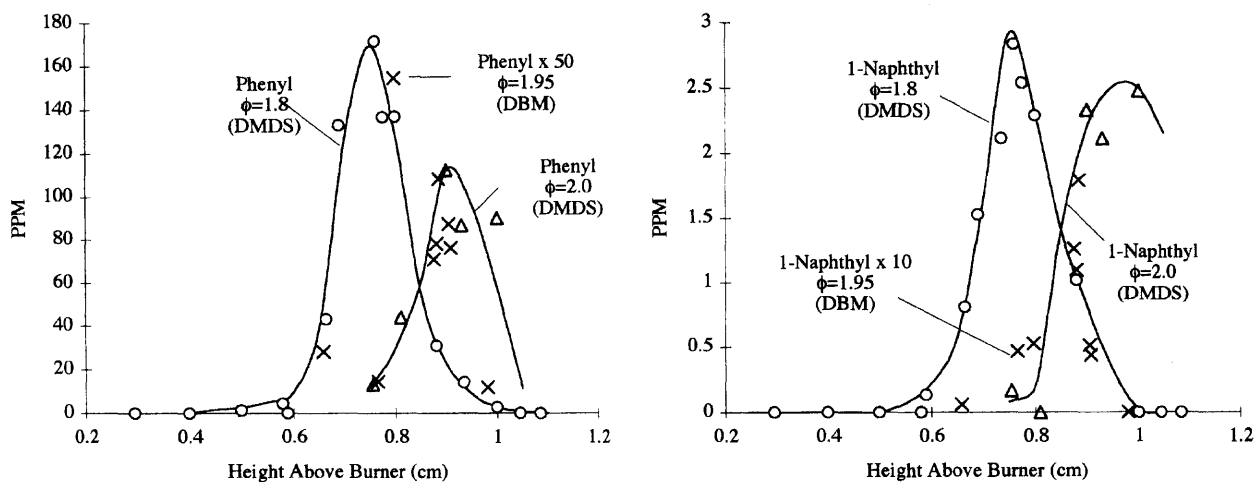


Figure A.2 PAH radical mole fractions determined from scavenging with dibromomethane (DBM) and dimethyl disulfide (DMDS)

Appendix B: Tabulated Mole Fractions

Table B.1 Measured Species Mole Fractions, $\phi=1.8$ flame, 0.3 to 0.74 cm HAB

Height Above Burner (cm)		0.30	0.40	0.50	0.58	0.59	0.67	0.69	0.74
Compound	MW								
Phenyl	77	0.00E+00	0.00E+00	1.42E-06	4.59E-06	0.00E+00	4.31E-05	1.33E-04	
Benzyl	91	0.00E+00	0.00E+00	2.68E-07	4.27E-07	7.62E-07	1.32E-06	0.00E+00	1.62E-06
Phenol	94	5.41E-04	4.38E-04	1.22E-03	1.29E-03	1.12E-03	6.54E-04	1.17E-03	
Phenylacetylene	102	4.14E-05	4.70E-05	1.22E-04	1.71E-04	2.50E-04	3.25E-04	4.37E-04	
Styrene	104	1.53E-05	1.82E-05	4.60E-05	6.38E-05	6.08E-05	4.97E-05	4.41E-05	4.52E-05
Indene	116	2.61E-05	2.25E-05	7.10E-05	9.92E-05	1.24E-04	1.21E-04	1.76E-04	
1-Naphthyl	127	0.00E+00	0.00E+00	0.00E+00	0.00E+00	1.36E-07	8.06E-07	1.52E-06	2.11E-06
2-Naphthyl	127	0.00E+00	0.00E+00	0.00E+00	0.00E+00	1.85E-07	1.07E-06	1.94E-06	2.52E-06
Naphthalene	128	3.05E-05	3.36E-05	9.34E-05	1.24E-04	1.71E-04	2.05E-04	2.42E-04	
1-Methylnaphthalene	142	2.44E-06	3.38E-06	9.14E-06	1.09E-05	1.43E-05	2.00E-05	1.43E-05	1.38E-05
1-Naphthol	144	5.18E-07	9.18E-07	4.88E-06	9.02E-06	7.00E-06	7.13E-06	4.86E-06	1.48E-06
2-Naphthol	144	1.11E-06	1.85E-06	6.78E-06	7.62E-06	6.41E-06	6.44E-06	4.92E-06	2.36E-06
1-Acenaphthyl	151	0.00E+00	0.00E+00	0.00E+00	0.00E+00	0.00E+00	0.00E+00	2.02E-07	8.99E-08
3-Acenaphthyl	151	0.00E+00	0.00E+00	0.00E+00	0.00E+00	0.00E+00	0.00E+00	5.27E-08	9.58E-08
4-Acenaphthyl	151	0.00E+00	0.00E+00	0.00E+00	0.00E+00	0.00E+00	8.52E-08	2.80E-07	3.90E-07
5-Acenaphthyl	151	0.00E+00	0.00E+00	0.00E+00	0.00E+00	0.00E+00	0.00E+00	7.65E-08	1.35E-07
2-Ethynylnaphthalene	152	0.00E+00	9.96E-07	5.65E-06	8.22E-06	1.06E-05	2.20E-05	2.38E-05	2.32E-05
1-Ethynylnaphthalene	152	0.00E+00	2.50E-07	1.47E-06	1.80E-06	2.38E-06	6.73E-06	7.75E-06	8.70E-06
Acenaphthylene	152	1.71E-06	1.29E-06	1.35E-05	2.71E-05	3.45E-05	5.55E-05	9.95E-05	
Biphenylene	152	0.00E+00	0.00E+00	2.10E-07	2.90E-07	3.99E-07	1.36E-06	1.54E-06	1.38E-06
2-Vinylnaphthalene	154	0.00E+00	2.14E-07	9.63E-07	1.04E-06	1.17E-06	1.86E-06	1.38E-06	1.09E-06
Biphenyl	154	6.85E-06	3.72E-06	2.53E-05	4.04E-05	4.70E-05	6.02E-05	7.92E-05	
Fluorine	166	2.08E-06	3.11E-06	1.16E-05	1.40E-05	1.74E-05	2.83E-05	2.41E-05	2.32E-05
Dibenzofuran	168	2.27E-06	2.77E-06	1.04E-05	1.10E-05	1.25E-05	1.87E-05	1.30E-05	1.27E-05
1-Acenaphthenone	168	7.36E-07	1.35E-06	4.24E-06	4.18E-06	4.99E-06	6.43E-06	5.61E-06	4.25E-06
1-Ethynylacenaphthylene	176	0.00E+00	0.00E+00	4.42E-07	8.68E-07	1.50E-06	3.45E-06	4.25E-06	5.20E-06
5-Ethynylacenaphthylene	176	0.00E+00	0.00E+00	6.06E-07	1.32E-06	1.48E-06	5.55E-06	5.32E-06	5.55E-06
Phenanthrene	178	1.73E-06	1.96E-06	6.50E-06	7.56E-06	1.25E-05	1.75E-05	2.28E-05	2.04E-05
Anthracene	178	0.00E+00	1.71E-07	1.29E-06	1.26E-06	2.14E-06	3.43E-06	3.88E-06	4.50E-06
9-Fluorenone	180	0.00E+00	2.09E-07	1.32E-06	1.50E-06	2.01E-06	5.06E-06	5.01E-06	5.94E-06
Perinaphthenone	180	0.00E+00	1.65E-07	1.53E-06	2.23E-06	2.49E-06	7.02E-06	6.83E-06	5.99E-06
Cyclopenta(def)phenanth.	190	1.30E-07	2.72E-07	1.26E-06	1.47E-06	2.56E-06	4.96E-06	4.81E-06	5.34E-06
Fluoranthenyl (total)	201	0.00E+00	0.00E+00	0.00E+00	0.00E+00	0.00E+00	0.00E+00	5.70E-08	1.18E-07
1-Pyrenyl	201	0.00E+00	0.00E+00	0.00E+00	0.00E+00	0.00E+00	0.00E+00	3.23E-08	6.71E-08
2-Pyrenyl	201	0.00E+00	0.00E+00	0.00E+00	0.00E+00	0.00E+00	0.00E+00	2.97E-08	6.20E-08
4-Pyrenyl	201	0.00E+00	0.00E+00	0.00E+00	0.00E+00	0.00E+00	0.00E+00	3.74E-08	7.54E-08
Fluoranthene	202	3.22E-07	5.59E-07	3.04E-06	3.20E-06	4.19E-06	8.87E-06	9.71E-06	1.13E-05
Acephenantrylene	202	4.65E-08	1.29E-07	1.29E-06	1.58E-06	2.01E-06	4.96E-06	5.14E-06	5.47E-06
Aceanthylene	202	0.00E+00	0.00E+00	4.31E-07	4.84E-07	5.75E-07	1.03E-06	1.05E-06	8.58E-07
Pyrene	202	3.13E-07	4.98E-07	2.21E-06	2.54E-06	3.35E-06	6.58E-06	8.03E-06	9.73E-06
1-Phenylnaphthalene	204	1.12E-07	0.00E+00	5.95E-07	7.37E-07	0.00E+00	8.11E-07	1.30E-06	8.58E-07
2-Phenylnaphthalene	204	1.99E-07	0.00E+00	1.02E-06	1.08E-06	0.00E+00	1.48E-06	2.21E-06	1.59E-06
Cyclopenta(cd)pyrene	226	0.00E+00	0.00E+00	9.43E-07	9.86E-07	1.37E-06	3.71E-06	2.96E-06	4.46E-06
Benzo(ghi)fluoranthene	226	0.00E+00	0.00E+00	6.59E-07	7.00E-07	7.89E-07	1.88E-06	1.72E-06	2.47E-06
Benzo(a)anthracene	228	2.84E-08	0.00E+00	3.22E-07	4.39E-07	0.00E+00	6.17E-07	7.46E-07	1.01E-08
Chrysene	228	5.85E-08	0.00E+00	5.82E-07	7.43E-07	0.00E+00	9.35E-07	1.13E-06	3.00E-08
Benzanthrone	230	2.31E-08	0.00E+00	2.18E-07	2.35E-07	0.00E+00	2.77E-07	2.46E-07	0.00E+00
Benzo(b)fluoranthene	252	8.22E-09	0.00E+00	9.95E-08	1.24E-07	0.00E+00	1.99E-07	1.97E-07	4.79E-09
Benzo(k)fluoranthene	252	6.08E-09	0.00E+00	6.08E-08	7.33E-08	0.00E+00	9.16E-08	8.23E-08	2.40E-09
Benzo(a)pyrene	252	1.04E-08	0.00E+00	1.03E-07	1.36E-07	0.00E+00	1.33E-07	1.71E-07	1.98E-09
Benzo(a)pyrenone	254	5.67E-09	0.00E+00	4.94E-08	1.20E-07	0.00E+00	7.19E-08	8.74E-08	0.00E+00
Indeno(1,2,3-cd)pyrene	276	0.00E+00	0.00E+00	2.33E-08	5.02E-08	0.00E+00	3.57E-08	5.20E-08	0.00E+00
Benzo(g,h,i)perylene	276	0.00E+00	0.00E+00	1.68E-08	5.83E-08	0.00E+00	2.87E-08	4.70E-08	0.00E+00

Table B.2 Measured Species Mole Fractions, $\phi=1.8$ Flame, 0.76 to 1.09 cm HAB

Height Above Burner (cm)		0.76	0.78	0.80	0.88	0.94	1.00	1.05	1.09
Compound	MW								
Phenyl	77	1.72E-04	1.37E-04	1.37E-04	3.10E-05	1.43E-05	2.86E-06	0.00E+00	0.00E+00
Benzyl	91	3.31E-06	1.24E-06	0.00E+00	2.71E-07		0.00E+00	0.00E+00	0.00E+00
Phenol	94	6.04E-04	3.95E-04	3.09E-04	4.53E-05	2.83E-05	0.00E+00	0.00E+00	0.00E+00
Phenylacetylene	102	5.88E-04	3.89E-04	3.82E-04	1.09E-04	2.32E-05	3.74E-06	2.14E-07	0.00E+00
Styrene	104	6.66E-05	3.31E-05	1.90E-05	4.55E-06		0.00E+00	0.00E+00	0.00E+00
Indene	116	2.24E-04	1.26E-04	1.27E-04	7.87E-06	1.55E-06	0.00E+00	0.00E+00	0.00E+00
1-Naphthyl	127	2.83E-06	2.53E-06	2.28E-06	1.02E-06		0.00E+00	0.00E+00	0.00E+00
2-Naphthyl	127	3.65E-06	3.32E-06	2.89E-06	1.38E-06		0.00E+00	0.00E+00	0.00E+00
Naphthalene	128	3.04E-04	2.26E-04	1.95E-04	3.27E-05	7.16E-06	0.00E+00	0.00E+00	0.00E+00
1-Methylnaphthalene	142	1.99E-05	7.32E-06	4.80E-06	4.90E-07		0.00E+00	0.00E+00	0.00E+00
1-Naphthol	144	5.79E-06	8.38E-07	1.56E-06	3.06E-08		0.00E+00	0.00E+00	0.00E+00
2-Naphthol	144	3.73E-06	2.58E-06	1.31E-06	2.92E-08		0.00E+00	0.00E+00	0.00E+00
1-Acenaphthyl	151	2.64E-07	0.00E+00	2.24E-07	2.18E-07		0.00E+00	0.00E+00	0.00E+00
3-Acenaphthyl	151	1.49E-07	0.00E+00	9.40E-08	1.04E-07		0.00E+00	0.00E+00	0.00E+00
4-Acenaphthyl	151	6.18E-07	7.90E-07	9.10E-07	5.95E-07		0.00E+00	0.00E+00	0.00E+00
5-Acenaphthyl	151	2.74E-07	0.00E+00	1.88E-07	1.84E-07		0.00E+00	0.00E+00	0.00E+00
2-Ethynylnaphthalene	152	5.51E-05	3.31E-05	2.75E-05	1.09E-05		0.00E+00	0.00E+00	0.00E+00
1-Ethynylnaphthalene	152	2.13E-05	1.33E-05	1.30E-05	7.12E-06		0.00E+00	0.00E+00	0.00E+00
Acenaphthylene	152	1.55E-04	1.23E-04	1.24E-04	3.44E-05	8.76E-06	0.00E+00	0.00E+00	9.13E-07
Biphenylene	152	3.54E-06	1.86E-06	1.27E-06	2.86E-07		0.00E+00	0.00E+00	0.00E+00
2-Vinylnaphthalene	154	3.09E-06	1.18E-06	6.68E-07	0.00E+00		0.00E+00	0.00E+00	0.00E+00
Biphenyl	154	8.13E-05	4.79E-05	2.98E-05	4.03E-07	1.11E-06	0.00E+00	0.00E+00	0.00E+00
Fluorine	166	4.17E-05	1.91E-05	1.32E-05	2.66E-06		0.00E+00	2.99E-08	2.09E-07
Dibenzofuran	168	2.04E-05	9.45E-06	5.61E-06	2.49E-06		0.00E+00	0.00E+00	5.47E-07
1-Acenaphthenone	168	6.88E-06	4.73E-06	2.51E-06	4.95E-07		0.00E+00	0.00E+00	0.00E+00
1-Ethynylacenaphthylene	176	1.21E-05	9.47E-06	9.19E-06	6.69E-06		0.00E+00	0.00E+00	0.00E+00
5-Ethynylacenaphthylene	176	1.73E-05	1.18E-05	1.04E-05	7.49E-06		0.00E+00	0.00E+00	0.00E+00
Phenanthrene	178	2.85E-05	2.61E-05	1.76E-05	3.29E-06		2.28E-07	1.53E-07	1.81E-07
Anthracene	178	5.25E-06	4.14E-06	3.28E-06	6.07E-07		0.00E+00	1.89E-08	0.00E+00
9-Fluorenone	180	9.60E-06	9.19E-06	3.71E-06	6.10E-07		0.00E+00	0.00E+00	0.00E+00
Perinaphthenone	180	1.57E-05	9.23E-06	4.65E-06	8.55E-07		0.00E+00	0.00E+00	0.00E+00
Cyclopenta(def)phenanth.	190	9.98E-06	6.26E-06	4.94E-06	2.05E-06		3.22E-08	0.00E+00	5.15E-08
Fluoranthenyl (total)	201	2.17E-07	2.75E-07	1.24E-07	1.59E-07		0.00E+00	0.00E+00	0.00E+00
1-Pyrenyl	201	1.32E-07	1.64E-07	7.72E-08	1.41E-07		2.29E-08	0.00E+00	0.00E+00
2-Pyrenyl	201	1.24E-07	1.48E-07	7.16E-08	1.20E-07		1.76E-08	0.00E+00	0.00E+00
4-Pyrenyl	201	1.92E-07	2.22E-07	1.25E-07	1.94E-07		2.97E-08	0.00E+00	0.00E+00
Fluoranthene	202	2.35E-05	1.80E-05	9.62E-06	5.60E-06		1.04E-07	9.39E-08	5.77E-07
Acephenantrylene	202	1.37E-05	9.65E-06	4.74E-06	2.52E-06		0.00E+00	0.00E+00	2.38E-07
Aceanthylene	202	3.30E-06	1.40E-06	1.02E-06	5.83E-07		0.00E+00	0.00E+00	0.00E+00
Pyrene	202	1.99E-05	1.84E-05	1.12E-05	1.07E-05		2.13E-07	9.26E-08	4.41E-07
1-Phenylnaphthalene	204	1.80E-06	1.52E-06	0.00E+00	1.52E-07		0.00E+00	0.00E+00	0.00E+00
2-Phenylnaphthalene	204	3.30E-06	3.01E-06	0.00E+00	3.08E-07		0.00E+00	0.00E+00	0.00E+00
Cyclopenta(cd)pyrene	226	9.96E-06	5.92E-06	5.15E-06	5.73E-06		6.08E-08	0.00E+00	0.00E+00
Benzo(ghi)fluoranthene	226	4.89E-06	4.06E-06	2.90E-06	3.20E-06		0.00E+00	0.00E+00	1.30E-07
Benzo(a)anthracene	228	2.70E-06	3.36E-08	5.85E-07	1.09E-08		0.00E+00	0.00E+00	0.00E+00
Chrysene	228	3.51E-06	6.41E-08	8.96E-07	5.10E-09		0.00E+00	0.00E+00	0.00E+00
Benzanthrone	230	9.84E-07	7.77E-09	1.48E-07	0.00E+00		0.00E+00	0.00E+00	0.00E+00
Benzo(b)fluoranthene	252	1.09E-06	2.26E-08	2.20E-07	0.00E+00		0.00E+00	0.00E+00	0.00E+00
Benzo(k)fluoranthene	252	4.22E-07	9.30E-09	1.07E-07	0.00E+00		0.00E+00	0.00E+00	0.00E+00
Benzo(a)pyrene	252	9.63E-07	2.12E-08	1.72E-07	0.00E+00		0.00E+00	0.00E+00	0.00E+00
Benzo(a)pyrenone	254	5.25E-07	2.06E-08	1.06E-07	0.00E+00		0.00E+00	0.00E+00	0.00E+00
Indeno(1,2,3-cd)pyrene	276	3.06E-07	1.13E-08	7.85E-08	0.00E+00		0.00E+00	0.00E+00	0.00E+00
Benzo(g,h,i)perylene	276	3.55E-07	2.33E-08	9.89E-08	0.00E+00		0.00E+00	0.00E+00	0.00E+00

Table B.3 Measured Species Mole Fractions, $\phi=2.0$ Flame

Height Above Burner (cm)		0.76	0.81	0.90	0.93	1.00
Compound	MW					
Phenyl	77	1.33E-05	4.39E-05	1.12E-04	8.69E-05	9.02E-05
Benzyl	91	6.19E-07	4.67E-07	2.29E-06	1.96E-06	5.65E-07
Phenol	94	1.11E-03	1.34E-03	4.75E-04	2.79E-04	6.04E-05
Phenylacetylene	102	3.30E-04	4.71E-04	6.03E-04	5.08E-04	2.63E-04
Styrene	104	6.99E-05	8.94E-05	4.75E-05	4.63E-05	9.29E-06
Indene	116	1.98E-04	2.59E-04	2.48E-04	1.76E-04	4.94E-05
1-Naphthyl	127	1.67E-07	0.00E+00	2.32E-06	2.10E-06	2.47E-06
2-Naphthyl	127	1.76E-07	0.00E+00	2.87E-06	2.61E-06	3.25E-06
Naphthalene	128	2.43E-04	2.86E-04	3.42E-04	2.77E-04	1.27E-04
1-Methylnaphthalene	142	1.78E-05	2.48E-05	2.07E-05	1.27E-05	1.57E-06
1-Naphthol	144	6.43E-06	4.34E-06	4.29E-06	2.51E-06	0.00E+00
2-Naphthol	144	4.59E-06	2.85E-06	3.41E-06	1.68E-06	0.00E+00
2-Ethynyl-naphthalene	152	1.51E-05	2.76E-05	4.45E-05	4.54E-05	2.91E-05
1-Ethynyl-naphthalene	152	5.28E-06	1.06E-05	1.71E-05	1.58E-05	1.41E-05
Acenaphthylene	152	6.44E-05	1.12E-04	1.61E-04	1.66E-04	1.18E-04
Biphenylene	152	5.36E-07	1.23E-06	2.25E-06	1.97E-06	7.21E-07
2-Vinylnaphthalene	154	1.51E-06	3.12E-06	2.38E-06	1.54E-06	5.20E-07
Biphenyl	154	6.58E-05	1.02E-04	8.35E-05	6.17E-05	1.17E-05
Fluorine	166	2.27E-05	3.34E-05	3.92E-05	2.93E-05	7.77E-06
Dibenzofuran	168	1.31E-05	1.65E-05	1.56E-05	1.10E-05	2.78E-06
1-Acenaphthenone	168	6.42E-06	5.57E-06	7.82E-06	3.58E-06	2.11E-06
1-Ethynylacenaphthylene	176	2.69E-08	4.77E-06	1.12E-05	1.28E-05	1.58E-05
5-Ethynylacenaphthylene	176	3.44E-06	6.41E-06	1.56E-05	1.62E-05	1.88E-05
Phenanthrene	178	1.66E-05	2.76E-05	4.41E-05	3.12E-05	1.60E-05
Anthracene	178	1.44E-06	1.93E-06	8.84E-06	4.67E-06	1.07E-06
9-Fluorenone	180	2.81E-06	4.05E-06	8.69E-06	8.21E-06	2.73E-06
Perinaphthenone	180	4.85E-06	3.22E-06	1.51E-05	9.38E-06	4.36E-06
Cyclopenta(def)phenanth.	190	4.55E-06	6.41E-06	1.36E-05	9.11E-06	5.65E-06
Fluoranthene	202	6.49E-06	9.18E-06	2.47E-05	1.75E-05	1.59E-05
Acephenantrylene	202	3.37E-06	4.40E-06	1.40E-05	9.49E-06	7.60E-06
Aceanthylene	202	4.29E-10	8.21E-07	2.75E-06	2.01E-06	1.20E-06
Pyrene	202	5.09E-06	7.29E-06	2.33E-05	1.78E-05	2.58E-05
Cyclopenta(cd)pyrene	226	2.82E-06	4.47E-06	9.35E-06	8.79E-06	1.24E-05
Benzo(ghi)fluoranthene	226	1.72E-06	2.22E-06	4.75E-06	4.97E-06	6.22E-06
Benz(a)anthracene	228	2.14E-07	0.00E+00	1.39E-06	5.51E-07	2.28E-07
Chrysene	228	5.00E-07	0.00E+00	2.59E-06	1.36E-06	7.14E-07
Benzo(b)fluoranthene	252	0.00E+00	0.00E+00	9.07E-07	4.72E-07	2.62E-07
Benzo(k)fluoranthene	252	0.00E+00	0.00E+00	4.75E-07	2.90E-07	1.54E-07
Benzo(e)pyrene	252	0.00E+00	0.00E+00	8.14E-07	5.28E-07	3.06E-07
Benzo(a)pyrene	252	0.00E+00	0.00E+00	1.12E-06	5.81E-07	4.11E-07

Appendix C: Detailed Sampling Procedure

The operation of the radical scavenging system designed for this work is presented in check-list format. The locations of the valves, pumps, and other operating equipment relative to the vacuum system are shown in Figure C.1.

System Start-up

Close valves:

- burner exhaust gate valve (G1)
- diffusion pump gate valves (G2,G3)
- roughing pump gate valve (G4)
- burner inlet (V1), scavenger valve (V2)
- nitrogen re-pressure valves (V3,V4,V8)
- stokes pump air-leak valves (V5,V6)
- manometer valves (M1,M2)
- benzene feed valves (B1,B2)
- benzene vent (B3)

Open burner bypass valve (B5) and manometer vent valves (M5,M6).

Turn on roughing pumps 1 and 2 (R1,R2).

Turn on cooling water (W1), and observe flows. Flow meters F1 and F2 should spin ~120 RPM.

Turn on cooling water auto-protection relay. Increase flows (W2,W3) if it doesn't engage.

Check that roughing pressures (P1,P2) are less than 50 mtorr, turn on diffusion pump heaters.

Turn on cooling water to stokes pump (R4), set for 1gpm.

Start stokes pump (r4).

Fill benzene tank with approx 1 liter benzene.

Turn on heat to benzene mass flow controller (H1=20V), line (H2=40V), and tank (H3=40V).

Fill dewer with liquid nitrogen, place LN2 trap inside and connect to lines with cajon fittings.

Open vacuum valve to trap (B6).

Open benzene feed valve (B2) and evacuate tank to 200 mbar, then shut valve

When mass flow controller thermocouple reads 0.130 ohms (80 °C), turn off the heater (H1).

Zero the mass flow controller.

Turn on benzene tank heater (level 10) for 2 min., then turn off. Turn on stirrer (level 4).

Open manometer bypass valves (M3,M4).

Zero O2 Manometer.

Record room temperature.

Close bypass valves (M3,M4) and turn on manometer backing pump (R5).

Adjust Ar manometer so that it reads the same as the O2 manometer.

Close the valves to atmosphere (M5,M6), open valves to control panel (M1,M2).

Open benzene feed valve (B2), set heat level 4.

Attach scavenger bottle (S) to system.

Evacuate scavenger bottle to 25 torr by opening and closing valve V7.

Set argon regulator to 20 psi., oxygen to 10 psi., acetylene to 5 psi., nitrogen to 2 psi.

Sample Collection

Open argon toggle valve (A1) and set flow (A2).

Set desired benzene flow rate.

Turn on roughing pump R3 and crack open gate valve G4.

Immediately but slowly open burner exhaust valve (G1).

Open burner inlet valve (V1).

Check that chamber pressure reaches 5 mtorr. (P6)

Start nitrogen flow to burner chamber through critical orifice (V3).

Set burner pressure (P3) using air leak valves (V5,V6)

Set burner height using cathetometer.

Position igniter above burner.

Start LN2 flow, start timer.

Open oxygen toggle valve (A3), adjust flow (A4).

Start scavenger flow (V2). Adjust with valve V8 to set pressure (P4,P5).

Record LN2 reading (X).

When LN2 thermocouple reading reaches -4.0 mV (approx 150 K), open C2H2 toggle valve (A5).

Turn on coil until flame ignites.

Adjust acetylene flow to produce a lean flame.

Move igniter out of position.

Close nitrogen to burner (V3).

Open benzene valve to burner (B1), and SLOWLY close valve to trap (B5).

Close acetylene toggle valve (A1).

Slowly open diffusion pump gate valves (G2,G3), and close roughing pump valve (G4).

When system pressure reaches 1 mtorr (P6), turn on ion gauge (P7).

Adjust LN2 flow so that a small amount of liquid flows into the small dewer.

Turn off roughing pump R3 and vent.

Sample removal

Turn off benzene flow (close B1, open B5).

Close toggle valves (A1,A3).

Close scavenger valve (V2).

Close diffusion pump gate valves (G2,G3).

Close burner exhaust (G1) and burner inlet (V1) valves.

Repressurize system with nitrogen (open V3,V4,V8).

When system pressure = 1 atm. (P8), turn off nitrogen flow (V3,V4,V8).

Release top flange and slowly raise cold trap into glove box using hoist.

Let trap thaw above sample bottle. When all has melted, rinse trap with DCM..

Wait 5 min. then rinse again.

Sample Analysis (performed as sampling system is put into stand-by mode)

Add 100 ml of prepared DPAH solution to sample.

Inject 1 ml of sample into GC/MS (Method KTTB2).

Place sample jar on heat plate and turn on blow-down nitrogen.

Briefly turn on heat to heat plate if crystals begin to form in the sample.

When sample volume equals 8 ml, transfer to small amber vial with pipette.

Continue blow-down until sample reaches 4 ml.

Inject 1 ml of sample into GC/MS.

Continue blow-down until sample reaches 0.1-0.4 ml.

Inject 1 ml of sample into GC/MS.

Inject 1 ml of DCM into GC/MS to clean column for next sample.

Return to Standby

Start roughing pump R3.

Open roughing pump valve (G4), burner exhaust (G1), and burner inlet (V1).

Open acetylene and oxygen toggle valves (A3,A5)

Turn on coil until flame ignites.

Adjust acetylene flow to produce a lean flame (A2).

Move igniter out of position.

Continue until carbon burns off of probe.

Close toggle valves (A3,A5).

Close burner exhaust (G1) and burner inlet (V1) valves.

Repressurize system with nitrogen (open V3,V4,V8).

When system pressure = 1 atm. (P8), turn off nitrogen flow (V3,V4,V8).

Wipe trap with DCM-soaked cloth.

Rinse trap with DCM.

Wipe scavenger doughnut and probe interior with DCM-soaked cloth.

Lower trap into vacuum chamber and clamp down top flange.

System Shutdown

Turn off diffusion pumps.

Turn on cooling fans.

Close benzene tank (B2)

Close argon, oxygen, and acetylene regulators.

Close manometer valves to control panel (M1,M2), open valves to atmosphere (M5,M6).

Turn off backing pump (R5).

Open manometer bypass valves slowly (M3,M4).

Open stokes air leak (V5) and turn off stokes pump (R4).

Turn off cooling water to stokes pump.

Wait until diffusion pumps are cool to the touch (2-3 hours).

Open roughing pump valve (G4)

Slowly open diffusion pump gate valves (G2,G3).

Turn off roughing pumps (R1,R2,R3).

Repressurize system with nitrogen (open V3,V4,V8).

When system pressure = 1 atm. (P8), turn off nitrogen flow (V3,V4,V8).

Turn off water to system (W1).

Turn off fans.

Close diffusion pump gate valves (G2,G3).

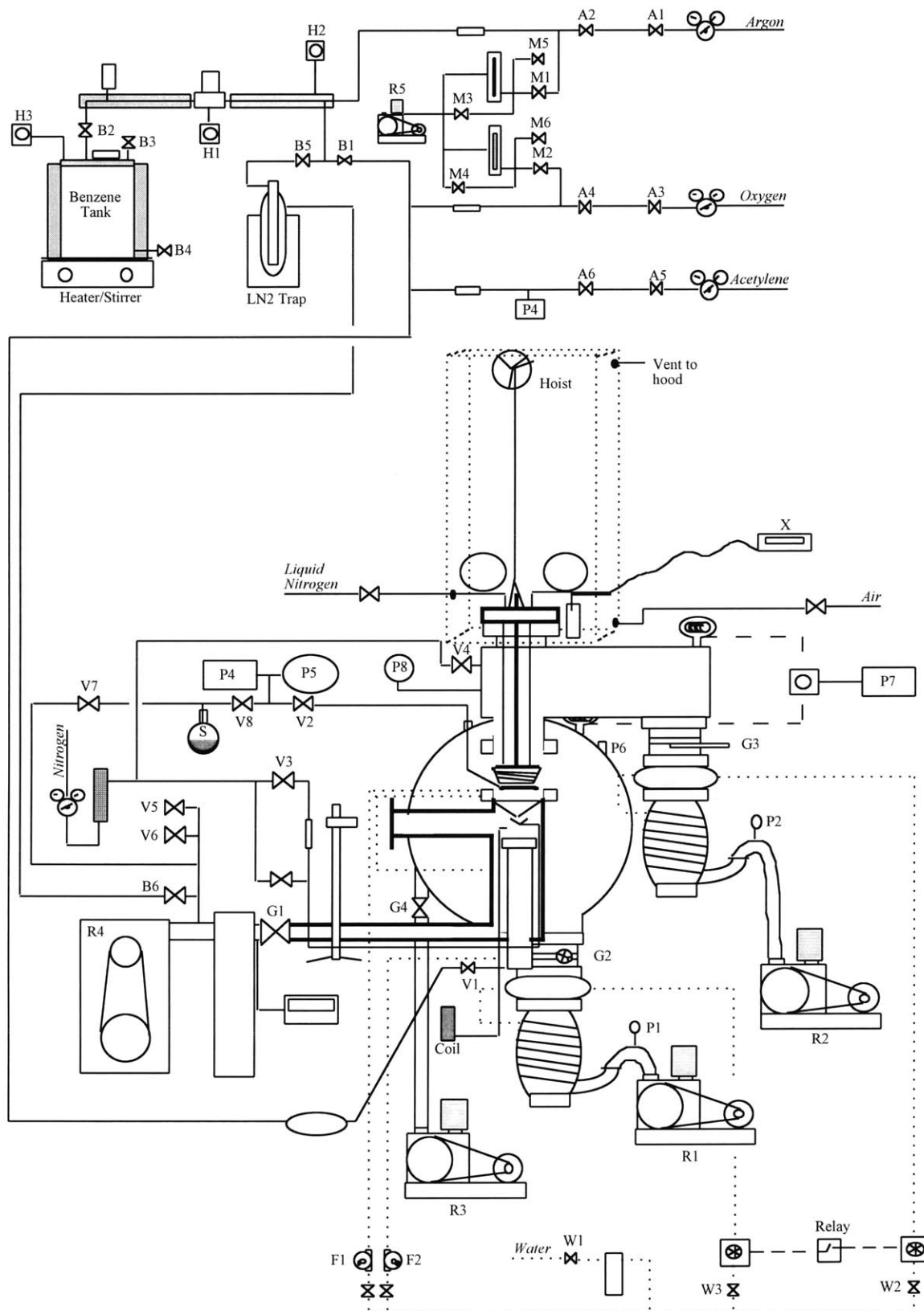


Figure C.1 Operating procedure reference schematic

Appendix D: Tabulated Thermodynamic Data from DFT Calculations

Table D.1 Formation and Zero-Point Energies from DFT Calculations

Compound	GGA Closed/Open Shell SCF Energy (Hartree) ^a	Zero-Point Vibrational Energy (Hartree) ^a
Benzene (C ₆ H ₆)	-232.17779987	0.09732755
Phenyl (C ₆ H ₅)	-231.49615801	0.08447825
Toluene (C ₇ H ₈)	-271.47495256	0.12376147
Benzyl (C ₇ H ₇)	-270.83054146	0.11083709
Naphthalene (C ₁₀ H ₈)	-385.77984388	0.14247648
1-Naphthyl (1-C ₁₀ H ₇)	-385.09868043	0.12975901
2-Naphthyl (2-C ₁₀ H ₇)	-385.09812176	0.12959603
Acenaphthylene (C ₁₂ H ₈)	-461.96065244	0.15379356
1-Acenaphthyl (1-C ₁₂ H ₇)	-461.27337153	0.14145376
3-Acenaphthyl (3-C ₁₂ H ₇)	-461.27994581	0.14127733
4-Acenaphthyl (4-C ₁₂ H ₇)	-461.27929676	0.14099108
5-Acenaphthyl (5-C ₁₂ H ₇)	-461.27876519	0.14124290
Cyclopenta[def]phenanthrene (C ₁₅ H ₁₀)	-577.47791127	0.19413308
4-Cyclopenta[def]phenanthryl (4-C ₁₅ H ₉)	-576.84706912	0.18146370
Pyrene (C ₁₆ H ₁₀)	-615.60326157	0.20003536
1-Pyrenyl (1-C ₁₆ H ₉)	-614.92139165	0.18749863
2-Pyrenyl (2-C ₁₆ H ₉)	-614.92168054	0.18726763
4-Pyrenyl (4-C ₁₆ H ₉)	-614.92204308	0.18748698
Cyclopenta[cd]pyrene (C ₁₈ H ₁₀)	-691.78321053	0.21131966
4-Cyclopenta[cd]pyrenyl (4-C ₁₈ H ₉)	-691.09568634	0.19899289
Ethylene (C ₂ H ₄)	-78.55750393	0.04927376
Vinyl (C ₂ H ₃)	-77.87664652	0.03528767
Ethane (C ₂ H ₆)	-79.11815812	0.05748614
Ethyl (C ₂ H ₅)	-79.78430236	0.07277241

^a1 hartree = 627.51 kcal/mol

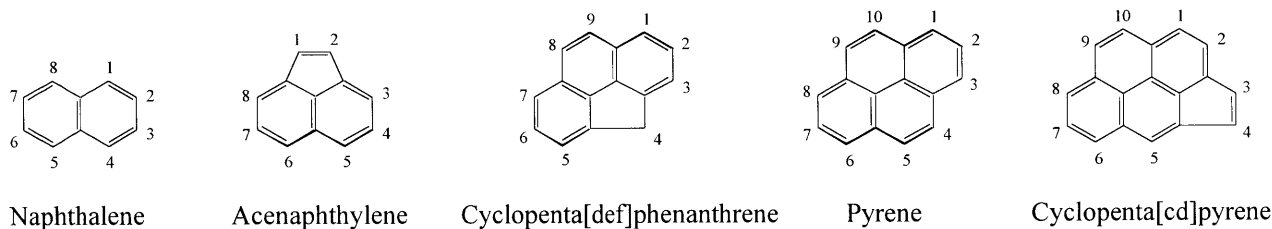


Figure D.1 Numbering schemes for select PAH.

Table D.2 Enthalpy Corrections^a and Entropies^b from DFT Calculations

	C ₆ H ₆	C ₆ H ₅	C ₇ H ₈	C ₇ H ₇	C ₁₀ H ₈	1-C ₁₀ H ₇	2-C ₁₀ H ₇	C ₁₂ H ₈	1-C ₁₂ H ₇
ΔH (273.15)	2.9619	2.9686	3.5197	5.7904	4.2994	4.3021	4.3008	4.7887	4.7879
ΔH (298.15)	3.4370	3.4382	4.1009	6.8906	5.0703	5.0653	5.0657	5.6746	5.6635
ΔH (400)	5.8523	5.7932	7.0264	12.4538	8.9654	8.8912	8.8979	10.1505	10.0535
ΔH (500)	8.9018	8.7219	10.6981	19.4137	13.8385	13.6350	13.6472	15.7363	15.4898
ΔH (600)	12.4997	12.1432	15.0305	27.5712	19.5507	19.1633	19.1803	22.2660	21.8154
ΔH (700)	16.5372	15.9555	19.9024	36.6789	25.9305	25.3118	25.3332	29.5403	28.8401
ΔH (800)	20.9316	20.0826	25.2188	46.5473	32.8478	31.9568	31.9822	37.4090	36.4207
ΔH (900)	25.6210	24.4683	30.9067	57.0344	40.2053	39.0064	39.0357	45.7609	44.4509
ΔH (1000)	30.5581	29.0697	36.9090	68.0320	47.9292	46.3912	46.4240	54.5116	52.8508
ΔH (1100)	35.7050	33.8530	43.1792	79.4560	55.9613	54.0567	54.0929	63.5960	61.5586
ΔH (1200)	41.0311	38.7912	49.6790	91.2389	64.2548	61.9598	61.9991	72.9617	70.5254
ΔH (1300)	46.5110	43.8618	56.3765	103.3264	72.7714	70.0650	70.1073	82.5667	79.7117
ΔH (1400)	52.1235	49.0464	63.2446	115.6739	81.4794	78.3433	78.3884	92.3763	89.0851
ΔH (1500)	57.8507	54.3294	70.2606	128.2444	90.3526	86.7707	86.8184	102.3617	98.6192
ΔH (1600)	63.6775	59.6978	77.4051	141.0074	99.3687	95.3269	95.3770	112.4991	108.2919
ΔH (1700)	69.5913	65.1404	84.6618	153.9373	108.5091	103.9950	104.0474	122.7685	118.0846
ΔH (1800)	75.5811	70.6481	92.0168	167.0124	117.7581	112.7609	112.8153	133.1529	127.9820
ΔH (1900)	81.6377	76.2129	99.4580	180.2147	127.1024	121.6123	121.6687	143.6380	137.9709
ΔH (2000)	87.7532	81.8280	106.9755	193.5287	136.5305	130.5391	130.5973	154.2118	148.0402
ΔH (2100)	93.9209	87.4875	114.5604	206.9412	146.0328	139.5324	139.5923	164.8639	158.1806
ΔH (2200)	100.1350	93.1866	122.2052	220.4411	155.6009	148.5848	148.6462	175.5854	168.3839
σ ^c	12	2	6	4	4	1	1	2	1
S (273.15)	62.9075	66.3582	69.4687	90.5450	77.7495	80.4753	80.3831	83.5805	84.8907
S (298.15)	64.5707	68.0018	71.5036	94.3963	80.4478	83.1470	83.0604	86.6815	87.9557
S (400)	71.4863	74.7480	79.8824	110.3288	91.6033	94.1071	94.0389	99.5009	100.5321
S (500)	78.2656	81.2604	88.0453	125.8038	102.4382	104.6562	104.6002	111.9212	112.6215
S (600)	84.8118	87.4859	95.9276	140.6473	112.8322	114.7161	114.6690	123.8031	124.1326
S (700)	91.0279	93.3557	103.4280	154.6701	122.6550	124.1832	124.1429	135.0034	134.9490
S (800)	96.8910	98.8625	110.5211	167.8374	131.8845	133.0497	133.0148	145.5027	145.0640
S (900)	102.4112	104.0254	117.2166	180.1829	140.5458	141.3487	141.3183	155.3347	154.5175
S (1000)	107.6108	108.8716	123.5379	191.7658	148.6806	149.1265	149.0998	164.5512	163.3646
S (1100)	112.5149	113.4293	129.5122	202.6510	156.3338	156.4306	156.4071	173.2072	171.6620
S (1200)	117.1482	117.7252	135.1664	212.9014	163.5486	163.3058	163.2851	181.3548	179.4626
S (1300)	121.5337	121.7832	140.5263	222.5751	170.3644	169.7924	169.7741	189.0418	186.8144
S (1400)	125.6924	125.6249	145.6154	231.7244	176.8170	175.9266	175.9103	196.3106	193.7601
S (1500)	129.6434	129.2695	150.4553	240.3964	182.9382	181.7403	181.7258	203.1992	200.3374
S (1600)	133.4036	132.7338	155.0659	248.6328	188.7566	187.2619	187.2490	209.7412	206.5795
S (1700)	136.9885	136.0332	159.4649	256.4710	194.2976	192.5167	192.5051	215.9666	212.5160
S (1800)	140.4120	139.1812	163.6686	263.9442	199.5839	197.5268	197.5165	221.9018	218.1729
S (1900)	143.6865	142.1898	167.6917	271.0820	204.6359	202.3124	202.3030	227.5706	223.5734
S (2000)	146.8232	145.0698	171.5475	277.9110	209.4717	206.8910	206.8827	232.9941	228.7381
S (2100)	149.8324	147.8310	175.2481	284.4548	214.1078	211.2788	211.2712	238.1911	233.6855
S (2200)	152.7231	150.4822	178.8043	290.7348	218.5587	215.4898	215.4830	243.1787	238.4320

^aΔH (T/K) = ΔH^o_T - ΔH^o_{0K}^bS (T/K) = ΔS^o_T; includes symmetry correction, -R[ln(σ)], which was not part of the program output^cσ = symmetry number.

Table D.2 cont.

	3-C ₁₂ H ₇	4-C ₁₂ H ₇	5-C ₁₂ H ₇	C ₁₅ H ₁₀	4-C ₁₅ H ₁₀	C ₁₆ H ₁₀	1-C ₁₆ H ₉	2-C ₁₆ H ₉	4-C ₁₆ H ₉
ΔH (273.15)	4.7752	4.8002	4.7903	5.7904	5.7177	6.0410	6.0263	6.0657	6.0553
ΔH (298.15)	5.6496	5.6804	5.6664	6.8906	6.8117	7.2057	7.1794	7.2262	7.2121
ΔH (400)	10.0400	10.0935	10.0621	12.4538	12.3292	13.0844	12.9708	13.0462	13.0186
ΔH (500)	15.4819	15.5546	15.5077	19.4137	19.1945	20.4174	20.1577	20.2560	20.2179
ΔH (600)	21.8155	21.9036	21.8438	27.5712	27.2020	28.9932	28.5351	28.6509	28.6045
ΔH (700)	28.8489	28.9492	28.8787	36.6789	36.1070	38.5521	37.8511	37.9801	37.9270
ΔH (800)	36.4377	36.5477	36.4684	46.5473	45.7252	48.8963	47.9139	48.0527	47.9939
ΔH (900)	44.4754	44.5933	44.5067	57.0344	55.9205	59.8778	58.5803	58.7263	58.6626
ΔH (1000)	52.8822	53.0064	52.9137	68.0320	66.5900	71.3843	69.7422	69.8935	69.8253
ΔH (1100)	61.5960	61.7256	61.6276	79.4560	77.6546	83.3285	81.3158	81.4708	81.3988
ΔH (1200)	70.5681	70.7020	70.5997	91.2389	89.0511	95.6411	93.2348	93.3925	93.3169
ΔH (1300)	79.7590	79.8967	79.7904	103.3264	100.7291	108.266	105.4459	105.6055	105.5266
ΔH (1400)	89.1366	89.2774	89.1678	115.6739	112.6470	121.1573	117.9056	118.0665	117.9846
ΔH (1500)	98.6743	98.8179	98.7053	128.2444	124.7708	134.2771	130.5783	130.7400	130.6554
ΔH (1600)	108.3502	108.4962	108.3809	141.0074	137.0722	147.5941	143.4343	143.5966	143.5095
ΔH (1700)	118.1459	118.2939	118.1763	153.9373	149.5274	161.0820	156.4491	156.6117	156.5223
ΔH (1800)	128.0459	128.1958	128.0761	167.0124	162.1166	174.7186	169.6020	169.7647	169.6731
ΔH (1900)	138.0372	138.1887	138.0671	180.2147	174.8231	188.4854	182.8756	183.0383	182.9447
ΔH (2000)	148.1087	148.2617	148.1383	193.5287	187.6327	202.3667	196.2552	196.4177	196.3223
ΔH (2100)	158.2510	158.4053	158.2804	206.9412	200.5331	216.3488	209.7282	209.8905	209.7935
ΔH (2200)	168.4561	168.6116	168.4852	220.4411	213.5141	230.4204	223.2839	223.4460	223.3474
σ	1	1	1	2	2	4	1	2	1
S (273.15)	84.8459	84.9228	84.9904	91.9223	91.3883	92.3412	94.9818	93.8084	95.2116
S (298.15)	87.9071	88.0039	88.0571	95.7736	95.2180	96.4183	99.0181	97.8709	99.2612
S (400)	100.4841	100.6466	100.6497	111.7061	111.0216	113.2559	115.6085	114.5439	115.8951
S (500)	112.5858	112.7912	112.7596	127.1811	126.2879	129.5613	131.5902	130.5768	131.9044
S (600)	124.1115	124.3451	124.2898	142.0246	140.8593	145.1662	146.8348	145.8535	147.1660
S (700)	134.9411	135.1937	135.1219	156.0474	154.5706	159.8841	161.1790	160.2181	161.5203
S (800)	145.0672	145.3328	145.2492	169.2147	167.4045	173.6864	174.6060	173.6583	174.9528
S (900)	154.5296	154.8045	154.7123	181.5602	179.4068	186.6140	187.1630	186.2238	187.5124
S (1000)	163.3839	163.6655	163.5669	193.1431	190.6443	198.7329	198.9191	197.9854	199.2694
S (1100)	171.6870	171.9736	171.8700	204.0283	201.1872	210.1140	209.9470	209.0170	210.2972
S (1200)	179.4922	179.7827	179.6752	214.2787	211.1016	220.8252	220.3159	219.3882	220.6654
S (1300)	186.8478	187.1412	187.0306	223.9524	220.4475	230.9289	230.0885	229.1624	230.4369
S (1400)	193.7965	194.0923	193.9792	233.1017	229.2786	240.4813	239.3211	238.3959	239.6683
S (1500)	200.3763	200.6740	200.5588	241.7737	237.6424	249.5322	248.0636	247.1390	248.4094
S (1600)	206.6205	206.9198	206.8029	250.0101	245.5810	258.1261	256.3601	255.4358	256.7047
S (1700)	212.5588	212.8593	212.7410	257.8483	253.1315	266.3026	264.2498	263.3257	264.5931
S (1800)	218.2172	218.5188	218.3992	265.3215	260.3269	274.0967	271.7674	270.8434	272.1096
S (1900)	223.6190	223.9214	223.8009	272.4593	267.1967	281.5398	278.9438	278.0198	279.2849
S (2000)	228.7848	229.0880	228.9666	279.2883	273.7669	288.6597	285.8064	284.8823	286.1465
S (2100)	233.7332	234.0370	233.9148	285.8321	280.0609	295.4814	292.3798	291.4556	292.7189
S (2200)	238.4804	238.7849	238.6620	292.1121	286.0996	302.0273	298.6857	297.7614	299.0241

Table D.2 cont.

	C ₁₈ H ₁₀	4-C ₁₈ H ₉	C ₂ H ₄	C ₂ H ₃	C ₂ H ₆	C ₂ H ₅
ΔH (273.15)	6.6101	6.6156	2.2761	2.3083	2.5061	2.8356
ΔH (298.15)	7.8900	7.8860	2.5295	2.5668	2.8052	3.1623
ΔH (400)	14.3447	14.2571	3.7153	3.7443	4.2195	4.6556
ΔH (500)	22.3832	22.1474	5.1163	5.0769	5.9274	6.3742
ΔH (600)	31.7694	31.3299	6.7249	6.5556	7.9331	8.3197
ΔH (700)	42.2170	41.5276	8.5111	8.1573	10.2041	10.4645
ΔH (800)	53.5078	52.5296	10.4507	9.8649	12.7090	12.7849
ΔH (900)	65.4795	64.1790	12.5241	11.6653	15.4198	15.2606
ΔH (1000)	78.0097	76.3575	14.7151	13.5478	18.3119	17.8739
ΔH (1100)	91.0035	88.9741	17.0095	15.5028	21.3629	20.6089
ΔH (1200)	104.3862	101.9570	19.3947	17.5218	24.5531	23.4510
ΔH (1300)	118.0976	115.2490	21.8598	19.5971	27.8649	26.3873
ΔH (1400)	132.0889	128.8034	24.3950	21.7220	31.2832	29.4064
ΔH (1500)	146.3198	142.5823	26.9917	23.8905	34.7944	32.4982
ΔH (1600)	160.7570	156.5541	29.6425	26.0974	38.3870	35.6537
ΔH (1700)	175.3728	170.6928	32.3410	28.3382	42.0511	38.8655
ΔH (1800)	190.1440	184.9764	35.0816	30.6089	45.7781	42.1268
ΔH (1900)	205.0511	199.3867	37.8593	32.9060	49.5604	45.4319
ΔH (2000)	220.0774	213.9081	40.6700	35.2266	53.3919	48.7758
ΔH (2100)	235.2088	228.5274	43.5101	37.5680	57.2668	52.1542
ΔH (2200)	250.4333	243.2333	46.3764	39.9282	61.1805	55.5634
σ	1	1	4	1	18	6
S (273.15)	100.1640	100.0853	51.6195	53.7559	51.3765	56.2282
S (298.15)	104.6444	104.5322	52.5066	54.6610	52.4235	57.3722
S (400)	123.1324	122.7841	55.9104	58.0447	56.4812	61.6621
S (500)	141.0070	140.3305	59.0275	61.0115	60.2795	65.4870
S (600)	158.0871	157.0406	61.9549	63.7039	63.9285	69.0281
S (700)	174.1734	172.7426	64.7051	66.1706	67.4243	72.3307
S (800)	189.2390	187.4231	67.2929	68.4493	70.7658	75.4267
S (900)	203.3326	201.1374	69.7337	70.5689	73.9565	78.3410
S (1000)	216.5297	213.9643	72.0411	72.5516	77.0020	81.0932
S (1100)	228.9110	225.9861	74.2271	74.4144	79.9088	83.6990
S (1200)	240.5532	237.2806	76.3020	76.1708	82.6838	86.1713
S (1300)	251.5266	247.9184	78.2747	77.8316	85.3341	88.5212
S (1400)	261.8940	257.9622	80.1532	79.4061	87.8668	90.7582
S (1500)	271.7114	267.4678	81.9445	80.9021	90.2890	92.8910
S (1600)	281.0283	276.4844	83.6552	82.3263	92.6074	94.9274
S (1700)	289.8886	285.0554	85.2910	83.6847	94.8285	96.8743
S (1800)	298.3312	293.2193	86.8573	84.9825	96.9586	98.7383
S (1900)	306.3907	301.0103	88.3591	86.2244	99.0035	100.5252
S (2000)	314.0980	308.4586	89.8007	87.4146	100.9687	102.2403
S (2100)	321.4804	315.5912	91.1863	88.5570	102.8592	103.8886
S (2200)	328.5627	322.4322	92.5197	89.6549	104.6798	105.4745

References

- Allen, J.O., Dookeran, N.M., Smith, K.A., Sarofim, A.F., Taghizadeh, K., and Lafleur, A.L., "Measurement of Polycyclic Aromatic Hydrocarbons Associated with Size-Segregated Atmospheric Aerosols in Massachusetts," *Env. Sci. Tech.*, 30, 1023-1031 (1996).
- Biordi, J.C., Lazzara, C.P., and Papp, J.F., "Molecular Beam Mass Spectrometry Applied to Determining the Kinetics of Reactions in Flames. I. Empirical Characterization of Flame Perturbation by Molecular Beam Sampling Probes," *Combustion and Flame*, 23, 73-82 (1974).
- Bittner, J.D., "A Molecular Beam Mass Spectrometric Study of Fuel-Rich and Sooting Benzene-Oxygen Flames," Sc.D. Thesis, Department of Chemical Engineering, Massachusetts Institute of Technology (1981).
- Bittner, J.D. and Howard, J.B., "Composition Profiles and Reaction Mechanisms in a Near-sooting Premixed Benzene/Oxygen/Argon Flame," *Eighteenth Symposium (International) on Combustion*, The Combustion Institute, 1105 (1981).
- Bockhorn, H., "General Discussion on Models for Soot Formation in Turbulent Flames," Soot Formation in Combustion, New York: Springer Verlag, 569 (1994).
- Bockhorn, H. and Schäfer, T., "Growth of Soot Particles in Premixed Flames by Surface Reactions," Soot Formation in Combustion, New York: Springer Verlag, 253-273 (1994).
- Bönig, M., Feldermann, C., Jander, H., Lüers, B., Rudolph, G., and Wagner, H.G., "Soot Formation in Premixed C₂H₄ Flat Flames at Elevated Pressure," *Twenty-Third Symposium (International) on Combustion*, The Combustion Institute, 1581-1587 (1990).
- Böhm, H., Feldermann, C., Heidermann, T., Jander, H., Lüers, B., and Wagner, H.G., "Soot Formation in Premixed C₂H₄-Air Flames for Pressures up to 100 bar," *Twenty-Fourth Symposium (International) on Combustion*, The Combustion Institute, 991-998 (1992).
- Bonne, U., Homann, K.H., and Wagner, H.G., "Carbon Formation in Premixed Flames," *Tenth Symposium (International) on Combustion*, The Combustion Institute, 503 (1965).
- Boyd, R.H., Christensen, R.L., and Pua, R., "The Heats of Combustion of Acenaphthene, Acenaphthylene, and Fluoranthene. Strain and Delocalization in Bridged Naphthalenes," *J. Am. Chem. Soc.*, 87 3554-3559 (1965).
- Brown, R.F.C., Choi, N., Coulston, K.J., Eastwood, F.W., Woersum, U.E., and Jenneskens, L.W., "Cyclopenta[a]indene (Benzopentalene): Generation by Flash Vacuum Pyrolysis and Subsequent Dimerisation," *Tetrahedron Letters*, 35, 4405-4408 (1994).
- Burrow, P.L. and Birks, J.W., "Flow Tube Kinetics Investigation of the Mechanism of Detection in the Sulfur Chemiluminescence Detector," *Anal. Chem.*, 69, 1299-1306 (1997)
- Castaldi, M.J., Marinov, N.M., Melius, C.F., Huang, J., Senkan, S.M., Pitz, W.J., and Westbrook, C.K., "Experimental and Modeling Investigation of Aromatic and Polycyclic Aromatic Hydrocarbon Formation in a Premixed Ethylene Flame," *Twenty-Sixth Symposium (International) on Combustion*, The Combustion Institute, 693-702 (1996).
- Chase, M.W., "NIST-JANAF Thermochemical Tables, Fourth Edition," J.Phys. Chem. Ref. Data, Monograph 9 (1998).

- Chen, R.H., Kafafi, S.A., and Stein, S.E., "Reactivity of Polycyclic Aromatic Aryl Radicals," *J. Am. Chem. Soc.*, 111, 1418-1423 (1989).
- Choi, M.Y., Mullholland, G.W., Hamins, A., and Kashiwagi, T., "Comparisons of the Soot Volume Fraction Using Gravimetric and Light Extinction Techniques," *Combustion and Flame*, 102, 161-169 (1995).
- Church, D.F., "Spin Trapping Organic Radicals," *Anal. Chem.*, 66, 419-427 (1994).
- Cioslowski, J., Liu, G., Martinov, M., Piskorz, P., and Moncrieff, D., "Energetics and Site Specificity of the Homolytic C-H Bond Cleavage in Benzenoid Hydrocarbons: An ab Initio Electronic Structure Study," *J. Am. Chem. Soc.*, 118, 5261-5264 (1996).
- Cole, J.A., "A Molecular-Beam Mass-Specrometric Study of Stoichiometric and Fuel-Rich 1,3-Butadiene Flames," M.S. Thesis, Department of Chemical Engineering, Massachusetts Institute of Technology (1982).
- Coleman, D.J. and Pilcher, G., "Heats of Combustion of Biphenyl, Bibenzyl, Naphthalene, Anthracene, and Phenanthrene," *Trans. Faraday Soc.*, 62, 821-827 (1966).
- Cosman, M., de los Santos, C., Radovan, F., Hingerty, B.E., Singh, S.B., Ibanez, V., Margulis, L.A., Live, D., Geacintov, N.E., Broyde, S., and Patel, D.J., "Solution Conformation of the Major Adduct Between the Carcinogen (+)-anti-Benzo[a]pyrene diol epoxide and DNA," *Proc. Natl. Acad. Sci. USA*, 89, 1914-1918 (1992).
- Delichatsios, M.A., "A Phenomenological Model for Smoke-Point and Soot Formation in Laminar Flames," *Combust. Sci. Tech.*, 100, 283-298 (1994).
- Dockery, D.W., Pope, C.A., Xu, X., Spengler, J.D., Ware, J.H., Fay, M.E., Ferris, B.G., Speizer, F.E., "An Association Between Air Pollution and Mortality in Six U.S. Cities," *New England Journal of Medicine*, 329, 1753-1808 (1993).
- Durant, J.L., Busby, W.F., Lafleur, A.L., Penman, B.W., and Crespi, C.L., "Human Cell Mutagenicity of Oxygenated, Nitrated, and Unsubstituted Polycyclic Aromatic Hydrocarbons Associated with Urban Aerosols," *Mutation Research*, 371, 123-157 (1996).
- Fahr, A. and Stein, S.E., "Reactions of Vinyl and Phenyl Radicals with Ethyne, Ethene and Benzene," *Twenty-Second Symposium (International) on Combustion*, The Combustion Institute., 1023-1029 (1989).
- Feitelberg, A.S., "The Effects of Metal Additives on Soot Formation," Ph.D. Thesis, Department of Chemical Engineering, Massachusetts Institute of Technology (1993).
- Foresman, J.B. and Frisch, M.J., *Exploring Chemistry with Electronic Structure Methods*, Gaussian, Inc. (1996).
- Fristrom, R.M. and Westenberg, K.P., *Flame Structure*, McGraw-Hill, 214-217 (1965).
- Fristrom, R.M., "Brief Communications: Comments on Quenching Mechanisms in the Microprobe Sampling of Flames," *Combustion and Flame*, 50, 239-242 (1983).
- Frenklach, M., Clary, D.W., Gardiner, W.C., and Stein, S.E., "Detailed Kinetic Modelling of Soot Formation in Shock-Tube Pyrolysis of Acetylene," *Twentieth Symposium (International) on Combustion*, The Combustion Institute., 887-901 (1984).
- Frenklach, M., "On the Driving Force of PAH Production," *Twenty-Second Symposium (International) on Combustion*, The Combustion Institute., 1075-1082 (1988).

- Harris, S.J. and Weiner, A.M., "Surface Growth of Soot Particles in Premixed Ethylene/Air Flames," *Combust Sci. Tech.*, 31, 155-167 (1983a).
- Harris, S.J. and Weiner, A.M., "Determination of the Rate Constant for Soot Surface Growth," *Combust Sci. Tech.*, 32, 267 (1983b).
- Harris, S. J. and Weiner, A. M., "A Picture of Soot Particle Inception," *Twenty-Second Symposium (International) on Combustion*, The Combustion Institute., 333-342 (1989).
- Hausmann, M. and Homann, K.H., "Analysis of Radicals from Flames by Scavenging with Dimethyl Disulfide," *Ber. Bunsenges. Phys. Chem.* 94, 1308-1312 (1990).
- Hausmann, M., Hebggen, P. and Homann, K.H., "Radicals in Flames: Analysis via Scavenging Reaction," *Twenty-Fourth Symposium (International) on Combustion*, The Combustion Institute, 793-801 (1992).
- Hausmann, M. and Homann, K.H., "Scavenging of Hydrocarbon Radicals from Flames with Dimethyl Disulfide," *Ber. Bunsenges. Phys. Chem.* 99 (1995).
- Haynes, B.S., Jander, H, and Wagner, H.G., "Optical Studies of Soot-Formation Processes in Premixed Flames," *Ber. Bunsenges. Phys. Chem.* 84, 585-592 (1980).
- Haynes, B.S. and Wagner, H.G., "The Surface Growth Phenomenon in Soot Formation," *Z. Phys. Chem.*, 133, 201-213 (1982).
- Haynes, B.S., "Soot and Hydrocarbons in Combustion," Fossil Fuel Combustion, Bartok, W. and Sarofim A. F., eds., John Wiley & Sons, 261-326 (1991).
- Homann, K.H., Mochizu, K.M., and Wagner, H.G., "Reactions in Rich Hydrocarbon-Oxygen Flames," *Z. Phys. Chem. N.F.*, 37, 299 (1963).
- Homann, K.H. and Wagner, H.G., "Untersuchung des Reaktionsablaufs in fetten Kohlenwasserstoff-Sauerstoff-Flammen bei niedrigem Druck," *Ber. Bunsenges. Phys. Chem.* 69, 20 (1965).
- Howard J. B. and Bittner, J. D., "Structure of Sooting Flames" Soot in Combustion Systems and its Toxic Properties, Lahaye, J., Prado, G. eds., New York: Plenum Press 57-92 (1983).
- Howard, J.B., "Carbon Addition and Oxidation Reactions in Heterogeneous Combustion and Soot Formation," *Twenty-Third Symposium (International) on Combustion*, The Combustion Institute, 1107-1127 (1990).
- Howard, J.B., Longwell, J.P, Marr, J.A., Pope, C.J., Busby, W.F., Lafleur, A.L. Taghizadeh, K., "Effects of PAH Isomerizations on Mutagenicity of Combustion Products," *Combustion and Flame*, 101, 262-270 (1995).
- Griesheimer, J. and Homann, K.H., "Aromatic Radicals and Intermediate PAHs in a Premixed Low-Pressure Naphthalene/Oxygen/Argon Flame," *Twenty-Seventh Symposium (International) on Combustion*, The Combustion Institute, (1998).
- Grieco, W.J., "Fullerenes and Carbon Nanostructures Formation in Flames," Ph.D. Thesis, Department of Chemical Engineering, Massachusetts Institute of Technology (1999).
- Kee, R.J., Grcar, J.F., Smooke, M.D., and Miller, J.A., "A FORTRAN Program for Modeling Steady Laminar One-Dimensional Premixed Flames," Sandia Report SAND85-8240 (1997).
- Kiefer, J.H., Mizerka, L.J., Patel, M.R., and Wei, H.-C., "A Shock Tube Investigation of Major Pathways in the High-Temperature Pyrolysis of Benzene," *J. Phys. Chem.*, 89, 2013-2019 (1985).

- Lagow, R.J., Kampa, J.J., Wei, H., Battle, S.L., Genge, J.W., Laude, D.A., Harper, C.J., Bau, R., Stevens, R.C., Haw, J.F., and Munson, E., "Synthesis of Linear Acetylenic Carbon: The 'sp' Carbon Allotrope," *Science*, 267, 362-367 (1995).
- Lam, F.W., Longwell, J.P., and Howard, J.B., "The Behavior of Polycyclic Aromatic Hydrocarbons During the Early Stages of Soot Formation," *Twenty-Second Symposium (International) on Combustion*, The Combustion Institute, 323-332 (1989).
- Lam, F.W., Longwell, J.P., and Howard, J.B., "The Effect of Ethylene and Benzene Addition on the Formation of Polycyclic Aromatic Hydrocarbons and Soot in a Jet-Stirred/Plug-Flow Reactor," *Twenty-Third Symposium (International) on Combustion*, The Combustion Institute, 1477-1484 (1991).
- Lindstedt, P.R., "Simplified Soot Nucleation and Surface Growth Steps for Non-Premixed Flames," *Soot Formation in Combustion*, New York: Springer Verlag, 417-441 (1994).
- Lindstedt, P., "Modeling of the Chemical Complexities of Flames," *Twenty-Seventh Symposium (International) on Combustion*, The Combustion Institute, (1998).
- Mackay, W., Benasutti, M., Drouin, E., and Loechler, E.L., "Mutagenesis by (+)-anti-B[a]P-N2-Gua, the Major Adduct of Activated Benzo[a]pyrene, when Studied in an Escherichia Coli Plasmid Using Site-directed Methods," *Carcinogenesis*, 13, 1415-1425 (1992).
- Madronich, S. and Felder, W., "Kinetics and Mechanism of the Reaction of OH with C₆H₆ over 790-1410 K," *J. Phys. Chem.*, 89, 3556-3561 (1985).
- Marinov, N.M. Pitz, C.K., Westbrook, C.K., Castaldi, M.J., and Senkan, S.M., "Modelling of Aromatic and Polycyclic Aromatic Hydrocarbon Formation in Premixed Methane and Ethane Flames," *Combust Sci. Tech.*, 116-117, 211-287 (1996).
- Marr, J. A., "PAH Chemistry in a Jet Stirred/Plug Flow Reactor System," Ph.D. Thesis, Department of Chemical Engineering, Massachusetts Institute of Technology (1993).
- Marr, J. A., Allison, D.M., Giovane, L.M., Yerkey, L.A., Monochamp, P., Longwell, J.P., and Howard, J.B., "The Effect of Chlorine on PAH, Soot, and Tar Yields From a Jet Stirred/Plug Flow Reactor System," *Combust Sci. Tech.*, 85, 65-76 (1992).
- Marr, J. A., Giovane, L.M., Longwell, J.P., Howard, J.B., and Lafleur, A.L., "Soot and Tar Production in a Jet-Stirred/Plug-Flow Reactor System: High and Low C₂H₂ Concentration Environments," *Combust Sci. Tech.*, 101, 301-309 (1994).
- Mauss, F., Schafer, T., and Bockhorn, F., "Inception of Growth and Soot Particles in Dependence on the Surrounding Gas Phase," *Combustion and Flame*, 99, 697-705 (1994).
- McKinnon, J.T., "Chemical and Physical Mechanisms of Soot Formation," Ph.D. Thesis, Department of Chemical Engineering, Massachusetts Institute of Technology (1989).
- McKinnon, J. T., and Howard, J. B., "The Role of PAH and Acetylene in Soot Nucleation and Growth," *Twenty-Fourth Symposium (International) on Combustion*, The Combustion Institute, 965-971 (1992).
- Pope, C.J., "Fluxes and Net Rates of High Molecular Weight Material in a Near-Sooting Benzene-Oxygen Flame," M.S. Thesis, Department of Chemical Engineering, Massachusetts Institute of Technology (1988).

Prosen, E.J., Johnson, W.H., and Rossini, F.D., "Heats of Combustion and Formation at 25°C of the Alkylbenzenes through C₁₀H₁₄ and of the Higher Normal Monoalkylbenzenes," *J. Res. NBS*, 36, 455-461 (1946).

Richter, H.R., *personal communication*, Feb. 7, 1999.

Richter, H.R., Grieco, W.J., and Howard, J.B., "Formation Mechanism of Polycyclic Aromatic Hydrocarbons and Fullerenes in Premixed Benzene Flames," *submitted to Combustion and Flame* (1999)

Ritter, E.R. and Bozzelli, J.W., "THERM: Thermodynamic Property Estimation for Gas Phase Radicals and Molecules," *Int. J. Chem. Kinet.*, 23, 767-778 (1991).

Schenker, M. "Air Pollution and Mortality," *New England Journal of Medicine*, 329, 1807-1808 (1993).

Schottler, M. and Homann, K.H., "Scavenging of Radicals from the Gas Phase by Freezing with Dimethyl Disulfide," *Ber. Bunsenges. Phys. Chem.* 91, 688-701 (1987).

Scott, L.T. and Roelfs, N.H., "Benzene Ring Contractions at High Temperatures. Evidence from the Thermal Interconversions of Aceanthrylene, Acephenanthrylene, and Fluoranthene," *J. Am. Chem. Soc.*, 109, 5461-5465 (1987).

Scott, L.T., *personal communication*, Feb. 2, 1999.

Shandross, R.A., "Experimental and Theoretical Study of Hydrogen and Benzene Destruction Chemistries," Ph.D. Thesis, Department of Chemical Engineering, Massachusetts Institute of Technology (1996).

Smedley, J. M., Williams, A., and Bartle, K.D., "A Mechanism for the Formation of Soot Particles," *Combustion and Flame*, 91, 71-82 (1992).

Smith, N.K., Stewart, R.C., Osborn, A.G., Scott, D.W., "Pyrene: Vapor Pressure, Enthalpy of Combustion, and Chemical Thermodynamic Properties," *J. Chem. Thermodyn.*, 12, 919-926 (1980).

Smyth, K.C. and Miller, J.H., "Chemistry of Molecular Growth Processes in Flames," *Science*, 236, 1540-1546 (1987).

Stepowski, D., Puechberty, D., and Cottureau, M., "The Use of Laser-Induced Fluorescence of OH to Study the Perturbation of a Flame by a Probe," *Eighteenth Symposium (International) on Combustion*, The Combustion Institute, 1567-1573 (1981).

Tang, H., Heaton, P., Brassard, B., and Dunbar, J., "A Study of Response Factors of Sulfur Compounds in a Sulfur Chemiluminescence Detector Coupled with GC," *American Laboratory*, 26-27 (Dec., 1997).

Tsang, W., "Heats of Formation of Organic Free Radicals by Kinetic Methods," *Energetics of Organic Free Radicals*, London: Blackie Academic and Professional, 22-58 (1996).

Wang, H., Frenklach, M., Detailed Kinetic Modeling Study of Aromatics Formation in Laminar Premixed Acetylene and Ethylene Flames," *Combustion and Flame*, 110, 173-221 (1997).

Weast, R.C. Ed., *CRC Handbook of Chemistry and Physics*, CRC Press, Inc. (1985).

Weischnowsky, U., Bockhorn, H, and Fetting, F., *Twenty-Second Symposium (International) on Combustion*, The Combustion Institute, 343-350 (1989).

Westmoreland, P.R., "Experimental and Theoretical Analysis of Oxidation and Growth Chemistry in a Fuel-Rich Acetylene Flame," Ph.D. Thesis, Department of Chemical Engineering, Massachusetts Institute of Technology (1986).

Wiersum, U.E. and Jenneskens, L.W., "Flash Vacuum Thermolysis of Biphenylene and Diphenic Anhydride. Formation of 6b,7,10,10a-Tetrahydro-as-indacenol[1,8-jk]fluoranthene. Evidence for the Intermediacy of as-Inacene on the C₁₂H₈ Potential Energy Surface," *Tetrahedron Letters*, 34, 6615-6618 (1993).

Woods, I.T., and Haynes, B.S., "Active Sites in Soot Growth," Soot Formation in Combustion, New York: Springer Verlag, 275-288 (1994).

D'Alessio, et al., "Precursor Formation and Soot Inception in Premixed Ethylene Flames," *Twenty-Fourth Symposium (International) on Combustion*, The Combustion Institute, 973-980 (1992).

Wersborg, B. L., et al., "Soot Concentration and Absorption Coefficient in a Low-Pressure Flame," *Combustion and Flame*, 24, 1-10 (1975).